

Energy Invariant Mechanisms

Kuppens, P.R.

DOI

[10.4233/uuid:579b7c68-8c13-493c-87d9-0f77d5fba34c](https://doi.org/10.4233/uuid:579b7c68-8c13-493c-87d9-0f77d5fba34c)

Publication date

2021

Document Version

Final published version

Citation (APA)

Kuppens, P. R. (2021). *Energy Invariant Mechanisms*. [Dissertation (TU Delft), Delft University of Technology]. <https://doi.org/10.4233/uuid:579b7c68-8c13-493c-87d9-0f77d5fba34c>

Important note

To cite this publication, please use the final published version (if applicable).
Please check the document version above.

Copyright

Other than for strictly personal use, it is not permitted to download, forward or distribute the text or part of it, without the consent of the author(s) and/or copyright holder(s), unless the work is under an open content license such as Creative Commons.

Takedown policy

Please contact us and provide details if you believe this document breaches copyrights.
We will remove access to the work immediately and investigate your claim.

Energy Invariant Mechanisms



Peter Reinier Kuppens

ENERGY INVARIANT MECHANISMS

Proefschrift

ter verkrijging van de graad van doctor
aan de Technische Universiteit Delft,
op gezag van de Rector Magnificus Prof. dr. ir. T.H.J.J. van der Hagen,
voorzitter van het College voor Promoties,
in het openbaar te verdedigen op
dinsdag 15 juni 2021 om 15:00 uur

door

Peter Reinier KUPPENS

Werktuigkundig ingenieur
Technische Universiteit Delft, Nederland
geboren te Gorinchem, Nederland

Dit proefschrift is goedgekeurd door de promotoren.

Samenstelling promotiecommissie:

Rector Magnificus	voorzitter
Prof. dr. ir. J.L. Herder	Technische Universiteit Delft, promotor
Dr. M.A. Bessa	Technische Universiteit Delft, copromotor

Onafhankelijke leden:	
Prof. dr. ir. P. Breedveld	Technische Universiteit Delft
Prof. dr. P.J. French	Technische Universiteit Delft
Prof. M.I. Frecker, PhD	Pennsylvania State University, USA
Dr. ir. M. Schenk	Bristol University, UK

Overige leden:	
Dr. N. Tolou	Flexous Mechanisms B.V., NL



TAGHeuer
SWISS AVANT-GARDE SINCE 1860

This research was instigated by and in close collaboration with TAG Heuer Institute, La Chaux de Fonds, 2300 Switzerland, and its Director, Mr G.A.(Guy) Sémon, and received funding from TAG Heuer Institute.

Printed by: Gildeprint

Front & Back: Reinier Loopik

Copyright © 2021 by P.R. Kuppens

ISBN 978-94-6384-227-3

An electronic version of this dissertation is available at
<http://repository.tudelft.nl/>

Demonstration videos are available at
https://www.youtube.com/channel/UCtyp20Z_z-yNESH7QLx1yCA

A machine that can bend? No way.

B.B. Rodríguez

CONTENTS

Summary	vii
Samenvatting	ix
1 Introduction	1
1.1 Energy invariance	2
1.2 Static balance at different scales	3
1.3 Statically balanced compliant mechanisms	5
1.4 Problem definition and research goals	6
1.5 Thesis outline	6
References	7
2 Static balancing of serial chains with virtual transmissions	15
2.1 Introduction	16
2.2 Method	17
2.2.1 Method in 2D	18
2.2.2 Method in 3D	20
2.3 Planar examples	21
2.3.1 Static balancing a single-link system	22
2.3.2 Static balancing a two-link system	23
2.3.3 Static balancing a two-link system with transmission	26
2.3.4 Static balancing a three-link system	28
2.4 Spatial example	32
2.4.1 One spring systems ($n = 1$)	33
2.4.2 Two spring systems ($n = 2$)	33
2.4.3 n -Spring systems ($n > 2$)	35
2.5 Independence of coefficients	36
2.6 Discussion	37
2.7 Conclusion	40
References	40
3 Dramatically different states of stiffness by opposing constant force	43
3.1 Introduction	44
3.2 Balancing method	45
3.2.1 Opposing constant force	45
3.2.2 Constant force and torque mechanisms	46
3.2.3 Preloading mechanisms	47
3.2.4 Finite element models	48
3.2.5 Final mechanism design and manufacturing	50
3.2.6 Measurements	51

3.3	Results	52
3.4	Discussion	53
3.5	Conclusion	54
	References	55
4	Binary stiffness mechanisms for mechanical digital machines	59
4.1	Introduction	60
4.2	Method for binary stiffness	62
4.2.1	Controlling the preloading	66
4.2.2	Modeling, design and fabrication	67
4.2.3	Measurements	68
4.3	Results	68
4.4	Conclusion	69
	References	70
5	Permanent stiffness reduction by thermal oxidation of silicon	77
5.1	Introduction	78
5.2	Stiffness reduction method	79
5.3	Minimum required film stress	80
5.4	Mechanism design	82
5.5	Manufacturing	83
5.6	Simulations	83
5.7	Measurements	85
5.8	Measurement results	85
5.8.1	Balance with oxide	88
5.8.2	Balance without oxide	89
5.9	Discussion	90
5.10	Conclusion	91
	References	92
6	Discussion and Conclusion	97
6.1	Scalability	98
6.2	Balancing quality	100
6.3	Conclusion	101
	References	102
A	Appendix	109
	About the author	117
	List of Publications	119
	Acknowledgements	121

SUMMARY

This thesis presents energy invariant mechanisms that can be scaled to micro size. They are also called statically balanced, because all static forces are balanced against each other. They enable effortless suspension of weight, and flexible devices without stiffness, seemingly defeating gravity and elasticity. In large scale applications such as movable bridges and ship lifts gravitational forces dominate elastic forces and counterweight balancing is the only practical approach. At small length scales, roles reverse: gravity becomes insignificant and elastic forces dominate. While other conservative forces such as magnetics or electrostatics also become relevant, focus will be placed on elastic forces.

Static balancing is investigated at various scales, working our way down as we progress through the chapters. This investigation starts with a method for the analysis and synthesis of energy invariance in rigid body mechanisms, which are often used to aid the more difficult design of compliant mechanisms. It allows symbolic derivation of balancing conditions for serial kinematic chains with any number of links and zero-free-length springs. Virtual transmissions are introduced to temporarily constrain the chain to single degree of freedom and ease solving. Examples are provided in 2D and 3D.

Static balancing is commonly used in civil engineering, robotics and large scale compliant mechanisms, where preloading is relatively easily applied by hand or preloading assembly. However, preloading becomes difficult at small scales and is identified as the primary reason the state of the art is not down-scalable. It is addressed by the design of various monolithic and planar architectures. The fully compliant mechanisms with linear and rotary motion incorporate a bistable mechanism that sustains the required preload in a reversible way. In one case, opposing constant force and torque achieves stiffness reduction by 98.5 % and 90.5 % respectively with increased relative range of motion (from 3.3 % to 6.6 %) and reduced complexity compared to the state of the art.

In the second case a new V-shape plate spring is used that minimizes and maximizes stiffness when preloaded and when not preloaded respectively. An unprecedented stiffness reduction of 99.9 % and 98.5 % is achieved under large deformations in fused model deposition prototypes made out of polylactic acid. In all four cases switching between soft and hard modes can be done reversibly by toggling the bistable switch directly. Alternatively, the soft mode can be entered by actuating the shuttle over a force threshold.

In addition, preloading is addressed by making it part of the manufacturing process by exploiting residual stress from thin film deposition. A stiffness reduction by a factor 9 to 46 is achieved over a range of 380 μm by thermal oxidation of silicon. The stiffness reduction is achieved in a passive way, allows for parallelized manufacturing, is space efficient and is scalable, since surface effects become more dominant at smaller scales.

Miniature statically balanced mechanisms will be an enabling technology for low frequency sensors, mechanical energy harvesting, mechanical watch oscillators, mechanical logic and computing, microrobotics, compliant transmission mechanisms, and make small scale compliant mechanisms more energy efficient.

SAMENVATTING

Deze thesis presenteert energie invariante mechanismen die naar microformaat gehaald kunnen worden. Een alternatieve naam is statisch gebalanceerde mechanismen, omdat alle statische krachten tegen elkaar worden uitgebalanceerd. Ze maken moeiteloze ophanging van gewicht en flexibele apparaten zonder stijfheid mogelijk, die schijnbaar de zwaartekracht en elasticiteit overwinnen. In toepassingen op grote schaal zoals beweegbare bruggen en scheepsliften domineert de zwaartekracht elastische krachten, zodat balanceren met contragewichten de enige praktische oplossing is. Op kleine schaal keren de rollen om: de zwaartekracht wordt onbeduidend en elastische krachten domineren. Terwijl andere conservatieve krachten zoals magnetisme en elektrostatica ook relevant worden, zal de focus worden gelegd op elastische krachten.

Statisch balanceren wordt op verschillende schalen onderzocht, waarbij we in ieder volgend hoofdstuk een steeds kleinere lengteschaal bekijken. Dit onderzoek begint met een methode voor de analyse en synthese van energie invariantie in mechanismen met rigide elementen, die vaak als voorloper op compliante mechanismen worden gebruikt in het ontwerpproces. Het maakt de afleiding van evenwichtscondities mogelijk voor seriële kinematische kettingen met een willekeurig aantal schakels en veren met een rustlengte van nul. Virtuele transmissies worden geïntroduceerd om de keten tijdelijk te beperken tot een enkele vrijheidsgraad en om het oplossen te vergemakkelijken. Er worden voorbeelden in 2D en 3D gegeven.

Statisch balanceren wordt vaak gebruikt in de civiele techniek, robotica en grotere compliante mechanismen, waar voorspanning relatief eenvoudig kan worden toegepast met de hand of voorspanningsconstructie. Voorspannen wordt echter moeilijk op kleine schaal en wordt gezien als de belangrijkste reden waarom huidige techniek niet kan worden verkleind. We bieden een oplossing door verschillende monolithische en platte architecturen te ontwerpen. De geheel compliante mechanismen, die linear end roterend bewegen, bevatten een bistabiel mechanisme dat de vereiste voorspanning op een omkeerbare manier aanbrengt. In het eerste type wordt door tegengestelde constante kracht en koppel een stijfheidsvermindering bereikt met respectievelijk 98.5 % en 90.5 % met een groter relatief bewegingsbereik (van 3.3 % tot 6.6 %) en verminderde complexiteit in vergelijking met de huidige techniek.

In het tweede type wordt een nieuwe V-vormige plaatveer gebruikt die de stijfheid minimaliseert en maximaliseert als deze respectievelijk is voorgespannen of niet. Een ongekende stijfheidsreductie van 99.9 % en 98.5 % wordt bereikt voor grote vervormingen in 3D geprinte prototypen van polylactide. In alle vier gevallen kan worden gewisseld tussen stijf en compliant door de bistabiele schakelaar om te zetten. Ook kan de compliante modus worden geactiveerd door de shuttle over een krachtdrempel te bewegen.

Bovendien wordt voorspannen bewerkstelligd als onderdeel van het fabricageproces door gebruik te maken van restspanning in een dunne filmafzetting. Stijfheidsreductie met een factor 9 tot 46 is bereikt over een domein van 380 μm door thermische oxida-

tie van silicium. Het is passief, ruimtebesparend en schaalbaar aangezien oppervlakte-effecten dominant worden op kleinere schaal.

Geminiaturiseerde statisch gebalanceerde mechanismen zullen het mogelijk maken nieuwe sensor technologie te ontwikkelen, maar ook mechanische energy opwekkers, oscillators voor mechanische horloges, mechanische logica en computers, microrobotica, compliante transmissiemechanismen en zullen kleinschalige compliante mechanismen meer energie efficiënt kunnen maken.

1

INTRODUCTION

This chapter explains what energy invariant mechanisms are and why they are useful and necessary. An overview of the state of the art shows that various principles for creating energy invariance dominate different length scales. This leads us to identify that little work at small scales (sub-centimeter) is done, because there are no straightforward approaches for preloading. We give the contributions and outline the structure of this thesis that is concerned with making energy invariant mechanisms scalable.

The way potential energy is stored and released affects the performance of many mechanical systems. For example, the constant pull of gravity requires excessive motor torque in robotic manipulators [1] and causes issues in the rehabilitation of human motor control impairment [2, 3]. Also, elasticity in compliant mechanisms causes part of the input energy to be stored as strain energy, which challenges energy efficiency and for example effective haptic feedback [4, 5].

A powerful solution is to prevent potential energy from entering and exiting the system. That is, to design for energy invariance over the complete motion domain of the system. These systems are called statically balanced [6] and in this thesis we work towards their design on small scales.

1.1. ENERGY INVARIANCE

Energy is an eternal shapeshifter that can only change form and is never truly lost. We are familiar with many of its faces such as thermal, chemical, nuclear and electric energy, but in classical mechanics only kinetic and potential energy are distinguished, i.e. the Hamiltonian or Lagrangian [7]. Kinetic energy measures the amount of work required to get a body in motion or to stop it, whereas potential energy is the capacity for motion. This study is only concerned with static bodies. This means motion is never concerned in a dynamical sense but always quasi-statically, which means the velocity is always close to zero ($v \approx 0$) and therefore the kinetic energy ($KE \propto v^2$) is insignificant.

Static systems that have a constant potential energy for all configurations are called statically balanced [6], because all conservative forces are balanced against each other. They can be moved effortlessly because restoring forces are eliminated which results in zero stiffness. Such a sustained equilibrium can be achieved in various ways, but the general approach is to add an energy buffer that is able to release and absorb the potential energy from the original system. It makes sure the potential energy flows within the system, incapacitating its true release and its natural tendency to cause motion.

Energy buffers are able to release energy, because they contain a predetermined amount of stored energy and are unstable when isolated. Mechanical systems with these properties exhibit negative stiffness, because the direction of motion and the direction

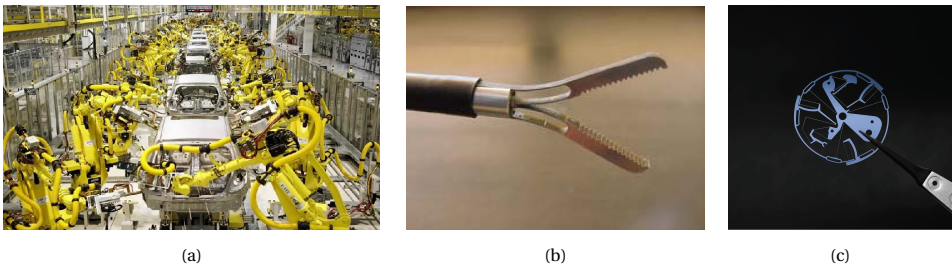


Figure 1.1: An army of robots fighting against gravity [8]. A fully compliant laparoscopic gripper with elastic equilibrium in the closed state [9, 10]. Fully compliant watch oscillator with a relatively high natural frequency (18Hz) compared to conventional watches (4Hz) [11].

of force are aligned. Arguably, one of the simplest examples of a negative stiffness mechanism is an inverted pendulum. If disturbed from its unstable equilibrium, force and displacement amplify each other, assuring permanent escape.

For elastic devices, negative stiffness means that the usual relation between force and displacement is reversed. This does not violate mechanics and is relatively easily created by preloading a spring system. Unstable systems are typically avoided in engineering science, because displacements can grow uncontrollably and cause damage. However, when integrated with a stable system, the combined system may exhibit marginal or neutral stability, that is, be energy invariant and statically balanced.

It is not hard to imagine that preloading poses different challenges at different scales. On large scale forces may become so big that heavy equipment is required, whereas on the centimeter scale simple hand tools or manual precision stages may be sufficient. But what should we do when systems become so small they cannot be seen by the naked eye and manipulation of any sort is very likely to damage the system?

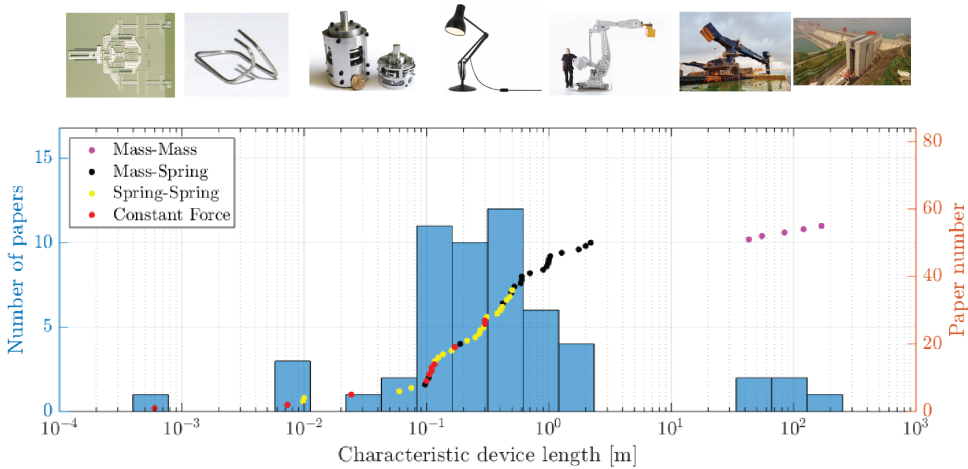


Figure 1.2: This graphs shows the characteristic device length of 54 devices from about as much scientific studies. Each data point represents one device corresponding to the paper on the right y-axis. The total number of devices at a particular scale is visualized with the histogram with the bin count on the left y-axis. We distinguish between four types, of which three are different types of static balancing. It can be seen that each type dominates a particular length scale and that most research is done on decimeter scale. On small scale ($< 1 \times 10^{-2}$) no statically balanced mechanisms are reported, only constant force mechanisms. All references are listed in appendix A.

1.2. STATIC BALANCE AT DIFFERENT SCALES

A plethora of statically balanced systems can be found in scientific literature, ranging from centimeter to hectometer scale. An overview is presented in figure 1.2 where each data point represents a mechanical device. Each device is plotted versus its characteristic length given in or inferred from the scientific study. Figure 1.2 distinguishes between four types of systems:

- Mass-mass balancing (figure 1.3a) uses counterweight balancing to cancel gravitational effects on a primary mass [12–14].
- Mass-spring balancing (figure 1.3b) also compensates gravitational effects but it does so with an elastic device [6, 15–32]. Elastic devices of this sort are almost exclusively comprised out of coiled extension or compression springs and use rigid body mechanisms to create the desired non-linear compensatory stiffness profiles.
- Spring-spring balancing (figure 1.3c) uses an elastic structure to cancel the elastic effect of another elastic structure [33–52].
- Constant force [53–58] and constant torque [59–61] mechanisms are not statically balanced, but they can be directly used to create static balance.

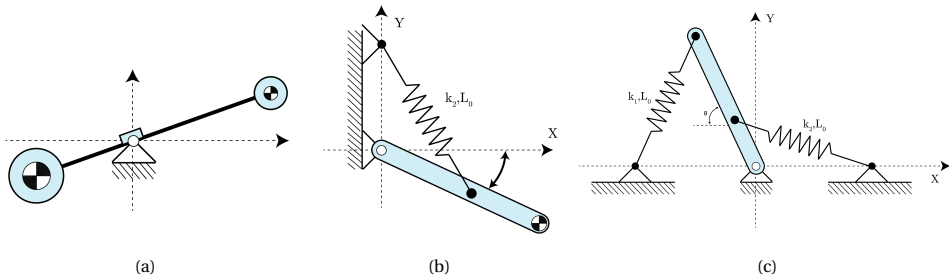


Figure 1.3: Schematic representations of three types of static balancing. (a) Mass-mass balancing, (b) mass-spring balancing and (c) spring-spring balancing [6].

Figure 1.2 reveals that each of the four device categories dominate a particular length scale. Unsurprisingly, mass-mass balancing is mainly used for extremely large systems ($> 1 \times 10^2$ m) predominantly in civil engineering structures such as movable bridges [13] and ship lifts [14], because it is the only reasonable approach. However, the added mass is often undesirable due to increased inertial forces during dynamical operation of industrial robotic systems, for example. Therefore, systems around the meter scale (~ 1 m), often robotic systems, resort to elastic systems to counteract gravity in order to reduce required motor torque.

The largest body of literature reports statically balanced mechanisms at the decimeter scale ($\sim 1 \times 10^{-1}$ m). At this scale compliant mechanisms come into play, because reasonable deflections can be obtained within material limits. In addition, manufacturing of complex geometries is relatively straightforward with conventional machine shop equipment and characterization of device properties is relatively straightforward with standard and low-cost laboratory equipment.

However, as we go into smaller scales in the centimeter ($\sim 1 \times 10^{-2}$ m), millimeter ($\sim 1 \times 10^{-3}$ m) and even sub-millimeter ($< 1 \times 10^{-3}$ m) range, less research is published.

Since compliant mechanisms are well suited for miniaturization, and a lot of micro-electromechanical systems (MEMS) research has been published [62–64], this raises the question why these devices are not more abundant. One reasonable explanation is that preloading is very difficult at a small scale.

1.3. STATICALLY BALANCED COMPLIANT MECHANISMS

Spring-spring balancing as it is shown in figure 1.3c is arguably pointless, because the system would behave the same way without springs. However, this type of balancing is important if there is parasitic stiffness; an undesirable elastic effect as a secondary property of the system. This happens almost exclusively in the domain of compliant mechanisms, where force and deflection are by their nature interrelated.

Compliant mechanisms achieve their mobility through elastic deformation of slender segments, such as plate and wire flexures. They enable engineers to design mechanisms without overlapping components that move relative to one another. This has many benefits such as the elimination of sliding friction resulting in less wear, noise and vibration which eliminates the need for lubrication, regular maintenance and enables applications in clean environments due to much reduced particle generation. Reduced relative motion between components means less backlash in kinematic pairs, which makes them perfect for high precision mechanical applications without the need for extreme control of tolerances [65]. Simultaneously, the number of individual components can be reduced up to a fully monolithic architecture, relaxing or even eliminating assembly. This may lower weight, increase compactness and opens up the opportunity for a two-dimensional embodiment. Monolithicity ensures good scalability and planarity makes them compatible with well established surface-micro-machining from semiconductor manufacturing such as photolithography.

However, in any unbalanced compliant mechanism, part of the input energy is stored as strain energy and is not available to the output [66]. The resulting restoring forces cause disturbances on force feedback in haptic interfaces [5] and compliant surgical tools [10]. Elastic effects may require high actuation forces [51] and hence challenge energy efficiency [4, 48, 67] in for example fully compliant micro transmission mechanisms [68, 69]. In addition this may limit the range of motion [70], transmit unwanted vibrations [71] and cause high natural frequencies of oscillation [64].

These adverse circumstances may be mitigated by geometric means, however they can never be resolved entirely this way. After all, the stiffness of plate and wire flexures is related to their length and cross section which cannot be reduced to zero. In addition, manufacturing constraints, desired kinematics and sufficient support stiffness may further limit the minimum dimensions.

Instead, an energy buffer may be added to create negative stiffness for balancing. However, this requires preloading, which makes their design even more difficult compared unbalanced compliant mechanism. On large scales (i.e. $> 1 \times 10^{-2}$ m) preloading is oftentimes done manually [48, 72, 73] or with a preloading assembly such as a lead-screw [74] or a precision stage [46]. However on small scales (i.e. $< 1 \times 10^{-2}$ m) manual handling is difficult and easily causes damage and assembly is economically unjustifiable [75]. Monolithic statically balanced compliant mechanisms without preloading assembly have been proposed [34, 42, 49], however they still need to be moved and kept

into their low stiffness domain by some form of physical manipulation. Even though topology optimization [66, 76] and building block approaches [46] may assist solving these multi objective design problems, more research is required for systematic design paradigms for micro-scale statically balanced compliant mechanisms.

1.4. PROBLEM DEFINITION AND RESEARCH GOALS

The primary challenge in the design and fabrication of energy invariant mechanisms is to create a geometry in which positive and negative stiffness exactly counteract by inserting a precise amount of potential energy into the system. In large scale systems applying preloading is relatively straightforward and most research has focused on creating appropriate geometries. However in small scale systems it is not obvious how preloading should be applied and consequently very little small scale (or downscalable) mechanism architectures have been proposed. Therefore the goal of this research is to investigate feasible preloading methods for energy invariant mechanisms at small scales and to develop new device architectures that can be scaled down. To achieve this research goal, several subgoals are formulated, which are addressed in subsequent chapters:

- Improve understanding of the required conditions for static balance by developing a mathematically precise method for the synthesis and analysis of rigid body spring mechanisms.
- Develop single-component and planar statically balanced compliant mechanisms that can be activated after production to make them compatible with conventional methods for micro-fabrication.
- Develop various essential building block components with linear and rotational kinematics for down-scalable statically balanced compliant mechanisms.
- Make preloading part of the manufacturing process by exploiting residual stress from thin film deposition.

The present work covers the system types from figure 1.2, except mass-mass balancing. The characteristic device length will reduce as we address each subgoal in subsequent chapters, as will become clear in the next section.

1.5. THESIS OUTLINE

In chapter 2 the balancing conditions for spring mechanisms with rigid links are investigated. Improving the understanding of static balance in linkages is useful with respect to our main research goal, because rigid body mechanisms are often used as a precursor in the design of miniaturizable compliant mechanisms. To be precise, a mathematical method for the design synthesis and analysis of mass-spring and spring-spring balanced serial chains is developed. The method generalizes among the number of links in 2D and 3D, the number of zero free length springs and includes transmissions. It uses homogeneous transformation matrices which make it compatible with conventions for robot kinematics such as the Denavit Hartenberg parameters [77]. The method is easily solvable because it temporarily constrains the system to a single degree of freedom with a

virtual transmission, but the algebraic balancing conditions generalize to all degrees of freedom afterwards.

In chapter 3 and chapter 4, four single-component and planar spring-spring balancers are developed. Device architectures like this are compatible with conventional micro-manufacturing techniques such as lithography, which enables their downsizing. To achieve static balance the substructure responsible for storing potential energy to generate negative stiffness has to be integrated seamlessly. This is done by exploiting fully compliant mechanical switches that exhibit bistable behavior. All four mechanisms from chapter 3 and chapter 4 can reversibly change between highly stiff and compliant configurations reducing both linear and torsional stiffness up to 99.9%, simply by toggling the switch.

The difference between chapters 3 and 4 is in what building blocks are used to establish balance. In Chapter 3 novel constant force and torque mechanisms, obtained by a linear buckling analysis, are preloaded against each other to bring about very low stiffness with reduced complexity, compared to the state of the art. In chapter 4 a novel V-shaped negative stiffness building block is introduced that is able to minimize stiffness when preloaded, yet it maximizes stiffness when it is not preloaded. In combination with a simple linear and rotational stage we achieve what is essentially binary stiffness. That is, a stiffness that can be turned on and off with the potential to be made on the micro-scale, which enables advanced mechanical digital machines and mechanical computers. For example, they could be directly used as rod-logical elements [78, 79].

In chapter 5 preloading is made part of the manufacturing process by exploiting residual thin film stress. Normally, such stresses are to be avoided, since they undesirably deform the silicon substrate and potentially damage device layers or alter their behavior. However, in the present study, compressive residual stress is exploited to elongate microbeams that generate negative stiffness resulting in constant force and spring-spring balanced mechanisms. Since thermal oxidation acts globally and is a commonly used step in the fabrication of microelectromechanical systems (MEMS) it readily enables batch fabrication of balanced micro-compliant mechanisms. Since surface effects become larger at smaller scales, this approach is promising for further miniaturization.

In chapter 6 preliminary results are reported to provide more evidence for the scalability of the proposed compliant mechanisms and methods. Apart from arguing scalability, we discuss the contributions of this thesis in light of the current scientific status, further possible applications and take a careful look into the future and make our final conclusions.

REFERENCES

- [1] V. Arakelian, *Gravity compensation in robotics*, *Advanced Robotics* **30**, 79 (2016).
- [2] S. K. Banala, S. K. Agrawal, A. Fattah, K. Rudolph, and J. P. Scholz, *A gravity balancing leg orthosis for robotic rehabilitation*, in *IEEE International Conference on Robotics and Automation, 2004. Proceedings. ICRA'04. 2004*, Vol. 3 (IEEE, 2004) pp. 2474–2479.
- [3] A. Alamdari, R. Haghghi, and V. Krovi, *Gravity-balancing of elastic articulated-cable leg-orthosis emulator*, *Mechanism and Machine Theory* **131**, 351 (2019).

- [4] J. A. Gallego and J. L. Herder, *Criteria for the static balancing of compliant mechanisms*, in *ASME 2010 International Design Engineering Technical Conferences and Computers and Information in Engineering Conference* (American Society of Mechanical Engineers, 2010) pp. 465–473.
- [5] L. C. Leishman, D. J. Ricks, and M. B. Colton, *Design and evaluation of statically balanced compliant mechanisms for haptic interfaces*, in *ASME 2010 Dynamic Systems and Control Conference* (American Society of Mechanical Engineers, 2010) pp. 859–866.
- [6] J. L. Herder, *Energy-free Systems; Theory, conception and design of statically balanced spring mechanisms* (2001).
- [7] A. J. Brizard, *An Introduction to Lagrangian Mechanics* (World Scientific Publishing Company, 2008).
- [8] *Hyundai industrial robots*, <https://roboticsandautomationnews.com/wp-content/uploads/2018/02/Industrial-Robots-Hyundai-Heavy.jpg>, accessed: 2021-02-28.
- [9] J. Herder and F. Van Den Berg, *Statically balanced compliant mechanisms (sbcms), an example and prospects*, in *Proceedings of the Design Engineering Technical Conferences and Computer in Engineering Conference, DETC2000/MECH-14144* (2000).
- [10] A. Stapel and J. L. Herder, *Feasibility study of a fully compliant statically balanced laparoscopic grasper*, in *ASME 2004 International Design Engineering Technical Conferences and Computers and Information in Engineering Conference* (American Society of Mechanical Engineers, 2004) pp. 635–643.
- [11] *Zenith watches*, <https://www.zenith-watches.com/int/collection/defy>, accessed: 2021-02-18.
- [12] C. M. Gosselin and J. Wang, *Static balancing of spatial six-degree-of-freedom parallel mechanisms with revolute actuators*, *Journal of Field Robotics* **17**, 159 (2000).
- [13] G. Stepanov, *Design of movable bridges*, *Structural Engineering International* **1**, 9 (1991).
- [14] J. Akkermann, T. Runte, and D. Krebs, *Ship lift at three gorges dam, china—design of steel structures*, *Steel Construction: Design and Research* **2**, 61 (2009).
- [15] A. Dunning, N. Tolou, and J. Herder, *A compact low-stiffness six degrees of freedom compliant precision stage*, *Precision Engineering* **37**, 380 (2013).
- [16] Z.-W. Yang and C.-C. Lan, *An adjustable gravity-balancing mechanism using planar extension and compression springs*, *Mechanism and Machine Theory* **92**, 314 (2015).
- [17] B. M. Wisse, W. D. Van Dorsser, R. Barents, and J. L. Herder, *Energy-free adjustment of gravity equilibrators using the virtual spring concept*, in *2007 IEEE 10th International Conference on Rehabilitation Robotics* (IEEE, 2007) pp. 742–750.

- [18] C. Cho, W. Lee, and S. Kang, *Static balancing of a manipulator with hemispherical work space*, in *2010 IEEE/ASME International Conference on Advanced Intelligent Mechatronics* (IEEE, 2010) pp. 1269–1274.
- [19] P.-Y. Lin, W.-B. Shieh, and D.-Z. Chen, *A theoretical study of weight-balanced mechanisms for design of spring assistive mobile arm support (mas)*, *Mechanism and Machine Theory* **61**, 156 (2013).
- [20] M. French and M. Widden, *The spring-and-lever balancing mechanism, george cardwaine and the anglepoise lamp*, *Proceedings of the Institution of Mechanical Engineers, Part C: Journal of Mechanical Engineering Science* **214**, 501 (2000).
- [21] R. Rizk, S. Krut, and E. Dombre, *Design of a 3d gravity balanced orthosis for upper limb*, in *2008 IEEE International Conference on Robotics and Automation* (IEEE, 2008) pp. 2447–2452.
- [22] B. G. Bijlsma, G. Radaelli, and J. L. Herder, *Design of a compact gravity equilibrator with an unlimited range of motion*, *Journal of Mechanisms and Robotics* **9**, 061003 (2017).
- [23] J. L. Herder, *Development of a statically balanced arm support: Armon*, in *9th International Conference on Rehabilitation Robotics, 2005. ICORR 2005*. (IEEE, 2005) pp. 281–286.
- [24] J. L. Herder and G. J. Tuijthof, *Two spatial gravity equilibrators*, in *Proc. of ASME 2000 Design Engineering Technical Conferences and Computers and Information in Engineering Conference* (2000) pp. 1–9.
- [25] S. K. Agrawal and A. Fattah, *Gravity-balancing of spatial robotic manipulators*, *Mechanism and machine theory* **39**, 1331 (2004).
- [26] G. Endo, H. Yamada, A. Yajima, M. Ogata, and S. Hirose, *A weight compensation mechanism with a non-circular pulley and a spring: Application to a parallel four-bar linkage arm*, *SICE Journal of Control, Measurement, and System Integration* **3**, 130 (2010).
- [27] S. K. Banala, S. K. Agrawal, A. Fattah, V. Krishnamoorthy, W.-L. Hsu, J. Scholz, and K. Rudolph, *Gravity-balancing leg orthosis and its performance evaluation*, *IEEE Transactions on robotics* **22**, 1228 (2006).
- [28] P.-Y. Lin, W.-B. Shieh, and D.-Z. Chen, *Design of statically balanced planar articulated manipulators with spring suspension*, *IEEE Transactions on Robotics* **28**, 12 (2011).
- [29] P.-Y. Lin, W.-B. Shieh, and D.-Z. Chen, *Design of a gravity-balanced general spatial serial-type manipulator*, *Journal of Mechanisms and Robotics* **2**, 031003 (2010).
- [30] A. Gopalswamy, P. Gupta, and M. Vidyasagar, *A new parallelogram linkage configuration for gravity compensation using torsional springs*, in *Proceedings 1992 IEEE International Conference on Robotics and Automation* (IEEE, 1992) pp. 664–669.

- [31] A. Alamdari and V. N. Krovi, *Static balancing of highly reconfigurable articulated wheeled vehicles for power consumption reduction of actuators*, *International Journal of Mechanisms and Robotic Systems* **3**, 15 (2016).
- [32] T. Laliberté, C. M. Gosselin, and M. Jean, *Static balancing of 3-dof planar parallel mechanisms*, *IEEE/ASME transactions on mechatronics* **4**, 363 (1999).
- [33] B. D. Jensen and C. H. Jenkins, *Design of small-scale statically balanced compliant joints*, in *ASME 2011 IDETC and CIE* (American Society of Mechanical Engineers, 2011) pp. 85–92.
- [34] N. Tolou, P. Estevez, and J. L. Herder, *Collinear-type statically balanced compliant micro mechanism (sb-cmm): experimental comparison between pre-curved and straight beams*, in *ASME 2011 IDETC and CIE* (American Society of Mechanical Engineers, 2011) pp. 113–117.
- [35] M. Plooij, T. Van Der Hoeven, G. Dunning, and M. Wisse, *Statically balanced brakes*, *Precision Engineering* **43**, 468 (2016).
- [36] A. Bruyas, F. Geiskopf, and P. Renaud, *Towards statically balanced compliant joints using multimaterial 3d printing*, in *International Design Engineering Technical Conferences and Computers and Information in Engineering Conference*, Vol. 46360 (American Society of Mechanical Engineers, 2014) p. V05AT08A033.
- [37] A. Lamers, J. A. G. Sánchez, and J. L. Herder, *Design of a statically balanced fully compliant grasper*, *Mechanism and machine theory* **92**, 230 (2015).
- [38] D. Sarojini, T. Lassche, J. Herder, and G. Ananthasuresh, *Statically balanced compliant two-port bistable mechanism*, *Mechanism and Machine Theory* **102**, 1 (2016).
- [39] D. F. Machekposhti, N. Tolou, and J. Herder, *A statically balanced fully compliant power transmission mechanism between parallel rotational axes*, *Mechanism and Machine Theory* **119**, 51 (2018).
- [40] J. Zhang, A. D. Shaw, M. Amoozgar, M. I. Friswell, and B. K. Woods, *Bidirectional torsional negative stiffness mechanism for energy balancing systems*, *Mechanism and Machine Theory* **131**, 261 (2019).
- [41] J. Lassooij, N. Tolou, G. Tortora, S. Caccavaro, A. Menciassi, and J. Herder, *A statically balanced and bi-stable compliant end effector combined with a laparoscopic 2dof robotic arm*, *Mechanical Sciences*, 3 (2), 2012 (2012).
- [42] G. Chen and S. Zhang, *Fully-compliant statically-balanced mechanisms without prestressing assembly: concepts and case studies*, *Mech. Sci* **2**, 169 (2011).
- [43] E. G. Merriam, M. Colton, S. Magleby, and L. L. Howell, *The design of a fully compliant statically balanced mechanism*, in *ASME 2013 International Design Engineering Technical Conferences and Computers and Information in Engineering Conference* (American Society of Mechanical Engineers, 2013) pp. V06AT07A035–V06AT07A035.

- [44] M. Barel, D. F. Machekposhti, J. Herder, N. Tolou, and M. Sitti, *Permanent preloading by acceleration for statically balancing mems devices*, in *2018 International Conference on Reconfigurable Mechanisms and Robots (ReMAR)* (IEEE, 2018) pp. 1–11.
- [45] L. Berntsen, D. H. Gosenshuis, and J. L. Herder, *Design of a compliant monolithic internally statically balanced four-bar mechanism*, in *ASME 2014 International Design Engineering Technical Conferences and Computers and Information in Engineering Conference* (American Society of Mechanical Engineers, 2014) pp. V05AT08A040–V05AT08A040.
- [46] K. Hoetmer, J. L. Herder, and C. J. Kim, *A building block approach for the design of statically balanced compliant mechanisms*, in *ASME 2009 IDETC and CIE* (American Society of Mechanical Engineers, 2009) pp. 313–323.
- [47] G. Radaelli, J. A. Gallego, and J. L. Herder, *An energy approach to static balancing of systems with torsion stiffness*, *Journal of Mechanical Design* **133**, 091006 (2011).
- [48] F. M. Morsch and J. L. Herder, *Design of a generic zero stiffness compliant joint*, in *ASME 2010 International Design Engineering Technical Conferences and Computers and Information in Engineering Conference* (American Society of Mechanical Engineers, 2010) pp. 427–435.
- [49] P. J. Pluimers, N. Tolou, B. D. Jensen, L. L. Howell, and J. L. Herder, *A compliant on/off connection mechanism for preloading statically balanced compliant mechanisms*, in *ASME 2012 IDETC and CIE* (American Society of Mechanical Engineers, 2012) pp. 373–377.
- [50] M. Schenk, J. L. Herder, and S. D. Guest, *Design of a statically balanced tensegrity mechanism*, in *International Design Engineering Technical Conferences and Computers and Information in Engineering Conference*, Vol. 42568 (2006) pp. 501–511.
- [51] S. R. Deepak, A. N. Hansoge, and G. Ananthasuresh, *Application of rigid-body-linkage static balancing techniques to reduce actuation effort in compliant mechanisms*, *Journal of Mechanisms and Robotics* **8**, 021005 (2016).
- [52] P. Pluimers, *Design for specified stiffness in precision engineering*, (2012).
- [53] S. A. Zirbel, Q. T. Aten, M. Easter, B. D. Jensen, and L. L. Howell, *Compliant constant-force micro-mechanism for enabling dual-stage motion*, in *International Design Engineering Technical Conferences and Computers and Information in Engineering Conference*, Vol. 45035 (American Society of Mechanical Engineers, 2012) pp. 191–198.
- [54] N. Tolou, P. Pluimers, B. D. Jensen, S. Magleby, L. Howell, and J. L. Herder, *Constant force micro mechanism out of carbon nanotube forest*, in *Proceedings of the 12th uspen International Conference Stockholm–Jun* (2011).
- [55] Y.-H. Chen and C.-C. Lan, *An adjustable constant-force mechanism for adaptive end-effector operations*, *Journal of Mechanical Design* **134**, 031005 (2012).

- [56] Q. Xu, *Design of a large-stroke bistable mechanism for the application in constant-force micropositioning stage*, Journal of Mechanisms and Robotics **9**, 011006 (2017).
- [57] J.-Y. Wang and C.-C. Lan, *A constant-force compliant gripper for handling objects of various sizes*, Journal of Mechanical Design **136**, 071008 (2014).
- [58] H. Pham and D. Wang, *A constant-force bistable mechanism for force regulation and overload protection*, Mechanism and Machine Theory (2011).
- [59] H. Nair Prakashah and H. Zhou, *Synthesis of constant torque compliant mechanisms*, Journal of Mechanisms and Robotics **8** (2016).
- [60] C.-W. Hou and C.-C. Lan, *Functional joint mechanisms with constant-torque outputs*, Mechanism and Machine Theory **62**, 166 (2013).
- [61] P. Bilancia, S. P. Smith, G. Berselli, S. P. Magleby, and L. L. Howell, *Zero torque compliant mechanisms employing pre-buckled beams*, Journal of Mechanical Design **142** (2020).
- [62] M. I. Younis, *MEMS linear and nonlinear statics and dynamics*, Vol. 20 (Springer Science & Business Media, 2011).
- [63] S. Iqbal and A. Malik, *A review on mems based micro displacement amplification mechanisms*, Sensors and Actuators A: Physical **300**, 111666 (2019).
- [64] M. de Laat, H. P. Garza, J. Herder, and M. Ghatkesar, *A review on in situ stiffness adjustment methods in mems*, Journal of Micromechanics and Microengineering **26**, 063001 (2016).
- [65] H. Soemers, *Design Principles for precision mechanisms* (T-Pointprint, 2011).
- [66] J. Gallego Sánchez, *Statically Balanced Compliant Mechanisms: Theory and Synthesis*, Ph.D. thesis, TU Delft, Delft University of Technology (2013).
- [67] A. Dunning, N. Tolou, and J. Herder, *Inventory of platforms towards the design of a statically balanced six degrees of freedom compliant precision stage*, Mechanical Sciences, 2, 2011 (2011).
- [68] D. Farhadi Machekposhti, J. L. Herder, and N. Tolou, *Frequency doubling in elastic mechanisms using buckling of microflexures*, Applied Physics Letters **115**, 143503 (2019).
- [69] D. F. Machekposhti, J. L. Herder, G. Sémon, and N. Tolou, *A compliant micro frequency quadrupler transmission utilizing singularity*, Journal of Microelectromechanical Systems **27**, 506 (2018).
- [70] N. Tolou, V. A. Henneken, and J. L. Herder, *Statically balanced compliant micro mechanisms (sb-mems): Concepts and simulation*, in *ASME 2010 International Design Engineering Technical Conferences and Computers and Information in Engineering Conference* (American Society of Mechanical Engineers, 2010) pp. 447–454.

- [71] T. D. Le and K. K. Ahn, *A vibration isolation system in low frequency excitation region using negative stiffness structure for vehicle seat*, *Journal of Sound and Vibration* **330**, 6311 (2011).
- [72] F. L. te Riele and J. L. Herder, *Perfect static balance with normal springs*, in *Proceedings of the 2001 ASME Design Engineering Technical Conferences, Pittsburg, PA, Sept (2001)* pp. 9–12.
- [73] I. Ebert-Uphoff and K. Johnson, *Practical considerations for the static balancing of mechanisms of parallel architecture*, *Proceedings of the Institution of Mechanical Engineers, Part K: Journal of Multi-body Dynamics* **216**, 73 (2002).
- [74] M. Zanaty and S. Henein, *Programmable constant-force multistable mechanisms*, in *International Design Engineering Technical Conferences and Computers and Information in Engineering Conference*, Vol. 51807 (American Society of Mechanical Engineers, 2018) p. V05AT07A002.
- [75] G. Ananthasuresh and L. L. Howell, *Mechanical design of compliant microsystems—a perspective and prospects*, *Journal of Mechanical Design* **127**, 736 (2005).
- [76] D. J. de Lange, M. Langelaar, and J. L. Herder, *Towards the design of a statically balanced compliant laparoscopic grasper using topology optimization*, in *ASME 2008 IDETC and CIE* (American Society of Mechanical Engineers, 2008) pp. 293–305.
- [77] J. Denavit, *A kinematic notation for lower-pair mechanisms based on matrices*. *Trans. of the ASME. Journal of Applied Mechanics* **22**, 215 (1955).
- [78] K. E. Drexler, *Rod logic and thermal noise in the mechanical nanocomputer*, in *Proc. Third Int. Symp. on Molecular Electronic Devices* (1988).
- [79] R. C. Merkle, *Two types of mechanical reversible logic*, *Nanotechnology* **4**, 114 (1993).

2

STATIC BALANCING OF SERIAL CHAINS WITH VIRTUAL TRANSMISSIONS

Static balancing can eliminate conservative forces caused by elasticity and gravity for example. In statically balanced systems, loads on for example compliant mechanisms, robot arms or human limbs are eliminated in every configuration by adding counteracting conservative forces. A myriad of examples of these systems exists, but general methods for their design synthesis are rare. In this paper we present a general and easy-to-solve method for statically balancing planar and spatial linkages with zero-free-length springs. We introduce virtual transmissions to temporarily constrain a linkage to a single degree of freedom and set the variation of the potential energy to zero to obtain balance for all degrees of freedom. In addition this enables the design of statically balanced systems with actual transmissions, such as gears, pulley systems and chain drives. Homogeneous transformation matrices make it compatible with the Denavit-Hartenberg parameters and allow easy extension to tree-structured linkages. Even though one may expect complicated systems to be increasingly difficult to solve, we show that algebraic conditions for large systems are as easily solved as a system with only a single link. Various examples are included to show efficacy.

This chapter will be submitted as a scientific article entitled *Static balancing of planar and spatial serial chains with virtual transmissions* to the journal of *Mechanisms and Machine theory* by P.R. Kuppens, M.A. Bessa and J.L. Herder

2.1. INTRODUCTION

Conservative forces caused by gravity and elasticity can negatively affect system performance. Elastic forces may challenge energy efficiency in compliant mechanisms [1], especially in transmission mechanisms as part of the input energy is stored [2, 3]. Gravitational forces may cause poor efficiency in robotics [4], cause significant physical strain on factory workers [5] and hamper the daily routines of people with reduced muscular force [6, 7]. Therefore these forces often need to be eliminated by static balancing.

A statically balanced system has invariant potential energy of the entire range of motion, implying static equilibrium in any position instead of one or few positions, so that it remains in any position without effort [8]. Gravity balancing oftentimes is done by counterweight balancing. However adding counterweight significantly increases system inertia, which is typically undesirable [4]. Instead, springs can be used to create a sustained equilibrium.

Many examples of statically balanced mechanisms exist in literature. For example the basic spring-force balancer, the double slider mechanism and their derivatives [8], four bar mechanisms [8, 9], pantograph linkages [10], tree-structured mechanisms [11], planar serial chains [12], gravity equilibrators [13] and numerous spatial mechanisms [14–16]. In many cases new mechanisms are found by adding auxiliary parallel links to essentially repeat the same balancing unit [8, 13, 17, 18] or clever kinematic transformations are used to maintain moment balance [8].

Although the conditions for static balance are well understood [1], general methods for their synthesis are scarce. Perfect balancing of kinematic chains with revolute joints of arbitrary length, open or closed loop, was first shown possible by adding auxiliary links by [13]. It was later extended by [17] to include all kinematic pairs. However, auxiliary links may limit the range of motion by link interference, need to consider tolerances, provide additional inertia to the system and may challenge robustness due to the increased number of components [12].

A method for statically balancing serial and tree-structured kinematic chains without auxiliary links was first proposed by [19] and later extended in [11]. It is based on the decomposition of springs and involves a recursive algorithm that places zero-free-length springs between links and the ground. Their method also applies to spatial mechanisms, while parallel mechanisms can be balanced by breaking the problem into sub-problems.

A method that more generally considers spring topology and does not require a recursive algorithm is presented in [12, 20] and extended to 3D in [21, 22]. They define a configuration-free stiffness block matrix to describe the potential energy over the entire motion domain. They show that potential energy is constant if the stiffness block matrix is diagonal. Conditions for a particular linkage are obtained by setting all its off-diagonal elements simultaneously to zero, which typically requires a computer algebra system.

In this paper we present a more general and easy to solve method for the design of statically balanced serial kinematic chains in 2D and 3D with zero-free-length springs that provides more physical understanding. The mathematical framework allows for a variable number of links and springs and makes no assumptions about the spring topology. It works by introducing a temporary and virtual transmission (the variables ρ_i) between all links and expressing the total potential energy U of the system over the entire configuration space in a single parameter α . The variation of the energy U is now a sin-

gle derivative and by equating it to zero the algebraic conditions for perfectly balanced mechanisms are derived. Since it is set to zero for all possible virtual transmissions (i.e. all values of ρ_i and α) the derived conditions generalize to all degrees of freedom.

Balancing conditions are also obtained for mechanisms with actual transmissions and we show that, for any linkage, there exists a topology of zero-free-length springs that results in an independent set of conditions that can be solved one by one. Zero-free-length springs enable us to derive conditions algebraically, because their potential energy is proportional to their length squared, this contrasts with normal springs. Although zero-free-length springs are not readily available, they are easily constructed from normal springs [8, 19, 23].

In addition, the method is directly compatible with the widely used Denavit-Hartenberg convention [24] and can be easily expanded to tree-structured mechanisms [11], because we use homogeneous transformation matrices.

We explain the method in section 2.2, for 2D in section 2.2.1 and 3D in section 2.2.2. It is followed by four planar examples in section 2.3. We start with the simplest of examples, a single link system in section 2.3.1, followed by a two link system in section 2.3.2. We then give an example of a two link system with an actual transmission in section 2.3.3, followed by a three link system in section 2.3.4. One spatial example is given in section 2.4. In section 2.5 we give a proof that an independent set of coefficients can be obtained for any linkage, followed by a discussion in section 2.6 and a conclusion in section 2.7. Various examples in 2D and 3D demonstrate the versatility of our method.

2.2. METHOD

The method statically balances a system by setting the variation of its total potential energy U to zero for all configurations. The energy U is the sum of the elastic potential energy U_e of the zero-free-length springs and gravitational potential energy U_g of the bodies. It is by definition a multivariate function for multiple degrees of freedom (DOFs). Consequently the variation of U is a set of partial derivatives that are required to be simultaneously zero for static balance, which is less easily solved than a single equation.

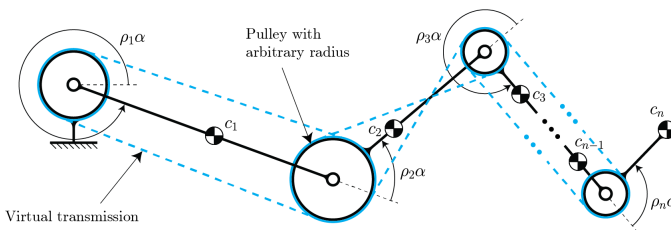


Figure 2.1: Virtual transmission conceptual drawing. The dashed lines represent a temporary and virtual transmission system. Although the pulley radii are fixed in this schematic they have an arbitrary radius, because the method computes solutions for all transmission ratios simultaneously.

This set of partial derivatives can be reduced to a single derivative by virtually and temporarily constraining the system to a single DOF with a virtual transmission, see figure 2.1. With a virtual transmission we temporarily impose constraints on the system by writing all generalized coordinates as a multiple ρ_i of a single generalized coordinate

α . As such the derivative of $U(\alpha)$ is a single equation in which energy variations of individual components are represented by sinusoidal functions of α and the transmission ratios ρ_i . Algebraic balancing conditions are obtained by setting the coefficients to these sinusoidal functions zero.

The transmission is virtual, because no actual transmission ratios have to be assumed in order to constrain the system. The ratios ρ_i can have any value, because they do not occur in the coefficients of the sinusoidal functions that we need to solve. This means that all pulleys shown in figure 2.1 have an arbitrary radius and that solutions are valid for all independent DOFs. As such, the obtained algebraic conditions for static balance generalize to the original unconstrained configuration space of the mechanisms.

Nonetheless, numerical substitution of the transmission ratios ρ_i is allowed which results in a system with an actual transmission, see section 2.3.3. The method is identical for planar and spatial linkages. However, because the method is more easily explained graphically in 2D, they will be separately discussed below.

2.2.1. METHOD IN 2D

Let us take a serial linkage with n links and attach to each link $i = 1, \dots, n$ a local coordinate frame O_i as shown in figure 2.2. A revolute joint is located at the origin of each O_i connecting link i and $i - 1$. The coordinate frame O_0 is global and represents the ground. The set of all coordinate frames is called $\mathcal{O} = \{O_0, O_1, \dots, O_n\}$.

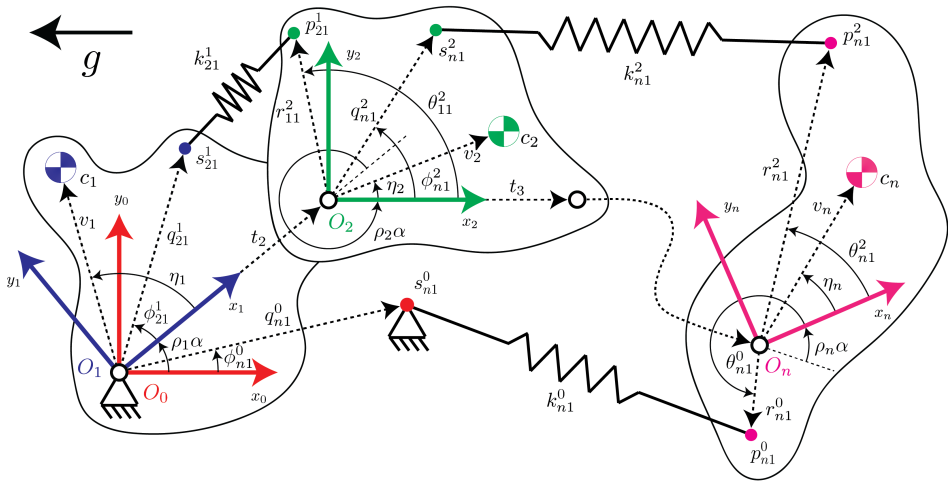


Figure 2.2: Schematic of the parametric model.

Each link i has a mass m_i and gravity works in the negative x_0 -direction. The initial center of mass location \mathbf{c}_i of each mass m_i in local coordinate frame O_i is defined in polar coordinates (v_i, η_i) by

$$\mathbf{c}_i = \begin{bmatrix} x_{ci} \\ y_{ci} \end{bmatrix} = \begin{bmatrix} v_i \cos(\eta_i) \\ v_i \sin(\eta_i) \end{bmatrix}, \quad i = 1, \dots, n. \quad (2.1)$$

A spring is attached to the linkage by choosing points for its endpoints in two distinct

coordinate frames O_i and O_j . All combinations of coordinate frames are given by $\mathcal{C} = \binom{\mathcal{O}}{2}$ which means there are $|\mathcal{C}| = \binom{n+1}{2}$ topologically distinct ways of connecting a spring. Next we define the index set $\mathcal{J} = \{(i, j) \mid \{O_i, O_j\} \in \mathcal{C} \text{ and } i < j\}$ which gives us the indices of each local frame for all distinct topological options.

For each possible spring topology $\mathcal{X} \in \mathcal{J}$ with $\mathcal{X} = (i, j)$ we define $n_{\mathcal{X}}$ springs ($n_{\mathcal{X}}$ can be 0 and distinct for each \mathcal{X}). We uniquely associate with each \mathcal{X} two matrices $S_{\mathcal{X}} = [\mathbf{s}_{\mathcal{X}1}, \dots, \mathbf{s}_{\mathcal{X}n_{\mathcal{X}}}]$ and $P_{\mathcal{X}} = [\mathbf{p}_{\mathcal{X}1}, \dots, \mathbf{p}_{\mathcal{X}n_{\mathcal{X}}}]$. The points $\mathbf{s}_{\mathcal{X}i}$ and $\mathbf{p}_{\mathcal{X}i}$ represent the origin and insertion of spring $\mathcal{X}i$ and for topology $\mathcal{X} = (i, j)$ the points in $S_{\mathcal{X}}$ are always associated with O_i and the points in $P_{\mathcal{X}}$ with O_j . In other words, $\mathbf{s}_{\mathcal{X}i}$ is always used in the local frame that is closest to O_0 . They are given by:

$$\begin{aligned} \mathbf{s}_{\mathcal{X}i} &= \begin{bmatrix} x_{s_{\mathcal{X}i}} \\ y_{s_{\mathcal{X}i}} \end{bmatrix} = \begin{bmatrix} q_{\mathcal{X}i} \cos(\phi_{\mathcal{X}i}) \\ q_{\mathcal{X}i} \sin(\phi_{\mathcal{X}i}) \end{bmatrix} \\ \mathbf{p}_{\mathcal{X}i} &= \begin{bmatrix} x_{p_{\mathcal{X}i}} \\ y_{p_{\mathcal{X}i}} \end{bmatrix} = \begin{bmatrix} r_{\mathcal{X}i} \cos(\theta_{\mathcal{X}i}) \\ r_{\mathcal{X}i} \sin(\theta_{\mathcal{X}i}) \end{bmatrix}, \quad \forall \mathcal{X} \in \mathcal{J}, \quad i = 1, \dots, n_{\mathcal{X}} \end{aligned} \quad (2.2)$$

where $(q_{\mathcal{X}i}, \phi_{\mathcal{X}i})$ and $(r_{\mathcal{X}i}, \theta_{\mathcal{X}i})$ are polar coordinates for each spring $\mathcal{X}i$ with topology $\mathcal{X} \in \mathcal{J}$ and spring number $i = 1, \dots, n_{\mathcal{X}}$. Please note that in the examples given in the following chapters, the topology $\mathcal{X} = (i, j)$ that belongs to a certain parameter can be expanded in the following way $n_{\mathcal{X}} = n_j^i$, $P_{\mathcal{X}} = P_j^i$, $S_{\mathcal{X}} = S_j^i$ and so on.

Virtual transmissions are now introduced as follows. Each frame O_i with $i \geq 1$ is rotated and translated in the preceding frame O_{i-1} with an angle $\rho_i \alpha$ and translation $[t_{xi}, t_{yi}] = [t_i, 0]$, where the variables ρ_i define a virtual transmission and can be regarded as an arbitrary scalar or function of α . The origins of O_0 and O_1 are coincident, such that $t_1 = 0$.

The relative motion of local coordinate frames is computed with n homogeneous matrices of the form

$$H_i^{i-1}(\alpha) = \begin{bmatrix} \cos(\rho_i \alpha) & -\sin(\rho_i \alpha) & t_i \\ \sin(\rho_i \alpha) & \cos(\rho_i \alpha) & 0 \\ 0 & 0 & 1 \end{bmatrix}, \quad i = 1, 2, \dots, n. \quad (2.3)$$

The length of a spring $\mathcal{X}i$ as a function of α is defined by $\|\mathbf{d}_{\mathcal{X}i}(\alpha)\|_2$ where $\mathbf{d}_{\mathcal{X}i}(\alpha)$ is a vector in the matrix $D_{\mathcal{X}} = [\mathbf{d}_{\mathcal{X}1}, \dots, \mathbf{d}_{\mathcal{X}n_{\mathcal{X}}}]$, which is given by

$$\begin{bmatrix} D_{\mathcal{X}}(\alpha) \\ \mathbf{1} \end{bmatrix} = \left(\prod_{k=1}^{j \in \mathcal{X}} H_k^{k-1}(\alpha) \right) \begin{bmatrix} P_{\mathcal{X}} \\ \mathbf{1} \end{bmatrix} - \left(\prod_{k=1}^{i \in \mathcal{X}} H_k^{k-1}(\alpha) \right) \begin{bmatrix} S_{\mathcal{X}} \\ \mathbf{1} \end{bmatrix} \quad (2.4)$$

The location of each center of mass as a function of α , $\mathbf{c}_i^*(\alpha)$, with $i = 1, \dots, n$ is given by

$$\begin{bmatrix} \mathbf{c}_i^*(\alpha) \\ 1 \end{bmatrix} = \begin{bmatrix} x_{ci}^*(\alpha) \\ y_{ci}^*(\alpha) \\ 1 \end{bmatrix} = \prod_{k=1}^i H_k^{k-1}(\alpha) \begin{bmatrix} \mathbf{c}_i \\ 1 \end{bmatrix} \quad (2.5)$$

The potential energy in the system is given by the sum of the elastic potential energy $U_e(\alpha)$ and gravitational potential energy $U_g(\alpha)$:

$$U(\alpha) = U_e(\alpha) + U_g(\alpha) \quad (2.6)$$

where, assuming zero-free-length springs

$$U_e(\alpha) = \sum_{\mathcal{X} \in \mathcal{J}} U_{\mathcal{X}}(\alpha) = \sum_{\mathcal{X} \in \mathcal{J}} \sum_{i=1}^{n_{\mathcal{X}}} \frac{1}{2} k_{\mathcal{X}i} \|\mathbf{d}_{\mathcal{X}i}(\alpha)\|_2^2 \quad (2.7)$$

and

$$U_g(\alpha) = \sum_{i=1}^n U_{g_i}(\alpha) = \sum_{i=1}^n g m_i x_{ci}^*(\alpha) + U_c \quad (2.8)$$

with $k_{\mathcal{X}i}$ the stiffness of spring $\mathcal{X}i$, g the gravitational constant and U_c a constant energy offset in the gravitational potential field. We have chosen gravity to act in the negative x_0 -direction, without loss of generality.

Static balance requires the potential energy to be constant over the whole motion domain, i.e. $U(\alpha) = C, \forall \alpha$. Equivalently the derivative of $U(\alpha)$ is zero over the whole domain, i.e.:

$$\frac{dU(\alpha)}{d\alpha} = 0, \quad \forall \alpha \quad (2.9)$$

Finding values for all variables that satisfy equation (2.9) will result in a perfectly statically balanced system. This involves the variables m_i, v_i, η_i, ρ_i and t_i with $i = 1, \dots, n$ and for $k_{\mathcal{X}i}, r_{\mathcal{X}i}, q_{\mathcal{X}i}, \theta_{\mathcal{X}i}, \phi_{\mathcal{X}i}$ with $i = 1, \dots, n_{\mathcal{X}}$ for each $\mathcal{X} \in \mathcal{Q} \subseteq \mathcal{J}$ where \mathcal{Q} is a nonempty subset of \mathcal{J} .

2.2.2. METHOD IN 3D

The method for 3D is identical to 2D, however revolute joints can be oriented along arbitrary axes and spherical coordinates are used instead of polar coordinates to define mass and spring locations. The center of mass location \mathbf{c}_i of each mass m_i in its respective coordinate frame O_i is given by

$$\mathbf{c}_i = \begin{bmatrix} x_{ci} \\ y_{ci} \\ z_{ci} \end{bmatrix} = \begin{bmatrix} v_i \sin(\xi_i) \cos(\psi_i) \\ v_i \sin(\xi_i) \sin(\psi_i) \\ v_i \cos(\xi_i) \end{bmatrix}, \quad i = 1, \dots, n. \quad (2.10)$$

For each topology \mathcal{X} the $n_{\mathcal{X}}$ spring endpoint locations $\mathbf{s}_{\mathcal{X}i}$ and $\mathbf{p}_{\mathcal{X}i}$ are given by:

$$\mathbf{s}_{\mathcal{X}i} = \begin{bmatrix} x_{s_{\mathcal{X}i}} \\ y_{s_{\mathcal{X}i}} \\ z_{s_{\mathcal{X}i}} \end{bmatrix} = \begin{bmatrix} q_i \sin(\gamma_i) \cos(\phi_i) \\ q_i \sin(\gamma_i) \sin(\phi_i) \\ q_i \cos(\gamma_i) \end{bmatrix} \quad (2.11)$$

$$\mathbf{p}_{\mathcal{X}i} = \begin{bmatrix} x_{p_{\mathcal{X}i}} \\ y_{p_{\mathcal{X}i}} \\ z_{p_{\mathcal{X}i}} \end{bmatrix} = \begin{bmatrix} r_i \sin(\zeta_i) \cos(\theta_i) \\ r_i \sin(\zeta_i) \sin(\theta_i) \\ r_i \cos(\zeta_i) \end{bmatrix}, \quad \forall \mathcal{X} \in \mathcal{J}, \quad i = 1, \dots, n_{\mathcal{X}}.$$

The length $\mathbf{d}_{\mathcal{X}i}(\alpha)$ of each spring $\mathcal{X}i$ from the matrix $D\mathcal{X} = [\mathbf{d}_{\mathcal{X}1}, \dots, \mathbf{d}_{\mathcal{X}n_{\mathcal{X}}}]$ is given by equation (2.4) where H_i^{i-1} is a homogeneous transformation matrix of the form:

$$H_i^{i-1}(\alpha) = \begin{bmatrix} R(\rho_i\alpha) & T_i \\ \mathbf{0} & 1 \end{bmatrix} \quad (2.12)$$

where $T_i = [t_i, 0, 0]^T$ is a translation vector, $T_1 = \mathbf{0}$ and $R(\rho_i\alpha)$ is a three dimensional rotation matrix, which could be of the form:

$$\begin{aligned} R_x &= \begin{bmatrix} 1 & 0 & 0 \\ 0 & \cos \rho_i\alpha & \sin \rho_i\alpha \\ 0 & -\sin \rho_i\alpha & \cos \rho_i\alpha \end{bmatrix}, & R_y &= \begin{bmatrix} \cos \rho_i\alpha & 0 & -\sin \rho_i\alpha \\ 0 & 1 & 0 \\ \sin \rho_i\alpha & 0 & \cos \rho_i\alpha \end{bmatrix}, \\ R_z &= \begin{bmatrix} \cos \rho_i\alpha & \sin \rho_i\alpha & 0 \\ -\sin \rho_i\alpha & \cos \rho_i\alpha & 0 \\ 0 & 0 & 1 \end{bmatrix} \end{aligned} \quad (2.13)$$

The location of each center of mass as a function of α , $\mathbf{c}_i^*(\alpha)$, is given by

$$\begin{bmatrix} \mathbf{c}_i^*(\alpha) \\ 1 \end{bmatrix} = \begin{bmatrix} x_{ci}^*(\alpha) \\ y_{ci}^*(\alpha) \\ z_{ci}^*(\alpha) \\ 1 \end{bmatrix} = \prod_{k=1}^i H_k^{k-1}(\alpha) \begin{bmatrix} \mathbf{c}_i \\ 1 \end{bmatrix} \quad (2.14)$$

Next the total potential energy in the system can be derived by equation (2.6) where U_e and U_g are given by equation (2.7) and equation (2.8). Finding values for all parameters that satisfy equation (2.9) will result in a spatial statically balanced system.

2.3. PLANAR EXAMPLES

Four planar examples with increasing complexity are worked out symbolically and solutions are numerically implemented and animated in Matlab. The examples are shown schematically in figure 2.3 and the animations and numerical implementations can be found in the supplementary material.

The first and simplest example from section 2.3.1 is a single-link with one DOF as shown in figure 2.3a. Although this system benefits least from our method, it illustrates the use of the virtual transmission ratios ρ_i in simplest form. A two-link system with two DOFs naturally follows as the second example in section 2.3.2, see figure 2.3b for a schematic. In section 2.3.3 we substitute numerical values for the transmission ratios ρ_1 and ρ_2 to end up with a two-link system with an actual transmission as shown in figure 2.3c. We show this enables previously unsuitable springs topologies to gravity balance. The final example from section 2.3.4 is a three-link system as shown in figure 2.3d.

The presented examples only use a subset of feasible spring topologies. We are not restricted to these chosen topologies and the method can be used to statically balance the same linkages in different ways.

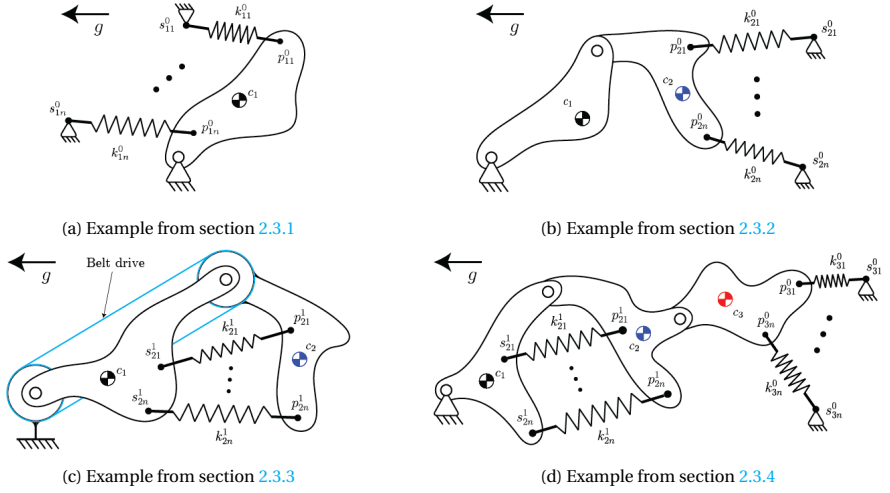


Figure 2.3: All planar examples that are worked out symbolically and implemented numerically and animated in Matlab. (a) Is a single-link system with one DOF. (b) Is a two-link system with two DOF. (c) Shows a two-link system with an actual transmission that reduces the DOFs to one. (d) Shows a three-link system. The center of mass location symbols are color associated with those in the animations.

2.3.1. STATIC BALANCING A SINGLE-LINK SYSTEM

The simplest case is a single link with one DOF as shown in figure 2.3a. Let us define two coordinate frames such that $\mathcal{O} = \{O_0, O_1\}$ and $\mathcal{J} = \{(0, 1)\}$. The matrix D_1^0 and vector $\mathbf{c}_1^*(\alpha)$ are then given by

$$\begin{bmatrix} D_1^0(\alpha) \\ \mathbf{1} \end{bmatrix} = H_1^0(\alpha) \begin{bmatrix} P_1^0 \\ \mathbf{1} \end{bmatrix} - \begin{bmatrix} S_1^0 \\ \mathbf{1} \end{bmatrix} \quad \text{and} \quad \begin{bmatrix} \mathbf{c}_1^*(\alpha) \\ 1 \end{bmatrix} = H_1^0(\alpha) \begin{bmatrix} \mathbf{c}_1 \\ 1 \end{bmatrix} \quad (2.15)$$

Please note that topology $\mathcal{X} = (i, j) = (0, 1)$ has been expanded and substituted, i.e. $D_{\mathcal{X}} = D_j^i = D_1^0$, $P_{\mathcal{X}} = P_j^i = P_1^0$ and so on. Substitution of eq. 2.15 into eq. 2.6 gives

$$U(\alpha) = U_1^0(\alpha) + U_g(\alpha) = \sum_{i=1}^{n_1^0} \frac{1}{2} k_{1i}^0 \|\mathbf{d}_{1i}^0(\alpha)\|_2^2 + g m_1 x_{c_1}^*(\alpha) \quad (2.16)$$

Working out equation (2.16), taking the derivative and setting it to zero gives

$$\frac{dU(\alpha)}{d\alpha} = \sum_{i=1}^{n_1^0} r_{1i}^0 q_{1i}^0 k_{1i}^0 \rho_1 \sin(\rho_1 \alpha + \theta_{1i}^0 - \phi_{1i}^0) - g m_1 v_1 \rho_1 \sin(\rho_1 \alpha + \eta_1) = 0 \quad (2.17)$$

Expanding the angle addition by $\sin(\alpha + \beta) = \cos(\beta) \sin(\alpha) + \sin(\beta) \cos(\alpha)$ gives

$$\begin{aligned} \frac{dU(\alpha)}{d\alpha} = & \left(\sum_{i=1}^{n_1^0} r_{1i}^0 q_{1i}^0 k_{1i}^0 \cos(\gamma_{1i}^0) \right) - g m_1 v_1 \cos(\eta_1) \Big) \rho_1 \sin(\rho_1 \alpha) \\ & + \left(\sum_{i=1}^{n_1^0} r_{1i}^0 q_{1i}^0 k_{1i}^0 \sin(\gamma_{1i}^0) \right) - g m_1 v_1 \sin(\eta_1) \Big) \rho_1 \cos(\rho_1 \alpha) = 0 \end{aligned} \quad (2.18)$$

where $\gamma_{1i}^0 = \theta_{1i}^0 - \phi_{1i}^0$. Equation (2.18) is solved for all α (and all ρ_1) if the coefficients of $\rho_1 \sin(\rho_1 \alpha)$ and $\rho_1 \cos(\rho_1 \alpha)$ are simultaneously zero:

$$\sum_{i=1}^{n_1^0} r_{1i}^0 q_{1i}^0 k_{1i}^0 \begin{bmatrix} \cos(\gamma_{1i}^0) \\ \sin(\gamma_{1i}^0) \end{bmatrix} - g m_1 v_1 \begin{bmatrix} \cos(\eta_1) \\ \sin(\eta_1) \end{bmatrix} \triangleq \sum_{i=1}^{n_1^0} \begin{bmatrix} a_{xi} \\ a_{yi} \end{bmatrix} - \begin{bmatrix} b_x \\ b_y \end{bmatrix} = \mathbf{0} \quad (2.19)$$

Since there are more than two variables in eq. 2.19 a solution can be constructed in many ways. We have chosen to construct a solution by arbitrarily defining m_1 , n_1^0 , k_{1i}^0 , r_{1i}^0 , q_{1i}^0 , θ_{1i}^0 and ϕ_{1i}^0 for $i = 1, \dots, n_1^0$ and then solve the system for v_1 and η_1 . We first calculate the values for b_x and b_y given by

$$\begin{bmatrix} b_x \\ b_y \end{bmatrix} = \sum_{i=1}^{n_1^0} \begin{bmatrix} a_{xi} \\ a_{yi} \end{bmatrix} = \sum_{i=1}^{n_1^0} r_{1i}^0 q_{1i}^0 k_{1i}^0 \begin{bmatrix} \cos(\theta_{1i}^0 - \phi_{1i}^0) \\ \sin(\theta_{1i}^0 - \phi_{1i}^0) \end{bmatrix} \quad (2.20)$$

and then solve for v_1 and η_1 by

$$v_1 = \frac{1}{g m_1} \sqrt{b_x^2 + b_y^2} \quad \text{and} \quad \eta_1 = \arctan\left(\frac{b_y}{b_x}\right) \quad (2.21)$$

Equations 2.20 and 2.21 show that an arbitrary number of randomly placed zero-free-length springs can gravity balance any mass. They also show that the basic spring force balancer, including all the modification rules (except shift) as given by [8], can be captured in a simple and compact rule. Two examples are shown in figures 2.4 and 2.5 with one and three springs respectively with $\rho_1 = 1$ and $\alpha = [0, 2\pi]$.

2.3.2. STATIC BALANCING A TWO-LINK SYSTEM

A system with two links as shown in figure 2.3b requires three coordinate frames, so $\mathcal{O} = \{O_0, O_1, O_2\}$ and $\mathcal{J} = \{(0, 1), (0, 2), (1, 2)\}$. The matrices $D_{\mathcal{X}}(\alpha)$ are given by

$$\begin{bmatrix} D_1^0(\alpha) \\ \mathbf{1} \end{bmatrix} = H_1^0(\alpha) \begin{bmatrix} P_1^0 \\ \mathbf{1} \end{bmatrix} - \begin{bmatrix} S_1^0 \\ \mathbf{1} \end{bmatrix} \quad (2.22)$$

$$\begin{bmatrix} D_2^0(\alpha) \\ \mathbf{1} \end{bmatrix} = H_1^0(\alpha) H_2^1(\alpha) \begin{bmatrix} P_2^0 \\ \mathbf{1} \end{bmatrix} - \begin{bmatrix} S_2^0 \\ \mathbf{1} \end{bmatrix} \quad (2.23)$$

$$\begin{bmatrix} D_2^1(\alpha) \\ \mathbf{1} \end{bmatrix} = H_1^0(\alpha) H_2^1(\alpha) \begin{bmatrix} P_2^1 \\ \mathbf{1} \end{bmatrix} - H_1^0(\alpha) \begin{bmatrix} S_2^1 \\ \mathbf{1} \end{bmatrix} \quad (2.24)$$

and the center of mass locations $\mathbf{c}_1^*(\alpha)$ and $\mathbf{c}_2^*(\alpha)$ are given by

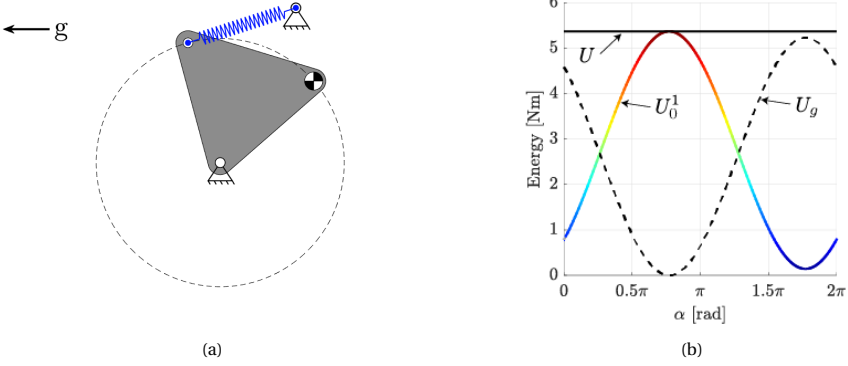


Figure 2.4: Gravity balancer with one DOF and one spring.

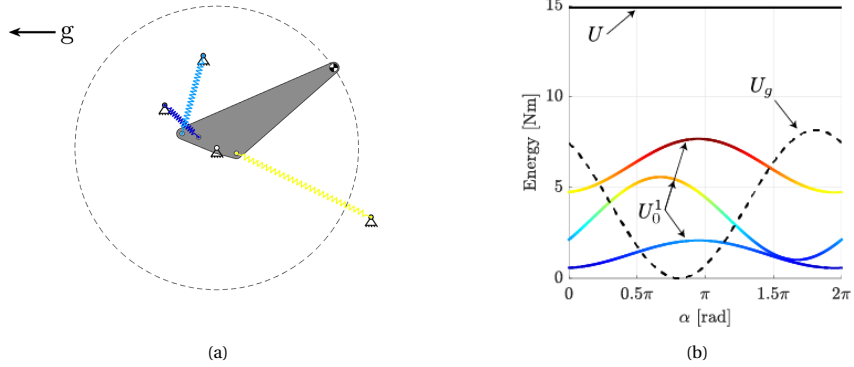


Figure 2.5: Gravity balancer with one DOF and three spring.

$$\begin{bmatrix} \mathbf{c}_1^* \\ 1 \end{bmatrix}(\alpha) = H_1^0(\alpha) \begin{bmatrix} \mathbf{c}_1 \\ 1 \end{bmatrix} \quad \text{and} \quad \begin{bmatrix} \mathbf{c}_2^* \\ 1 \end{bmatrix}(\alpha) = H_1^0(\alpha) H_2^1(\alpha) \begin{bmatrix} \mathbf{c}_2 \\ 1 \end{bmatrix} \quad (2.25)$$

If springs are attached in all topologically distinct ways, the total potential energy $U(\alpha)$ in the system is given by

$$U(\alpha) = U_1^0 + U_2^0 + U_2^1 + U_{g1} + U_{g2} \quad (2.26)$$

A statically balanced system is obtained when the derivative of $U(\alpha)$ is zero, i.e.:

$$\frac{dU(\alpha)}{d\alpha} = \frac{dU_1^0}{d\alpha} + \frac{dU_2^0}{d\alpha} + \frac{dU_2^1}{d\alpha} + \frac{dU_{g1}}{d\alpha} + \frac{dU_{g2}}{d\alpha} = 0 \quad (2.27)$$

where $\frac{dU_{\mathcal{X}\in\mathcal{J}}}{d\alpha}$ and $\frac{dU_{g_i}}{d\alpha}$ are given by

$$\frac{dU_1^0}{d\alpha} = \sum_{i=1}^{n_1^0} r_{1i}^0 q_{1i}^0 k_{1i}^0 \rho_1 \sin(\rho_1 \alpha + \theta_{1i}^0 - \phi_{1i}^0) \quad (2.28)$$

$$\begin{aligned} \frac{dU_2^0}{d\alpha} = \sum_{i=1}^{n_2^0} & \left(r_{2i}^0 q_{2i}^0 k_{2i}^0 (\rho_1 + \rho_2) \sin((\rho_1 + \rho_2) \alpha + \theta_{2i}^0 - \phi_{2i}^0) \right. \\ & \left. - r_{2i}^0 k_{2i}^0 t_2 \rho_2 \sin(\rho_2 \alpha + \theta_{2i}^0) + q_{2i}^0 k_{2i}^0 t_2 \rho_1 \sin(\rho_1 \alpha - \phi_{2i}^0) \right) \end{aligned} \quad (2.29)$$

$$\begin{aligned} \frac{dU_2^1}{d\alpha} = \sum_{i=1}^{n_2^1} & \left(r_{2i}^1 q_{2i}^1 k_{2i}^1 \rho_2 \sin(\rho_2 \alpha + \theta_{2i}^1 - \phi_{2i}^1) \right. \\ & \left. - r_{2i}^1 k_{2i}^1 t_2 \rho_2 \sin(\rho_2 \alpha + \theta_{2i}^1) \right) \end{aligned} \quad (2.30)$$

$$\frac{dU_{g1}}{d\alpha} = -g m_1 v_1 \rho_1 \sin(\rho_1 \alpha + \eta_1) \quad (2.31)$$

$$\frac{dU_{g2}}{d\alpha} = -g m_2 v_2 (\rho_1 + \rho_2) \sin((\rho_1 + \rho_2) \alpha + \eta_2) - g m_2 t_2 \rho_1 \sin(\rho_1 \alpha) \quad (2.32)$$

The above equations (2.28) to (2.32) are all sinusoidal functions at various frequencies. An overview of their frequency dependency is given in table 2.1. Three frequencies can be identified; $\rho_1 \alpha$, $\rho_2 \alpha$ and $(\rho_1 + \rho_2) \alpha$. The variation of potential energy of a single spring or mass can thus be considered a signal at particular frequencies. To eliminate the energy of a specific mechanical element, an element with energy at the same frequencies is required. The sinusoidal signals can then destructively interfere if amplitude and phase of each element is chosen properly.

Springs with the same topology \mathcal{X} vary their energies at the same frequencies. This is apparent in equations (2.28) to (2.30) from the sums over the number of springs $n_{\mathcal{X}}$. Multiple springs with the same topology can thus always destructively interfere. The variation of the gravitational energy (equations (2.31) and (2.32)) is not a sum of sinusoids itself, such that springs at the same frequency are required. That is, link one (equation (2.31)) requires springs with frequency $\rho_1 \alpha$ and link two (equation (2.32)) springs with a frequency $\rho_1 \alpha$ and $(\rho_1 + \rho_2) \alpha$.

This analysis allows us to see that the single link system $\frac{dU_1^0}{d\alpha} + \frac{dU_{g1}}{d\alpha} = 0$ can be solved, because both are a function of $\rho_1 \alpha$. However, a two link system $\frac{dU_2^0}{d\alpha} + \frac{dU_{g1}}{d\alpha} + \frac{dU_{g2}}{d\alpha} = 0$ cannot be solved, because the spring is at frequency $\rho_2 \alpha$ while gravity is at the frequencies $\rho_1 \alpha$ and $(\rho_1 + \rho_2) \alpha$.

Solving equation (2.27) for any ρ_1 and ρ_2 yields a statically balanced two degree of freedom system. Table 2.1 shows that two links can be balanced by using springs with topology $\mathcal{X} = (0, 2)$. Therefore we will solve the equation:

$$\frac{dU(\alpha)}{d\alpha} = \frac{dU_2^0}{d\alpha} + \frac{dU_{g1}}{d\alpha} + \frac{dU_{g2}}{d\alpha} = 0 \quad (2.33)$$

Substitution of equations (2.29), (2.31) and (2.32) in equation (2.33) yields:

$$\begin{aligned} \frac{dU(\alpha)}{d\alpha} = & \sum_{i=1}^{n_2^0} \left(r_{2i}^0 q_{2i}^0 k_{2i}^0 (\rho_1 + \rho_2) \sin((\rho_1 + \rho_2)\alpha + \theta_{2i}^0 - \phi_{2i}^0) \right. \\ & - r_{2i}^0 k_{2i}^0 t_2 \rho_2 \sin(\rho_2 \alpha + \theta_{2i}^0) + q_{2i}^0 k_{2i}^0 t_2 \rho_1 \sin(\rho_1 \alpha - \phi_{2i}^0) \Big) \\ & - g m_2 v_2 (\rho_1 + \rho_2) \sin((\rho_1 + \rho_2)\alpha + \eta_2) - g m_2 t_2 \rho_1 \sin(\rho_1 \alpha) \\ & - g m_1 v_1 \rho_1 \sin(\rho_1 \alpha + \eta_1) = 0 \end{aligned} \quad (2.34)$$

By expanding angle addition and collecting coefficients of the sine and cosine functions (i.e. $\rho_1 \sin(\rho_1 \alpha)$, $\rho_1 \cos(\rho_1 \alpha)$, $\rho_2 \sin(\rho_2 \alpha)$, $\rho_2 \cos(\rho_2 \alpha)$, $(\rho_1 + \rho_2) \sin((\rho_1 + \rho_2)\alpha)$ and $(\rho_1 + \rho_2) \cos((\rho_1 + \rho_2)\alpha)$) we can solve equation (2.33) by setting those coefficients simultaneously to zero:

$$\sum_{i=1}^{n_2^0} \begin{bmatrix} r_{2i}^0 k_{2i}^0 t_2 \cos(\phi_{2i}^0) \\ q_{2i}^0 k_{2i}^0 t_2 \sin(\phi_{2i}^0) \end{bmatrix} + \begin{bmatrix} -g m_1 v_1 \cos(\eta_1) \\ g m_1 v_1 \sin(\eta_1) \end{bmatrix} - \begin{bmatrix} g m_2 t_2 \\ 0 \end{bmatrix} = \mathbf{0} \quad (2.35)$$

$$\sum_{i=1}^{n_2^0} \begin{bmatrix} r_{2i}^0 k_{2i}^0 t_2 \cos(\theta_{2i}^0) \\ r_{2i}^0 k_{2i}^0 t_2 \sin(\theta_{2i}^0) \end{bmatrix} = \mathbf{0} \quad (2.36)$$

$$\sum_{i=1}^{n_2^0} \begin{bmatrix} r_{2i}^0 q_{2i}^0 k_{2i}^0 \cos(\theta_{2i}^0 - \phi_{2i}^0) \\ r_{2i}^0 q_{2i}^0 k_{2i}^0 \sin(\theta_{2i}^0 - \phi_{2i}^0) \end{bmatrix} - \begin{bmatrix} g m_2 v_2 \cos(\eta_2) \\ g m_2 v_2 \sin(\eta_2) \end{bmatrix} = \mathbf{0} \quad (2.37)$$

Equations (2.35) to (2.37) can be solved in many different ways, because this system of six equations has $5n_1^0 + 7$ unknowns. One could for example pick six variables and find explicit expressions for them in terms of the remaining $5n_1^0 + 1$ variables by solving the system at once. However, a closer inspection of equations (2.35) to (2.37) shows that they are independent in certain variables. This allows us to solve equations (2.35) to (2.37) sequentially in the same way we solved equation (2.19).

Let us pick random numerical values for all variables but η_1 , v_1 , r_{21}^0 , θ_{21}^0 , η_2 and v_2 . We then proceed to solve equation (2.35), then equation (2.36) and lastly equation (2.37) by using the same approach from equations (2.20) and (2.21). Regardless of any particular solution we can tell from the coefficients that a minimum of two springs is required, because equation (2.36) contains only a sum of springs. An example of this minimum system is shown in figure 2.6 with values $\rho_1 = 1$, $\rho_2 = 2$ and $\alpha = [0, 2\pi]$. An example with five springs is shown in figure 2.7. Please note that the solutions hold for all ρ_1 and ρ_2 .

2.3.3. STATIC BALANCING A TWO-LINK SYSTEM WITH TRANSMISSION

This example considers a two-link system with an actual transmission as shown in figure 2.3c. The transmission reduces the DOFs to one, which is achieved by numerical substitution of the values ρ_1 and ρ_2 . Assuming numerical values for ρ_1 and ρ_2 effectively changes the frequencies the energies are dependent on. This allows U_2^1 to cancel U_{g1} and U_{g2} even though their frequencies originally mismatched.

Let us first assume $\rho_1 = 1$, which leaves us with four options for ρ_2 . The first option is to assign an arbitrary value to ρ_2 . Now all frequencies are distinct and since ρ_2 is arbitrary it is effectively a degree of freedom which is solved in section 2.3.2.

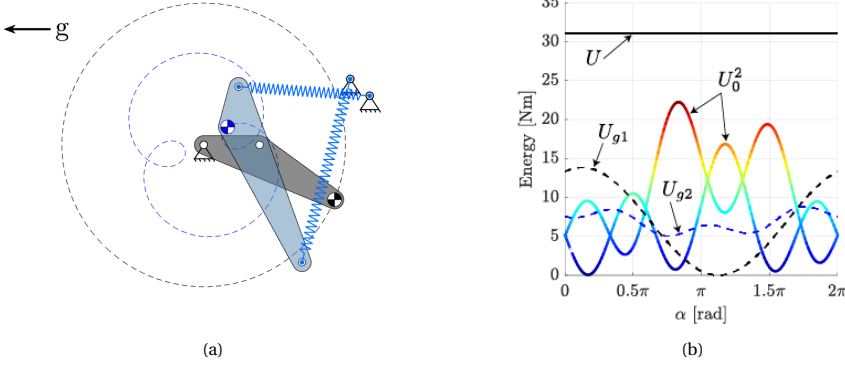


Figure 2.6: Gravity balancer with two DOF and two springs.

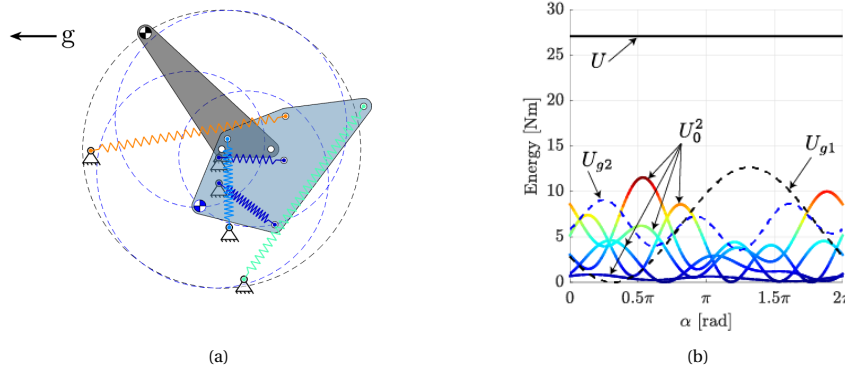


Figure 2.7: Gravity balancer with two DOF and five springs.

The other options are to set $\rho_2 = 0$, $\rho_2 = 1$ or $\rho_2 = -1$, because these simplify the resulting frequency dependencies as is shown in table 2.1. Consequently they also change possible balancing topologies. For example, with $\rho_2 = -1$ it is now possible to balance the two-link system with any spring, because all energies depend on frequency α . Although the system without transmission is not solvable, it is now possible to solve:

$$\frac{dU(\alpha)}{d\alpha} = \frac{dU_2^1}{d\alpha} + \frac{dU_{g1}}{d\alpha} + \frac{dU_{g2}}{d\alpha} = 0. \tag{2.38}$$

The total energy $U(\alpha)$ of a two-link system with $\rho_1 = -1$ and $\rho_2 = -1$ is given by:

$$\begin{aligned} \frac{dU(\alpha)}{d\alpha} = \sum_{i=1}^{n_2^1} & \left(r_{2i}^1 q_{2i}^1 k_{2i}^1 \sin(\alpha + \phi_{2i}^1 - \theta_{2i}^1) - r_{2i}^1 k_{2i}^1 t_2 \sin(\alpha - \theta_{2i}^1) \right) \\ & - g m_1 v_1 \sin(\alpha + \eta_1) - g m_2 t_2 \sin(\alpha) = 0 \end{aligned} \tag{2.39}$$

Table 2.1: Frequency dependency for each variational energy for different values of ρ_2 with $\rho_1 = 1$

Energy	U_1^0	U_2^1	U_2^0			U_{g1}	U_{g2}	
	Frequency	$\rho_1\alpha$	$\rho_2\alpha$	$\rho_1\alpha$	$\rho_2\alpha$	$(\rho_2 + \rho_1)\alpha$	$\rho_1\alpha$	$\rho_2\alpha$
$\rho_2 = 0$	α	0	α	0	α	α	α	α
$\rho_2 = 1$	α	α	α	α	2α	α	α	2α
$\rho_2 = -1$	α	α	α	α	0	α	α	0

Expanding angle addition and collecting coefficients yields:

$$\frac{dU(\alpha)}{d\alpha} = \left(\left(\sum_{i=1}^{n_2^1} a_i \cos(\gamma_{2i}^1) - b_i \cos(\theta_{2i}^1) \right) - c \cos(\eta_1) - d \right) \sin(\alpha) \quad (2.40)$$

$$\left(\left(\sum_{i=1}^{n_2^1} a_i \sin(\gamma_{2i}^1) + b_i \sin(\theta_{2i}^1) \right) - c \sin(\eta_1) \right) \cos(\alpha)$$

where $a_i = r_{2i}^1 q_{2i}^1 k_{2i}^1$, $b_i = r_{2i}^1 k_{2i}^1 t_2$, $c = g m_1 v_1$, $d = g m_2 t_2$ and $\gamma_{2i}^1 = \phi_{2i}^1 - \theta_{2i}^1$.

$$\sum_{i=1}^{n_2^1} a_i \begin{bmatrix} \cos(\gamma_i) \\ \sin(\gamma_i) \end{bmatrix} + \sum_{i=1}^{n_2^1} b_i \begin{bmatrix} -\cos(\theta_i) \\ \sin(\theta_i) \end{bmatrix} - c \begin{bmatrix} \cos(\eta_1) \\ \sin(\eta_1) \end{bmatrix} - \begin{bmatrix} d \\ 0 \end{bmatrix} \quad (2.41)$$

$$\triangleq \sum_{i=1}^{n_2^1} \begin{bmatrix} a_{xi} \\ a_{yi} \end{bmatrix} + \sum_{i=1}^{n_2^1} \begin{bmatrix} -b_{xi} \\ b_{yi} \end{bmatrix} - \begin{bmatrix} c_x \\ c_y \end{bmatrix} - \begin{bmatrix} d \\ 0 \end{bmatrix} = \mathbf{0}$$

A statically balanced mechanism is now easily constructed by choosing a_{xi} , a_{yi} , b_{xi} , b_{yi} , c_x , c_y and d such that equation (2.41) is satisfied. Equation (2.21) is then used to uncover a_i , b_i , c , γ_{2i}^1 , θ_{2i}^1 and η_1 . Subsequently we determine ϕ_{2i}^1 , r_{2i}^1 , q_{2i}^1 , k_{2i}^1 , t_2 , m_1 , m_2 and v_1 . Two examples are given in figures 2.8 and 2.9 with one and three springs. This solution is only valid for $\rho = 1$ and $\rho = -1$ which prevents rotation of the second center of mass (blue).

2.3.4. STATIC BALANCING A THREE-LINK SYSTEM

Statically balancing a three-link system as shown in figure 2.3d against gravity requires the gravitational terms U_{g1} , U_{g2} and U_{g3} . Their derivatives are given by

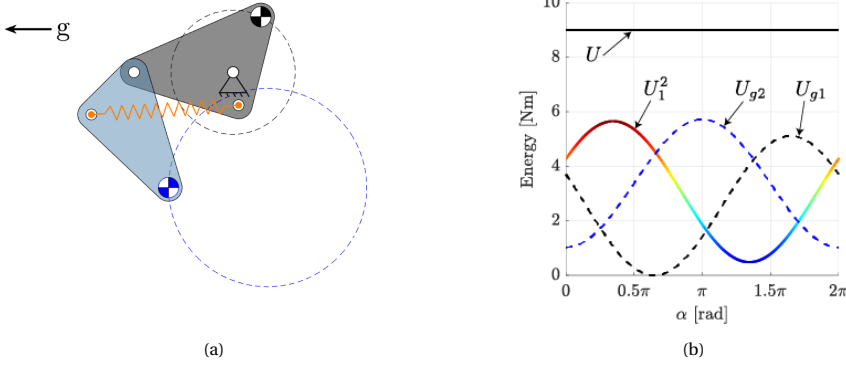


Figure 2.8: Gravity balancer with one DOF, one spring and an actual transmission.

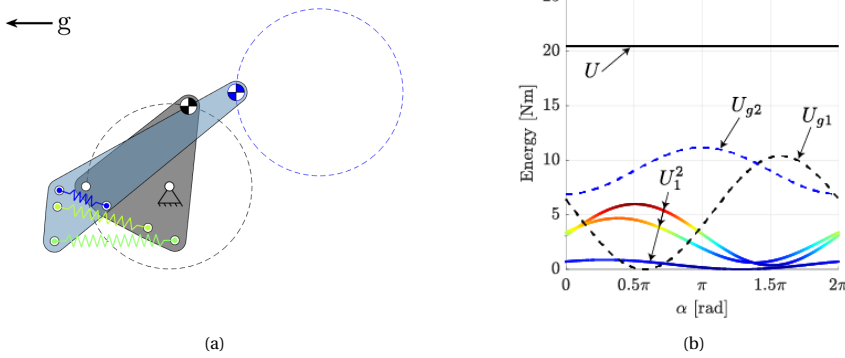


Figure 2.9: Gravity balancer with one DOF, three springs and an actual transmission.

$$\begin{aligned}
 \frac{dU_{g1}}{d\alpha} &= -g m_1 v_1 \rho_1 \sin(\rho_1 \alpha + \eta_1) \\
 \frac{dU_{g2}}{d\alpha} &= -g m_2 t_2 \rho_1 \sin(\rho_1 \alpha) \\
 &\quad - g m_2 v_2 (\rho_1 + \rho_2) \sin((\rho_1 + \rho_2) \alpha + \eta_2) \\
 \frac{dU_{g3}}{d\alpha} &= -g m_3 t_2 \rho_1 \sin(\rho_1 \alpha) \\
 &\quad - g m_3 t_3 (\rho_1 + \rho_2) \sin((\rho_1 + \rho_2) \alpha) \\
 &\quad - g m_3 v_3 (\rho_1 + \rho_2 + \rho_3) \sin((\rho_1 + \rho_2 + \rho_3) \alpha + \eta_3)
 \end{aligned} \tag{2.42}$$

which contain the frequencies $\rho_1 \alpha$, $(\rho_1 + \rho_2) \alpha$ and $(\rho_1 + \rho_2 + \rho_3) \alpha$. Springs with energies at the same frequencies are required to obtain balance against gravity. All frequency dependencies for all springs are summarized in figure 2.14. It shows that at least a spring with topology $\mathcal{X} = (0, 3)$ is needed. The derivative of U_3^0 is given by

$$\begin{aligned}
\frac{dU_3^0}{d\alpha} = \sum_{i=1}^{n_3^0} & \left[k_{3i}^0 q_{3i}^0 t_3 (\rho_1 + \rho_2) \sin((\rho_1 + \rho_2) \alpha - \phi_{3i}^0) \right. \\
& - k_{3i}^0 r_{3i}^0 t_2 (\rho_2 + \rho_3) \sin((\rho_2 + \rho_3) \alpha + \theta_{3i}^0) \\
& + k_{3i}^0 r_{3i}^0 q_{3i}^0 (\rho_1 + \rho_2 + \rho_3) \sin((\rho_1 + \rho_2 + \rho_3) \alpha + \theta_{3i}^0 - \phi_{3i}^0) \\
& - k_{3i}^0 r_{3i}^0 t_3 \rho_3 \sin(\rho_3 \alpha + \theta_{3i}^0) \\
& + k_{3i}^0 q_{3i}^0 t_2 \rho_1 \sin(\rho_1 \alpha - \phi_{3i}^0) \\
& \left. - k_{3i}^0 t_2 t_3 \rho_2 \sin(\rho_2 \alpha) \right] \quad (2.43)
\end{aligned}$$

Even though equation (2.43) contains all frequencies from the gravitational energy terms, it is not sufficient for balance. A close look shows that the term with frequency $\rho_2 \alpha$ is only summed over the stiffness k_{3i}^0 . Since stiffness should be positive, the coefficient $k_{3i}^0 t_2 t_3$ can never be zero and therefore the energy will change with a frequency $\rho_2 \alpha$. Additional springs are needed in order to cancel energy variations with frequency $\rho_2 \alpha$. The only spring that depends on $\rho_2 \alpha$ has topology $\mathcal{X} = (1, 2)$, see figure 2.14. The variation of its energy U_2^1 is given by

$$\frac{dU_2^1}{d\alpha} = \sum_{i=1}^{n_2^1} k_{2i}^1 r_{2i}^1 q_{2i}^1 \rho_2 \sin(\rho_2 \alpha + \theta_{2i}^1 - \phi_{2i}^1) - k_{2i}^1 r_{2i}^1 \rho_2 t_2 \sin(\rho_2 \alpha + \theta_{2i}^1) \quad (2.44)$$

We add all energy variations together and set it to zero to get:

$$\frac{dU_{g1}}{d\alpha} + \frac{dU_{g2}}{d\alpha} + \frac{dU_{g3}}{d\alpha} + \frac{dU_3^0}{d\alpha} + \frac{dU_2^1}{d\alpha} = 0 \quad (2.45)$$

By expanding angle addition we can collect the coefficients of all sine and cosine functions at all frequencies. Setting all coefficients simultaneously zero will result in a statically balanced system. These balancing conditions can be written as:

$$\sum_{i=1}^{n_3^0} \begin{bmatrix} k_{3i}^0 q_{3i}^0 t_2 \cos(\phi_{3i}^0) \\ -k_{3i}^0 q_{3i}^0 t_2 \sin(\phi_{3i}^0) \end{bmatrix} - \begin{bmatrix} g m_1 v_1 \cos(\eta_1) \\ g m_1 v_1 \sin(\eta_1) \end{bmatrix} - \begin{bmatrix} g m_2 t_2 \\ 0 \end{bmatrix} - \begin{bmatrix} g m_3 t_2 \\ 0 \end{bmatrix} = \mathbf{0} \quad (2.46)$$

$$\sum_{i=1}^{n_3^0} \begin{bmatrix} k_{3i}^0 t_2 t_3 \\ 0 \end{bmatrix} + \sum_{i=1}^{n_2^1} \begin{bmatrix} k_{2i}^1 q_{2i}^1 r_{2i}^1 \cos(\theta_{2i}^1 - \phi_{2i}^1) - k_{2i}^1 r_{2i}^1 t_2 \cos(\theta_{2i}^1) \\ k_{2i}^1 q_{2i}^1 r_{2i}^1 \sin(\theta_{2i}^1 - \phi_{2i}^1) - k_{2i}^1 r_{2i}^1 t_2 \sin(\theta_{2i}^1) \end{bmatrix} = \mathbf{0} \quad (2.47)$$

$$\sum_{i=1}^{n_3^0} \begin{bmatrix} k_{3i}^0 r_{3i}^0 t_2 \cos(\theta_{3i}^0) \\ k_{3i}^0 r_{3i}^0 t_2 \sin(\theta_{3i}^0) \end{bmatrix} = \mathbf{0} \quad \longrightarrow \quad \sum_{i=1}^{n_3^0} \begin{bmatrix} k_{3i}^0 r_{3i}^0 \cos(\theta_{3i}^0) \\ k_{3i}^0 r_{3i}^0 \sin(\theta_{3i}^0) \end{bmatrix} = \mathbf{0} \quad (2.48)$$

$$\sum_{i=1}^{n_3^0} \begin{bmatrix} k_{3i}^0 r_{3i}^0 t_3 \cos(\theta_{3i}^0) \\ k_{3i}^0 r_{3i}^0 t_3 \sin(\theta_{3i}^0) \end{bmatrix} = \mathbf{0} \quad \longrightarrow \quad \sum_{i=1}^{n_3^0} \begin{bmatrix} k_{3i}^0 r_{3i}^0 \cos(\theta_{3i}^0) \\ k_{3i}^0 r_{3i}^0 \sin(\theta_{3i}^0) \end{bmatrix} = \mathbf{0} \quad (2.49)$$

$$\sum_{i=1}^{n_3^0} \begin{bmatrix} k_{3i}^0 q_{3i}^0 t_3 \cos(\phi_{3i}^0) \\ -k_{3i}^0 q_{3i}^0 t_3 \sin(\phi_{3i}^0) \end{bmatrix} - \begin{bmatrix} g m_2 v_2 \cos(\eta_2) \\ g m_2 v_2 \sin(\eta_2) \end{bmatrix} - \begin{bmatrix} g m_3 t_3 \\ 0 \end{bmatrix} = \mathbf{0} \quad (2.50)$$

$$\sum_{i=1}^{n_3^0} \begin{bmatrix} k_{3i}^0 q_{3i}^0 r_{3i}^0 \cos(\theta_{3i}^0 - \phi_{3i}^0) \\ k_{3i}^0 q_{3i}^0 r_{3i}^0 \sin(\theta_{3i}^0 - \phi_{3i}^0) \end{bmatrix} - \begin{bmatrix} g m_3 v_3 \cos(\eta_3) \\ g m_3 v_3 \sin(\eta_3) \end{bmatrix} = \mathbf{0} \quad (2.51)$$

It would be expected that the balancing conditions become more difficult to solve as links are added, but this is not the case. We can solve the coefficients sequentially one by one, in the same way as for a single link system. It is shown in section 2.5 we can do this for any number of links.

Let us again pick random numerical values for all variables but θ_{31}^0 , r_{31}^0 , ϕ_{31}^0 , q_{31}^0 , η_1 , v_1 , η_3 , ϕ_{21}^1 and q_{21}^1 . We then proceed to solve equations (2.46) to (2.51) one by one. Please note that the conditions from equations (2.48) and (2.49) are identical, because t_2 and t_3 can be taken out of the summation. Inspection of the balancing conditions from equations (2.46) to (2.51) tells us that a minimum of two springs with topology $\mathcal{X} = (0, 3)$

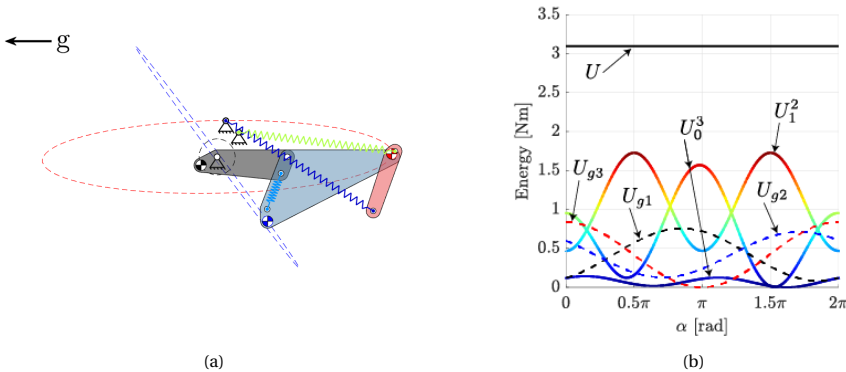


Figure 2.10: Gravity balancer with three DOFs and three springs.

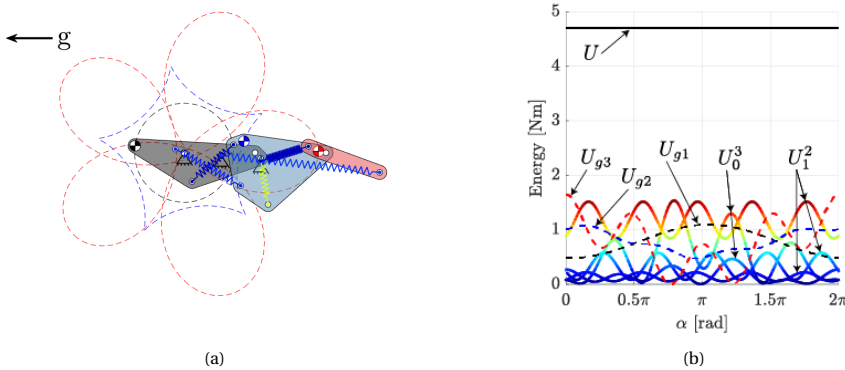


Figure 2.11: Gravity balancer with three DOFs and five springs.

and one spring with topology $\mathcal{X} = (1, 2)$ is needed for static balance. An example with the minimum number of springs is shown in figure 2.10 with $\rho_1 = 1$, $\rho_2 = -2$, $\rho_3 = 2$ and $\alpha = [0, 2\pi]$ and with five springs and $\rho_1 = 1$, $\rho_2 = -5$, $\rho_3 = 2$ in figure 2.11. Please note that the solutions hold for all ρ_1 , ρ_2 and ρ_3 .

2

2.4. SPATIAL EXAMPLE

One spatial example is given in this section for which solutions are also given in [16]. It concerns a single body with a spherical joint with three DOFs as shown in figure 2.12. A local coordinate frame is created for the ground and each DOF such that $\mathcal{O} = \{O_0, O_1, O_2, O_3\}$. Since we have only one body we will only consider the spring topology $\mathcal{X} = (0, 3)$.

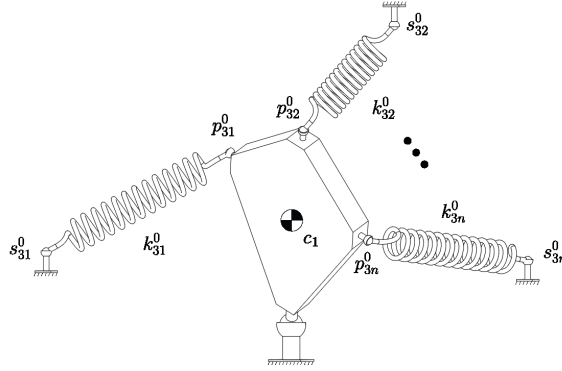


Figure 2.12: Schematic drawing of the spatial single-body mechanisms with a spherical joint with three DOFs.

The matrix $D_{(0,3)}(\alpha)$ and vector $\mathbf{c}_1^*(\alpha)$ are given by

$$\begin{bmatrix} D_3^0(\alpha) \\ \mathbf{1} \end{bmatrix} = H_1^0 H_2^1 H_3^2(\alpha) \begin{bmatrix} P_3^0 \\ \mathbf{1} \end{bmatrix} - \begin{bmatrix} S_3^0 \\ \mathbf{1} \end{bmatrix} \quad \text{and} \quad \begin{bmatrix} \mathbf{c}_1^*(\alpha) \\ \mathbf{1} \end{bmatrix} = H_1^0 H_2^1 H_3^2(\alpha) \begin{bmatrix} \mathbf{c}_1 \\ \mathbf{1} \end{bmatrix} \quad (2.52)$$

where

$$H_1^0(\alpha) = \begin{bmatrix} R_x(\rho_1 \alpha) & T_1 \\ \mathbf{0} & \mathbf{1} \end{bmatrix}, \quad H_2^1(\alpha) = \begin{bmatrix} R_y(\rho_2 \alpha) & T_2 \\ \mathbf{0} & \mathbf{1} \end{bmatrix}, \quad H_3^2(\alpha) = \begin{bmatrix} R_z(\rho_3 \alpha) & T_3 \\ \mathbf{0} & \mathbf{1} \end{bmatrix} \quad (2.53)$$

with $T_1 = T_2 = T_3 = \mathbf{0}$ and R_x , R_y and R_z given by equation (2.13). Substitution of equation (2.52) into equation (2.6) yields

$$U(\alpha) = U_3^0(\alpha) + U_{g1}(\alpha) = \sum_{i=1}^{n_3^0} \frac{1}{2} k_{3i}^0 \|\mathbf{d}_{3i}^0(\alpha)\|_2^2 + g m_1 c_{1x}^* \quad (2.54)$$

Working out equation (2.54) and setting the derivative to zero according to equation (2.9) allows us to identify 9 unique coefficients to be simultaneously zero. In the following the subscript \mathcal{X} is dropped for conciseness, i.e. $\mathbf{p}_{3i}^0 = \mathbf{p}_i$. The coefficients are given by

$$\sum_{i=1}^n k_i r_i q_i \begin{bmatrix} \sin(\zeta_i) \cos(\theta_i) \sin(\gamma_i) \cos(\phi_i) \\ \sin(\zeta_i) \cos(\theta_i) \sin(\gamma_i) \sin(\phi_i) \\ \sin(\zeta_i) \cos(\theta_i) \sin(\gamma_i) \\ \sin(\zeta_i) \sin(\theta_i) \sin(\gamma_i) \cos(\phi_i) \\ \sin(\zeta_i) \sin(\theta_i) \sin(\gamma_i) \sin(\phi_i) \\ \sin(\zeta_i) \sin(\theta_i) \sin(\gamma_i) \\ \cos(\zeta_i) \sin(\gamma_i) \cos(\phi_i) \\ \cos(\zeta_i) \sin(\gamma_i) \sin(\phi_i) \\ \cos(\zeta_i) \cos(\gamma_i) \end{bmatrix} - \begin{bmatrix} g m_1 v_1 \sin(\xi_1) \cos(\psi_1) \\ 0 \\ 0 \\ g m_1 v_1 \sin(\xi_1) \sin(\psi_1) \\ 0 \\ 0 \\ 0 \\ g m_1 v_1 \cos(\xi_1) \\ 0 \\ 0 \end{bmatrix} = \mathbf{0} \quad (2.55)$$

which can be rewritten in the form:

$$\sum_{i=1}^n k_i \begin{bmatrix} x_{p_i} x_{s_i} \\ x_{p_i} y_{s_i} \\ x_{p_i} z_{s_i} \\ y_{p_i} x_{s_i} \\ y_{p_i} y_{s_i} \\ y_{p_i} z_{s_i} \\ z_{p_i} x_{s_i} \\ z_{p_i} y_{s_i} \\ z_{p_i} z_{s_i} \end{bmatrix} - \begin{bmatrix} g m_1 x_{c1} \\ 0 \\ 0 \\ g m_1 y_{c1} \\ 0 \\ 0 \\ g m_1 z_{c1} \\ 0 \\ 0 \end{bmatrix} = \mathbf{0} \quad (2.56)$$

Three different solutions can be found for equation (2.56). Distinct solutions exist with only one spring ($n = 1$), with two springs ($n = 2$) and with more than two springs $n > 2$. These three cases are discussed in the sections 2.4.1 to 2.4.3 below. The results are shown in figure 2.13 with $\rho_1 = 1$, $\rho_2 = \sqrt{2}$, $\rho_3 = \pi$ and $\alpha = [0, 2\pi]$, but all solutions are valid for all values of ρ_1 , ρ_2 and ρ_3 .

2.4.1. ONE SPRING SYSTEMS ($n = 1$)

Equation (2.56) can be solved with 5 unknowns for $n = 1$, i.e. x_{c1} , y_{c1} , z_{c1} , y_{s1} and z_{s1} . The conditions for these variables are given by

$$x_{c1} = \frac{k_1 x_{p1} x_{s1}}{g m_1}, \quad y_{c1} = \frac{k_1 y_{p1} x_{s1}}{g m_1}, \quad z_{c1} = \frac{k_1 z_{p1} x_{s1}}{g m_1}, \quad y_{s1} = z_{s1} = 0 \quad (2.57)$$

which can be simplified to

$$\mathbf{c}_1 = \frac{k_1 x_{s1}}{g m_1} \mathbf{p}_1, \quad y_{s1} = z_{s1} = 0 \quad (2.58)$$

Geometrically this means that the points \mathbf{c}_1 and \mathbf{p}_1 must be on the same line scaled by a factor $\frac{k_1 x_{s1}}{g m_1}$ and that the other end of the spring, point \mathbf{s}_1 , must be above the spherical joint at the origin of O_0 . These conditions are identical to those given by [16].

2.4.2. TWO SPRING SYSTEMS ($n = 2$)

Equation (2.56) can be solved with 7 unknowns for $n = 2$, i.e. x_{c1} , y_{c1} , z_{c1} , x_{p1} , y_{p1} , z_{p1} , z_{s1} . The conditions for these variables are given by

$$\mathbf{c}_1 = -\frac{k_2(x_{s_1}y_{s_2} - x_{s_2}y_{s_1})}{gm_1y_{s_1}}\mathbf{p}_2, \quad \mathbf{p}_1 = -\frac{k_2y_{s_2}}{k_1y_{s_1}}\mathbf{p}_2, \quad z_{s_1}y_{s_2} = z_{s_2}y_{s_1} \quad (2.59)$$

Equation (2.59) shows that \mathbf{c}_1 , \mathbf{p}_1 and \mathbf{p}_2 need to be collinear and that the line defined by the points \mathbf{s}_1 and \mathbf{s}_2 needs to intersect the x-axis of the coordinate frame O_0 , given that z_{s_1} , y_{s_1} , z_{s_2} and y_{s_2} are nonzero. For $z_{s_1} = y_{s_1} = z_{s_2} = y_{s_2} = 0$ equation (2.56) reduces to

$$\sum_{i=1}^2 k_i \begin{bmatrix} x_{p_i}x_{s_i} \\ y_{p_i}x_{s_i} \\ z_{p_i}x_{s_i} \end{bmatrix} - \begin{bmatrix} gm_1x_{c1} \\ gm_1y_{c1} \\ gm_1z_{c1} \end{bmatrix} = \mathbf{0} \quad (2.60)$$

with solution:

$$\mathbf{c}_1 = \frac{k_1x_{s_1}}{gm_1}\mathbf{p}_1 + \frac{k_2x_{s_2}}{gm_1}\mathbf{p}_2 \quad (2.61)$$

which means the points \mathbf{c}_1 , \mathbf{p}_1 and \mathbf{p}_2 are co-planar and the points \mathbf{s}_1 and \mathbf{s}_2 are on the x-axis of O_0 . These conditions are identical to those given by [16].

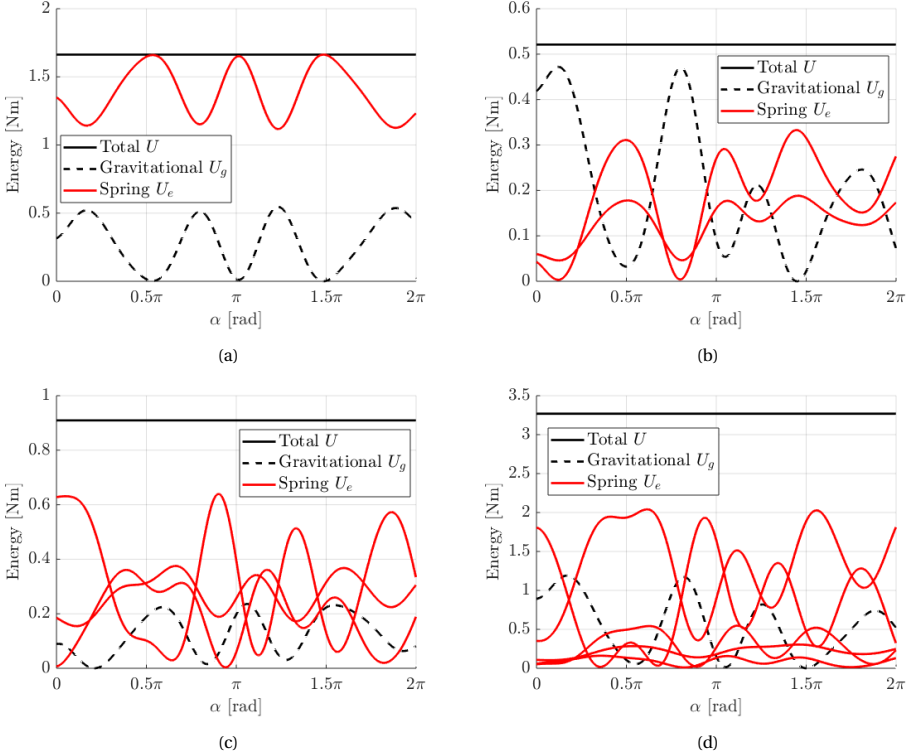


Figure 2.13: Energy diagrams of spatial three DOF example with (a) one spring, (b) two springs, (c) three springs and (d) five springs.

2.4.3. N-SPRING SYSTEMS ($n > 2$)

For $n > 2$ springs, 9 unknowns are required. To generalize for n springs we rewrite equation (2.56) in the following form:

$$\begin{bmatrix} C_1 \\ C_2 \\ C_3 \\ C_4 \\ C_5 \\ C_6 \\ C_7 \\ C_8 \\ C_9 \end{bmatrix} + k_1 \begin{bmatrix} x_{p_1} x_{s_1} \\ x_{p_1} y_{s_1} \\ x_{p_1} z_{s_1} \\ y_{p_1} x_{s_1} \\ y_{p_1} y_{s_1} \\ y_{p_1} z_{s_1} \\ z_{p_1} x_{s_1} \\ z_{p_1} y_{s_1} \\ z_{p_1} z_{s_1} \end{bmatrix} + k_2 \begin{bmatrix} x_{p_2} x_{s_2} \\ x_{p_2} y_{s_2} \\ x_{p_2} z_{s_2} \\ y_{p_2} x_{s_2} \\ y_{p_2} y_{s_2} \\ y_{p_2} z_{s_2} \\ z_{p_2} x_{s_2} \\ z_{p_2} y_{s_2} \\ z_{p_2} z_{s_2} \end{bmatrix} - \begin{bmatrix} gm_1 x_{c_1} \\ 0 \\ 0 \\ gm_1 y_{c_1} \\ 0 \\ 0 \\ gm_1 z_{c_1} \\ 0 \\ 0 \end{bmatrix} = \mathbf{0} \quad (2.62)$$

Solving this system for x_{c_1} , y_{c_1} , z_{c_1} , x_{p_1} , x_{p_2} , y_{p_1} , y_{p_2} , z_{p_1} and z_{p_2} yields

$$\begin{aligned} x_{c_1} &= \frac{C_1 y_{s_1} z_{s_2} - C_1 y_{s_2} z_{s_1} - C_2 x_{s_1} z_{s_2} + C_2 x_{s_2} z_{s_1} + C_3 x_{s_1} y_{s_2} - C_3 x_{s_2} y_{s_1}}{gm_1 (y_{s_1} z_{s_2} - y_{s_2} z_{s_1})}, \\ y_{c_1} &= \frac{C_4 y_{s_1} z_{s_2} - C_4 y_{s_2} z_{s_1} - C_5 x_{s_1} z_{s_2} + C_5 x_{s_2} z_{s_1} + C_6 x_{s_1} y_{s_2} - C_6 x_{s_2} y_{s_1}}{gm_1 (y_{s_1} z_{s_2} - y_{s_2} z_{s_1})}, \\ z_{c_1} &= \frac{C_7 y_{s_1} z_{s_2} - C_7 y_{s_2} z_{s_1} - C_8 x_{s_1} z_{s_2} + C_8 x_{s_2} z_{s_1} + C_9 x_{s_1} y_{s_2} - C_9 x_{s_2} y_{s_1}}{gm_1 (y_{s_1} z_{s_2} - y_{s_2} z_{s_1})}, \\ x_{p_1} &= -\frac{C_2 z_{s_2} - C_3 y_{s_2}}{k_1 (y_{s_1} z_{s_2} - y_{s_2} z_{s_1})}, & x_{p_2} &= \frac{C_2 z_{s_1} - C_3 y_{s_1}}{k_2 (y_{s_1} z_{s_2} - y_{s_2} z_{s_1})}, \\ y_{p_1} &= -\frac{C_5 z_{s_2} - C_6 y_{s_2}}{k_1 (y_{s_1} z_{s_2} - y_{s_2} z_{s_1})}, & y_{p_2} &= \frac{C_5 z_{s_1} - C_6 y_{s_1}}{k_2 (y_{s_1} z_{s_2} - y_{s_2} z_{s_1})}, \\ z_{p_1} &= -\frac{C_8 z_{s_2} - C_9 y_{s_2}}{k_1 (y_{s_1} z_{s_2} - y_{s_2} z_{s_1})}, & z_{p_2} &= \frac{C_8 z_{s_1} - C_9 y_{s_1}}{k_2 (y_{s_1} z_{s_2} - y_{s_2} z_{s_1})} \end{aligned} \quad (2.63)$$

The above equation (2.63) is a general solution to equation (2.56). This solution is by no means unique, since it could be solved for any nine variables. An alternative and simpler way of solving equation (2.56) is by reducing it by setting $y_{s_i} = z_{s_i} = 0$ for $i = 1, \dots, n$, which yields

$$\sum_{i=1}^n k_i \begin{bmatrix} x_{p_i} x_{s_i} \\ y_{p_i} x_{s_i} \\ z_{p_i} x_{s_i} \end{bmatrix} - \begin{bmatrix} gm_1 x_{c_1} \\ gm_1 y_{c_1} \\ gm_1 z_{c_1} \end{bmatrix} = \sum_{i=1}^n k_i x_{s_i} \mathbf{p}_i - gm_1 \mathbf{c}_1 = \mathbf{0} \quad (2.64)$$

A solution is obtained by rewriting equation (2.64) explicitly for \mathbf{c}_1 . And the balancing conditions become

$$\mathbf{c}_1 = \sum_{i=1}^n \frac{k_i x_{s_i}}{gm_1} \mathbf{p}_i \quad \text{and} \quad y_{s_i} = z_{s_i} = 0, \quad i = 1, \dots, n. \quad (2.65)$$

These conditions show that the location \mathbf{c}_1 of the mass \mathbf{m}_1 is a linear combination of all n spring locations \mathbf{p}_i on the mass, given that all springs are connected to the x-axis in O_0 .

2.5. INDEPENDENCE OF COEFFICIENTS

The balancing conditions for a two and three link system are as easily solved as for a system with a single link, see section 2.3. In these examples, each set of two coefficients can be individually solved, because they are independent. We will now show that a set of independent coefficients can be created for any number of links, which in turn proves that a solution exists for any number of links.

2

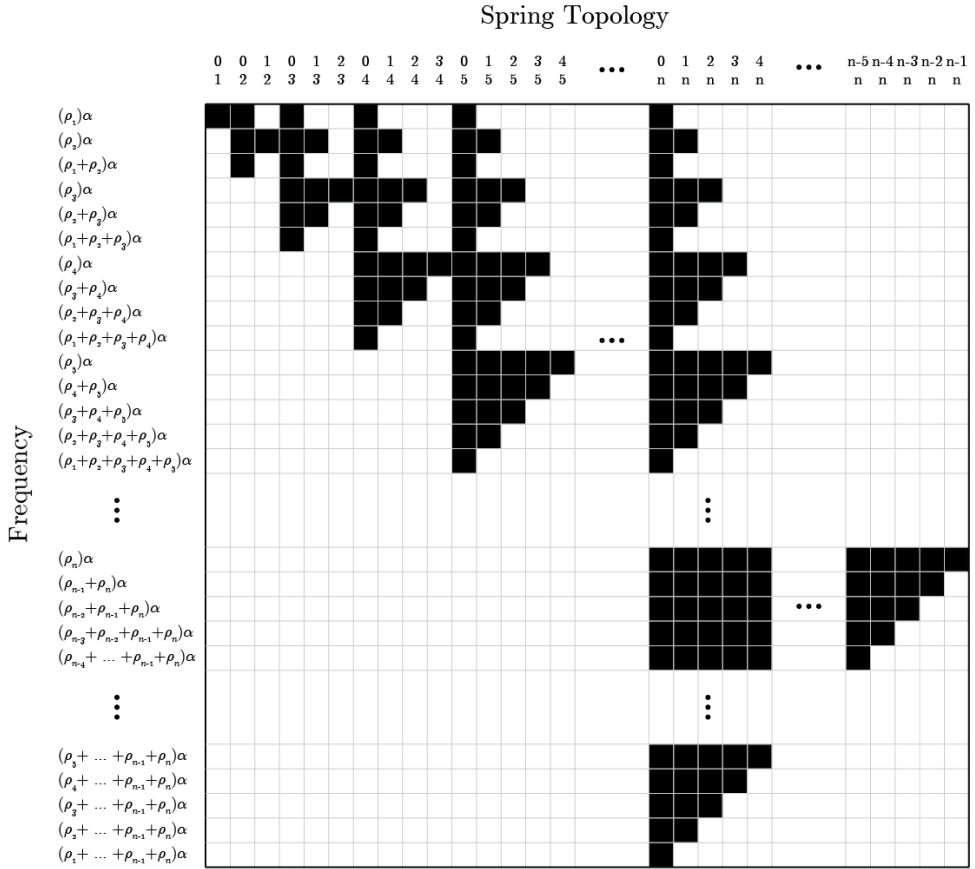


Figure 2.14: Frequency dependency \mathcal{F} for each spring topology \mathcal{X} in a system with n links.

An independent set of coefficients can be created for static balancing both gravitational and elastic forces. Let us first investigate a system without gravity by looking at the frequencies $\mathcal{F}_{\mathcal{X}}$ that belong to spring topologies $\mathcal{X} \in \mathcal{J}$. For a serial kinematic chain of length n there are $m = \binom{n+1}{2}$ distinct frequencies. The frequencies each spring topology is dependent on, are given by the set of all possible sums of consecutive angular coordinates $\rho_i \alpha$ that affect the length of a spring.

For example, the length of a spring with topology $\mathcal{X} = (0, 3)$ is affected by $\rho_1 \alpha, \rho_2 \alpha$

and $\rho_3\alpha$. The set \mathcal{F}_3^0 of all frequencies that it depends on is then given by

$$\mathcal{F}_3^0 = \{\rho_1\alpha, \rho_2\alpha, \rho_3\alpha, (\rho_1 + \rho_2)\alpha, (\rho_2 + \rho_3)\alpha, (\rho_1 + \rho_2 + \rho_3)\alpha\}. \quad (2.66)$$

A spring with topology $\mathcal{X} = (1, 3)$ is dependent on the angles $\rho_2\alpha$ and $\rho_3\alpha$ such that all possible frequencies are given by $\mathcal{F}_3^1 = \{\rho_2\alpha, \rho_3\alpha, (\rho_2 + \rho_3)\alpha\}$ and a spring with $\mathcal{X} = (2, 3)$ is only dependent on $\rho_3\alpha$ such that $\mathcal{F}_3^2 = \{\rho_3\alpha\}$.

For a serial chain with n links all possible sets of frequencies $\mathcal{F}_{\mathcal{X} \in \mathcal{J}}$ can be organized in a repeating structure. This pattern is shown in figure 2.14. Frequencies are listed vertically and spring topologies horizontally, a black square indicates a dependency.

A set of $2m$ coefficients is independent if in each remaining unsolved set there is at least one set of two coefficients with two unique parameters. This means there is at least one mechanical element that is left only dependent on a single frequency. In figure 2.14, n such independent mechanical elements can be readily identified. Each spring with topology $\mathcal{X} = (i-1, i)$ for $i = 1, \dots, n$ is only a function of frequency $(\rho_i)\alpha$. Consequently, we can solve the coefficients of these frequencies independently of all other frequencies.

The remaining unsolved set of $2(m-n)$ coefficients can be visualized by removing the columns with topology $\mathcal{X} = (i-1, i)$ and rows with frequency $(\rho_i)\alpha$ for $i = 1, \dots, n$ from figure 2.14. The structure of this reduced set is identical to the original set, which means the pattern of frequency-dependencies is self similar under the operation of solving independent coefficients. Consequently, we can sequentially solve independent coefficients until we have solved for all frequencies.

The self similar reduction of a set of m frequencies with $2m$ coefficients should be repeated n times to solve the entire system. At each reduction step $k = 1, \dots, n$ the springs $\mathcal{X} = (i-k, i)$ are only dependent on the frequencies

$$F_i^{(i-k)} = \left(\sum_{y=0}^{k-1} \rho_{i-y} \right) \alpha, \quad i = k, \dots, n. \quad (2.67)$$

Equation (2.67) shows that at each reduction step k there are $n-k+1$ frequencies that can be independently solved for. It also shows that after $n-1$ steps we end up with a single spring topology $\mathcal{X} = (0, n)$ that is left dependent on only one set of coefficients that belong to the frequency $F_n^0 = \left(\sum_{i=1}^n \rho_i \right) \alpha$.

The above procedure requires the use of all springs. However, we can relax this requirement by accounting for gravity. The pattern of frequency dependency for the gravitational potential energy is shown in figure 2.15. One can easily see that it is possible to sequentially solve and reduce for the frequencies $\sum_{y=1}^i \rho_y$ for $i = 1, \dots, n$. Once one has solved for these frequencies, they can be removed from the pattern in figure 2.14, which gives us more options for the selection of springs.

2.6. DISCUSSION

In this chapter we presented a general method for the design of statically balanced serial chains with any number of links and springs. We introduced virtual transmissions to constrain any linkage to a single degree of freedom. As such, the derivative of the potential energy is a single equation that is set to zero, from which algebraic balancing

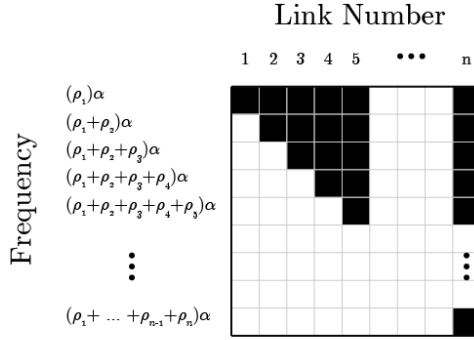


Figure 2.15: Frequency dependency \mathcal{F} for each link i

conditions for all DOF result. Substitution of numerical values for the virtual transmissions resulted in balanced systems with actual transmissions. Various examples in 2D and 3D demonstrated the versatility of our method.

With the use of virtual transmissions, the variation of the potential energy of a single mechanical element (i.e. a spring or link) can be written as a sum of sinusoidal functions at particular frequencies. A balanced system is obtained by having all these sinusoidal functions destructively interfere. This is done by isolating the coefficients at all frequencies and setting them simultaneously zero. Although the number of coefficients increases for longer chains, we show they are not more difficult to solve. For any number of links, a set of independent coefficients can be obtained that can be solved sequentially one by one with the same simple equation (2.21). This can be done for gravity balancing but also for spring-force balancing.

The homogeneous transformation matrices that we use describe general rotation in 2D and 3D. It is however possible to readily substitute other homogeneous transformation matrices in equations (2.4), (2.5) and (2.14) for the potential energies. This allows conventions such as the Denavit-Hartenberg (DH) parameters [24] used for spatial serial chains in robotics, to be directly compatible with our method. In addition, since homogeneous transformation matrices can model all lower kinematic pairs [24], our method is suited for mechanisms with spherical, planar, cylindric, screw, prismatic and revolute pairs.

The method can be expanded to include tree-structured mechanisms as well, similar to the mechanisms in [11, 19]. To generalize for such parallel branches we need a set \mathcal{K} that defines kinematic topology, in addition to \mathcal{J} for spring topologies. This set defines for each local coordinate frame O_i with $i > 0$ how to compute the global coordinates in O_0 . For a very simple parallel 3 link mechanism this set may be given by $\mathcal{K} = \{(0, 1), (0, 1, 2), (0, 1, 3)\}$, which says that link 1 is directly connected to the ground and links 2 and 3 are both connected to link 1, such that \mathbf{c}_1^* , \mathbf{c}_2^* and \mathbf{c}_3^* are given by:

$$\begin{bmatrix} \mathbf{c}_1^* \\ 1 \end{bmatrix} = H_1^0 \begin{bmatrix} \mathbf{c}_1 \\ 1 \end{bmatrix}, \quad \begin{bmatrix} \mathbf{c}_2^* \\ 1 \end{bmatrix} = H_1^0 H_2^1 \begin{bmatrix} \mathbf{c}_2 \\ 1 \end{bmatrix}, \quad \begin{bmatrix} \mathbf{c}_3^* \\ 1 \end{bmatrix} = H_1^0 H_3^1 \begin{bmatrix} \mathbf{c}_3 \\ 1 \end{bmatrix} \quad (2.68)$$

Similarly equation (2.4) will change.

We have claimed our method is able to balance any open serial kinematic chain. We can expand this claim by saying that it can also balance any closed serial kinematic chain. This claim is justified by the configuration space of a closed kinematic chain being a subset of an open chain with the same number of links. Similarly, we can claim that the expanded method could balance any mechanism, including parallel chains. By the same token, the configuration space of a parallel mechanism is a subset of the configuration space of its equivalent tree-structured mechanism.

We believe to be improving upon the state of the art with a more versatile synthesis tool for static balancing, but we can also learn important lessons from interpreting the balancing conditions geometrically, as done for a single link in 3D in section 2.4. Here we learned for example that the center of mass is always a linear combination of the vectors \mathbf{p}_i if all springs i are grounded on the x_0 -axis, similar to [16], and that any such system with any number of random springs can always be balanced by adding just one additional spring.

Many interesting properties can even be obtained without ever solving any of the equations. An analysis of the energy variation in terms of frequency can reveal whether a solution can be found at all, as done in section 2.3.4. By numerical substitution of values for the virtual transmissions ρ_i actual transmissions can be readily implemented and designed for. For particular values of ρ_i the frequency dependencies change and energy equations simplify. This allows gravity balancing by springs that were previously unable to do so, see section 2.3.3.

Most ρ_i will not simplify the system, but can be used to create rectilinear motion. If a zero-free-length spring moves over a rectilinear trajectory, it can be replaced with a normal spring [8, 14, 25]. A well-known example is the elliptic trammel which can be spring-spring balanced [8] and is based on the tusi-couple [26, 27]. An extended version with three normal springs that is designed with our method is shown in figure 2.16.

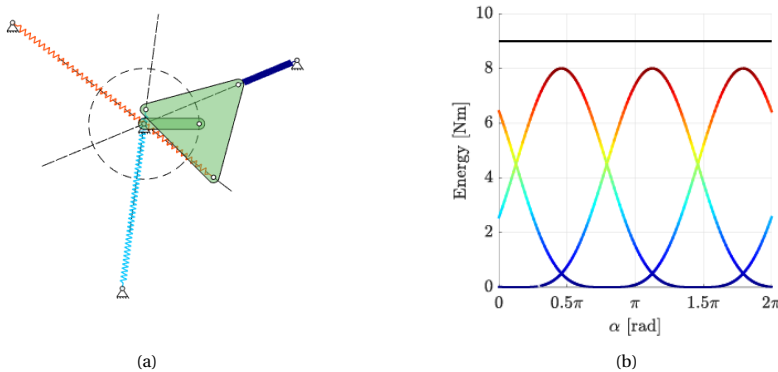


Figure 2.16: A possible future direction that uses actual transmissions to create linear motion which enables balancing by normal springs. The figure shows a perfectly spring-spring balanced mechanism with normal springs based on the elliptic trammel and the tusi couple.

2.7. CONCLUSION

In this chapter we have presented a method for static balancing of serial kinematic chains without adding auxiliary links. Systems in 2D and 3D can be gravity and spring-force balanced with an arbitrary number of links and springs. This is achieved by introducing virtual transmissions between all links that reduce any system initially to a single degree of freedom. This allows us to derive the variation of the potential energy with a single derivative which is a sum of sinusoidal functions at frequencies determined by the transmissions. Static balance over the entire unconstrained configuration space is obtained by setting all coefficients of these sinusoidal functions simultaneously to zero. Substitution of numerical values for the virtual transmissions allows the design of statically balanced kinematic chains that include actual transmissions. We prove that the equations are independent and are equally simple to solve for any number of links.

Homogeneous transformation matrices are used to describe the kinematics which makes the method compatible with for example the Denavit-Hartenberg convention, widely used to compute forward kinematics in robotics. Homogeneous transformations not only allow the use of revolute and spherical kinematic pairs, but planar, cylindrical, screw and prismatic pairs can also be included.

Multiple examples in 2D and 3D, with and without transmissions are given to demonstrate the versatility of our method. The method is easily expanded to include tree-structured mechanisms, by introducing a mathematical structure that describes kinematic topology. In addition we show that it enables the design of mechanisms with normal springs by including transmissions. And lastly, we argue that this method can be used for static balancing of any mechanism, because the configuration space of closed loop mechanisms are a subset of open loop mechanisms.

REFERENCES

- [1] J. A. Gallego and J. L. Herder, *Criteria for the static balancing of compliant mechanisms*, in *ASME 2010 International Design Engineering Technical Conferences and Computers and Information in Engineering Conference* (American Society of Mechanical Engineers, 2010) pp. 465–473.
- [2] D. Farhadi Machekposhti, J. L. Herder, and N. Tolou, *Frequency doubling in elastic mechanisms using buckling of microflexures*, *Applied Physics Letters* **115**, 143503 (2019).
- [3] D. F. Machekposhti, J. L. Herder, G. Sémon, and N. Tolou, *A compliant micro frequency quadrupler transmission utilizing singularity*, *Journal of Microelectromechanical Systems* **27**, 506 (2018).
- [4] V. Arakelian, *Gravity compensation in robotics*, *Advanced Robotics* **30**, 79 (2016).
- [5] T. Bosch, J. van Eck, K. Knitel, and M. de Looze, *The effects of a passive exoskeleton on muscle activity, discomfort and endurance time in forward bending work*, *Applied ergonomics* **54**, 212 (2016).

- [6] R. Rizk, S. Krut, and E. Dombre, *Design of a 3d gravity balanced orthosis for upper limb*, in *2008 IEEE International Conference on Robotics and Automation (IEEE, 2008)* pp. 2447–2452.
- [7] P.-Y. Lin, W.-B. Shieh, and D.-Z. Chen, *A theoretical study of weight-balanced mechanisms for design of spring assistive mobile arm support (mas)*, *Mechanism and Machine Theory* **61**, 156 (2013).
- [8] J. L. Herder, *Energy-free Systems; Theory, conception and design of statically balanced spring mechanisms* (2001).
- [9] S. R. Deepak and G. Ananthasuresh, *Static balancing of a four-bar linkage and its cognates*, *Mechanism and Machine Theory* **48**, 62 (2012).
- [10] E. Shin and D. A. Streit, *Spring equilibrators theory for static balancing of planar pantograph linkages*, *Mechanism and machine theory* **26**, 645 (1991).
- [11] S. R. Deepak and G. Ananthasuresh, *Perfect static balance of linkages by addition of springs but not auxiliary bodies*, *Journal of mechanisms and robotics* **4**, 021014 (2012).
- [12] P.-Y. Lin, W.-B. Shieh, and D.-Z. Chen, *A stiffness matrix approach for the design of statically balanced planar articulated manipulators*, *Mechanism and Machine Theory* **45**, 1877 (2010).
- [13] R. Nathan, *A constant force generation mechanism*, *Journal of Mechanisms, Transmissions, and Automation in Design* **107**, 508 (1985).
- [14] F. L. te Riele, E. E. Hekman, and J. L. Herder, *Planar and spatial gravity balancing with normal springs*, in *ASME 2004 International Design Engineering Technical Conferences and Computers and Information in Engineering Conference* (American Society of Mechanical Engineers, 2004) pp. 415–424.
- [15] F. L. te Riele, J. L. Herder, and E. E. Hekman, *Spatial static gravity balancing with ideal springs*, in *ASME 2004 International Design Engineering Technical Conferences and Computers and Information in Engineering Conference* (American Society of Mechanical Engineers, 2004) pp. 425–432.
- [16] C. M. Gosselin, *Static balancing of spherical 3-dof parallel mechanisms and manipulators*, *The International Journal of Robotics Research* **18**, 819 (1999).
- [17] D. Streit and E. Shin, *Equilibrators for planar linkages*, *Journal of Mechanical Design* **115**, 604 (1993).
- [18] C. M. Gosselin and J. Wang, *Static balancing of spatial six-degree-of-freedom parallel mechanisms with revolute actuators*, *Journal of Field Robotics* **17**, 159 (2000).
- [19] S. R. Deepak and G. Ananthasuresh, *Static balancing of spring-loaded planar revolute-joint linkages without auxiliary links*, in *14th National Conference on Machines and Mechanisms (NaCoMM09)*, NIT, Durgapur, India (2009).

- [20] P.-Y. Lin, W.-B. Shieh, and D.-Z. Chen, *Design of statically balanced planar articulated manipulators with spring suspension*, IEEE Transactions on Robotics **28**, 12 (2011).
- [21] P.-Y. Lin, W.-B. Shieh, and D.-Z. Chen, *Design of a gravity-balanced general spatial serial-type manipulator*, Journal of Mechanisms and Robotics **2**, 031003 (2010).
- [22] P.-Y. Lin, *Design of statically balanced spatial mechanisms with spring suspensions*, Journal of Mechanisms and Robotics **4**, 021015 (2012).
- [23] A. A. Delissen, G. Radaelli, and J. L. Herder, *Design and optimization of a general planar zero free length spring*, Mechanism and Machine Theory **117**, 56 (2017).
- [24] J. Denavit, *A kinematic notation for lower-pair mechanisms based on matrices*. Trans. of the ASME. Journal of Applied Mechanics **22**, 215 (1955).
- [25] F. L. te Riele and J. L. Herder, *Perfect static balance with normal springs*, in *Proceedings of the 2001 ASME Design Engineering Technical Conferences, Pittsburg, PA, Sept (2001)* pp. 9–12.
- [26] C. Kren, *The rolling device of nasir al-din al-tusi in the de spera of nicole oresme?* Isis **62**, 490 (1971).
- [27] E. A. Dijkman, *Motion geometry of mechanisms* (CUP Archive, 1976).

3

DRAMATICALLY DIFFERENT STATES OF STIFFNESS BY OPPOSING CONSTANT FORCE

Stiffness in compliant mechanisms can be dramatically altered and even eliminated entirely by using static balancing. This requires elastic energy to be inserted before operation, which is most often done with an additional device or preloading assembly. Adding such devices contrasts starkly with primary motivations for using compliant mechanisms, such as part count reduction, increased precision and miniaturization. Yet, statically balanced compliant mechanisms with a fully monolithic architecture are rare.

In this paper we introduce two novel statically balanced compliant mechanisms with linear and rotary kinematics that do not require preloading assembly, enabling miniaturization. Static balance is achieved by the principle of opposing constant force and extended to a rotational device by using opposing constant torque mechanisms for the first time. A constant force mechanism based on existing work is used and inspired a novel constant torque mechanism.

A single piece device is obtained by monolithically integrating a bistable switch for preloading, which allows static balance to be turned on and off. The linear device reduces stiffness by 98.5% over 10 mm, has significantly reduced device complexity and doubled relative range of motion from 3.3% to 6.6% compared to the state of the art. The rotary device reduces stiffness by 90.5% over 0.35 rad.

This chapter has been published as a scientific article: P. R. Kuppens, M. A. Bessa, J. L. Herder, and J. B. Hopkins. *Compliant mechanisms that use static balancing to achieve dramatically different states of stiffness.* Journal of Mechanisms and Robotics, 13(2), 2021. doi: 10.1115/1.4049438

3.1. INTRODUCTION

Fully compliant mechanisms (CM) improve upon their multi-component rigid-body counterparts in many respects. Their monolithic nature increases precision and reliability, reduces friction and wear and eliminates assembly which makes them perfect for micro-scale applications in for example MEMS [1–7] and laparoscopic tools [8–11].

However, they store a significant part of the input energy as strain energy, because their functionality arises from deformation of slender segments. This may reduce range of motion, hamper energy efficiency or cause high natural frequencies [12]. This inherent and often undesired stiffness may be compensated for by adding an equal but opposite negative stiffness in parallel.

An isolated mechanism with negative stiffness is unstable and requires some form of preloading. During preloading potential elastic energy is inserted into the device. Upon motion, energy flows out of the unstable negative stiffness part and enters the stable part with positive stiffness, keeping the total elastic potential energy constant. It follows that all internal forces are in sustained static equilibrium. Hence these systems are called statically balanced.

Preloading is often done manually [13, 14] but can also be done as part of the manufacturing process in small scale devices such as MEMS [15]. Manual preloading often relies on a preloading assembly; an external device using for example screw lead. This contrasts starkly with the motivation for using CM in the first place and eliminates any possibility for miniaturization.

Few examples of CM without preloading assembly exist. Among them are a fully compliant gripper [16] and linear stage [17, 18] with on and off switch, a linear stage based on multistable mechanisms [19] and a statically balanced linear stage preloaded once with hooks [20]. Some of the aforementioned examples have relatively complicated geometry, limiting the ratio between device footprint and range of motion. Some use contact between components to ensure preloading and some are not properly constrained. All aforementioned examples only consider rectilinear motion and it is not immediately obvious how a rotational system could be devised.

In this paper we introduce two novel statically balanced fully compliant mechanisms with rectilinear and rotational kinematics that do not require a preloading assembly. In the linear case, static balance is reversibly achieved by the principle of opposing constant force (OCF), first introduced by [17, 18]. We use a constant force mechanism based on the work from [15] resulting in statically balanced compliant mechanism with reduced complexity and improved range of motion compared to [17, 18]. We have expanded the principle of OCF to rotary devices by using opposing constant torque (OCT) mechanisms for the first time. A novel constant torque mechanism is used that is based on the same principles as the constant force mechanism from [15]. A monolithic architecture is achieved by integrating a fully compliant bistable switch for preloading. Toggling the bistable switch allows static balance to be turned on and off, effectively switching between high and low stiffness configurations.

The mechanisms presented may find applications in low-frequency sensor technology [4], low-frequency mechanical energy harvesters [21] and make compliant micro transmission mechanisms more efficient [7, 22]. In addition they may be perfect for protecting sensitive instruments for space applications. Upon launch the high stiffness

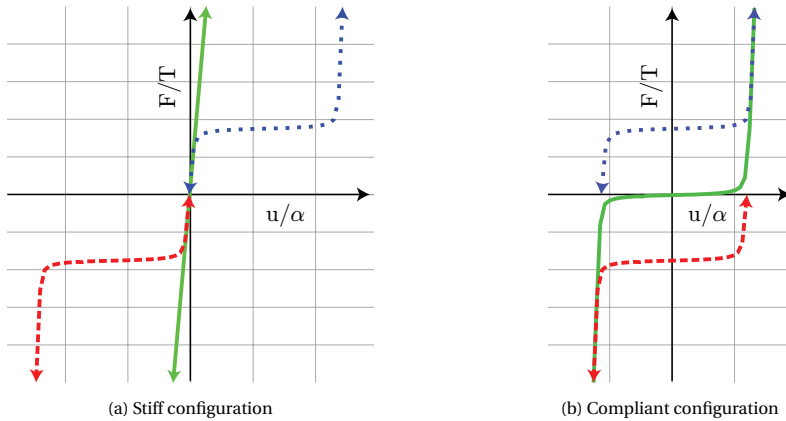


Figure 3.1: Principle of static balance by opposing constant force and torque. (a) Shows force (F) and torque (T) versus deflection (u) and angular displacement (α) in the stiff configuration. (b) Shows the compliant configuration.

provides robustness and protection. Once in orbit, the highly sensitive and compliant state may be activated.

3.2. BALANCING METHOD

Static balancing can be done in two distinctive ways. By far the most common and well known approach is to add a spring with negative stiffness in parallel to the functional positive stiffness part [8, 10, 15, 23]. A second and less frequently used method opposes two constant forces. In a constant force mechanism (CFM) force is constant over some part of its motion domain. By preloading two such mechanisms against each other, the constant forces cancel out resulting in zero force. The only mechanism to exploit this principle of opposing constant force (OCF) for stiffness reduction is reported in [16, 18].

3.2.1. OPPOSING CONSTANT FORCE

A balanced system can be created by preloading two CFMs against each other. A graphical explanation is given in Fig. 3.1. The dashed and dotted curves are force (F) deflection (u) characteristics of two CFMs with their degree of freedom in the opposite direction. If left unconnected, one CFM (dotted) will have positive constant force if moved to the right. The other CFM (dashed) will have negative constant force if moved to the left. By connecting the CFMs in parallel the force deflection can be simply added to uncover the combined behavior. If done in their undeformed state, the high stiffness away from the constant force domain is dominant. The combined stiffness is therefore very high, as shown by the solid line in Fig. 3.1a.

When both CFM are displaced over half their motion domain when unconnected, their stiffness curves essentially slide over each other. By connecting them in this preloaded state, the positive and negative constant force cancel out resulting in the solid curve in Fig. 3.1b. The concept of OCF can be readily extended to rotational devices by considering an opposing constant torque (OCT) mechanism. Connecting two preloaded

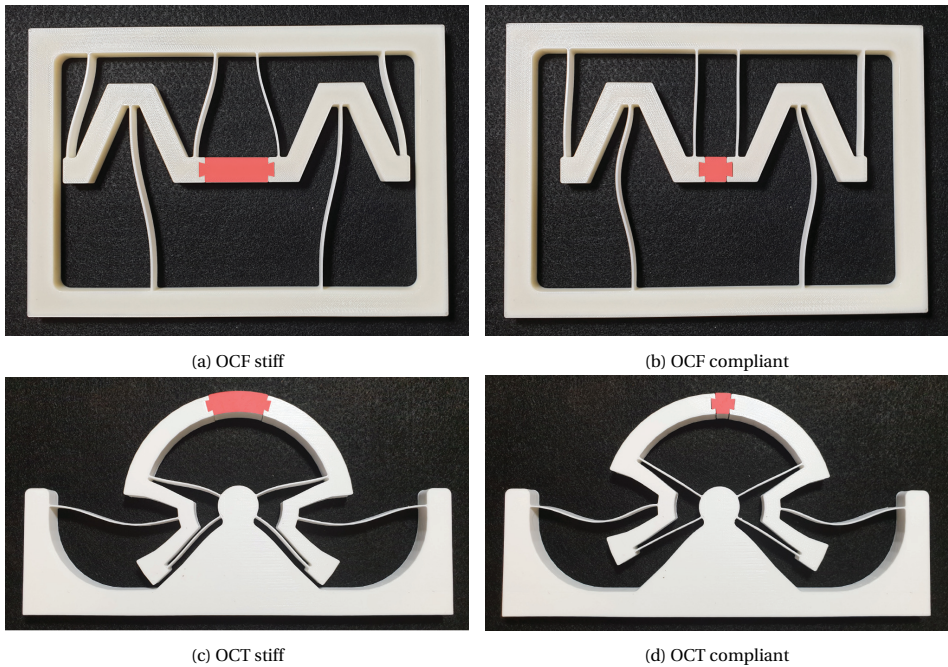


Figure 3.2: Photos of 3D printed OCF and OCT mechanisms with dovetail inserts in stiff and compliant configuration

constant torque mechanisms (CTM) in parallel, cancels the constant torques in exactly the same way. Fabricated mechanisms with OCF and OCT in their stiff and compliant configuration are shown in Fig. 3.2. In each case, the mechanisms are connected with an insert with dovetails. As a monolithic alternative bistable mechanisms will replace these inserts.

3.2.2. CONSTANT FORCE AND TORQUE MECHANISMS

A constant force mechanism (CFM) is created when a positive stiffness is combined in parallel with a bistable mechanism [24, 25]. In [24] and [25] these components can be individually identified. However, in [15] a constant force mechanisms is reported where no such distinction can be made.

It is comprised out of two parallel plate springs, to form a simple linear stage, and an additional plate spring at the bottom, initially overconstraining the system. A thermally induced expansion of all plate springs is used to compute the first buckling mode shape with a linear buckling analysis. The constant force mechanisms is obtained by assuming a scaled version of this shape as new geometry.

Scaling the solution of the buckling analysis allows control over the size of the low stiffness domain and magnitude of the constant force. The length of the plate spring at the bottom (parameters L_{ns} and r_{ns} in Fig. 3.5) allows control over the slope of the low stiffness domain. For short plate springs the slope over the low stiffness range becomes

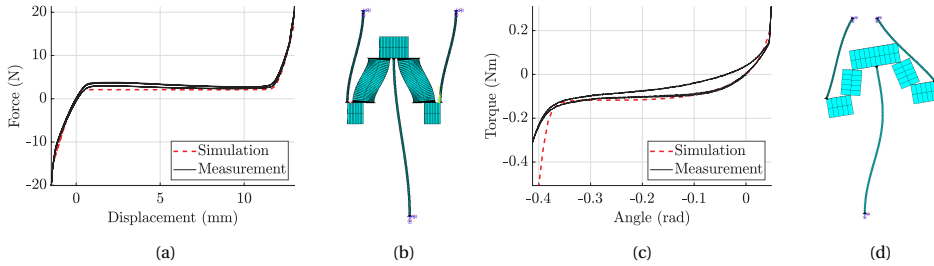


Figure 3.3: Constant force and torque mechanisms. (a) Simulation and measurement of the CFM. (b) Finite element model of CFM. (c) Simulation and measurement of CTM. (d) Finite element model of CTM.

negative and for long plate springs positive [15]. Its length is chosen right where behavior transitions from a negative to positive slope, resulting in minimal stiffness. A simulation and a measurement of the CFM is shown in Fig. 3.3a.

Various CTMs can be found in literature [26, 27]. Both these mechanisms rely on shape optimized radial plate springs with complex geometry. What we propose instead is a slight modification of the CFM from [15]. FACT [28, 29] tells us that an instantaneous center of rotation is created at the point of virtual intersection of two plate springs. Parallel plate springs, which intersect at infinity, will therefore cause rectilinear motion. Rotation is simply obtained by tilting the plate springs inwards, see 3.3d. Constant torque behavior is obtained by computing the first buckling mode shape and assuming a scaled version of this shape to be the new geometry. A simulation and a measurement of the CTM is shown in Fig. 3.3c.

3.2.3. PRELOADING MECHANISMS

A monolithic alternative to the inserts with dovetails from Fig. 3.2 is to use a bistable mechanism. A bistable mechanism has two stable configurations, can stay in either equilibrium indefinitely and can be switched reversibly. One equilibrium (the fabricated configuration) will replace the long insert and the other will replace the short insert.

Many fully compliant bistable mechanisms are reported in literature, both macro- and micro-scale and both translational [30, 31] and rotational [32, 33]. In this paper we will use bistable mechanisms similar to [31] since they are proven to work on micro-scale. The shape of these curved-beam bistable elements is given by

$$w(x) = \frac{h}{2} \left[1 - \cos\left(2\pi \frac{x}{L}\right) \right] \quad (3.1)$$

where h is the amplitude or initial apex of the beam, L the total length and $x \in [0, L]$.

If boundary conditions are infinitely stiff each additional bistable element in parallel adds to an increased magnitude of the bistability. However, since more bistable elements in parallel also increase the force on the boundaries there is a limit to the number of bistable elements in practice. We found that a total number of 3 parallel bistable elements worked well in this design.

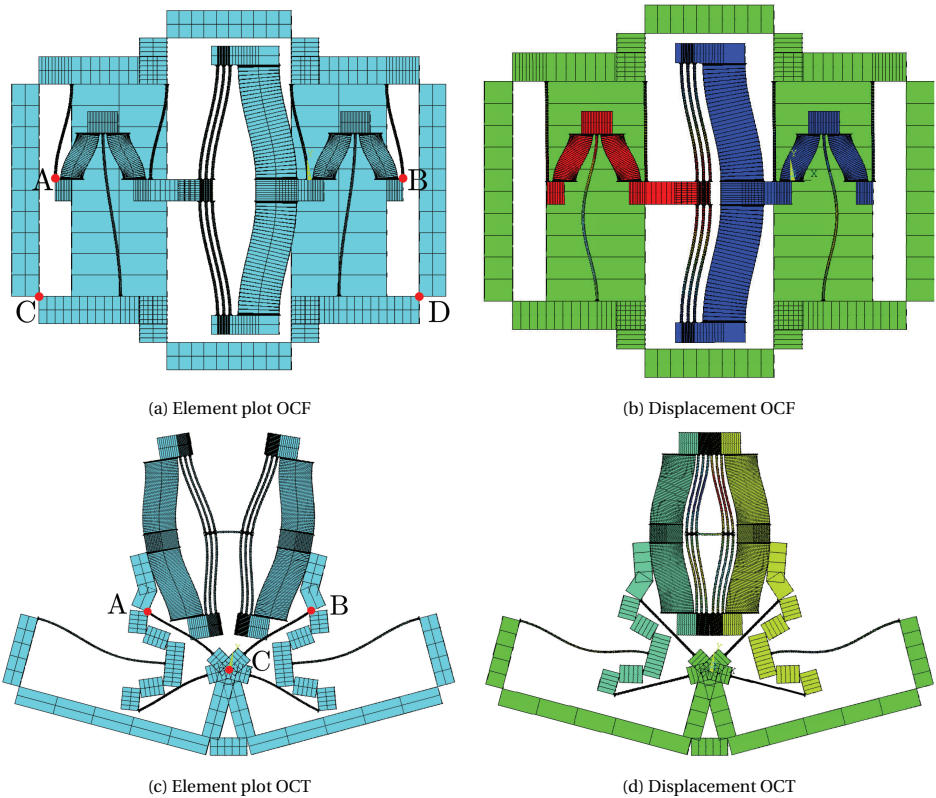


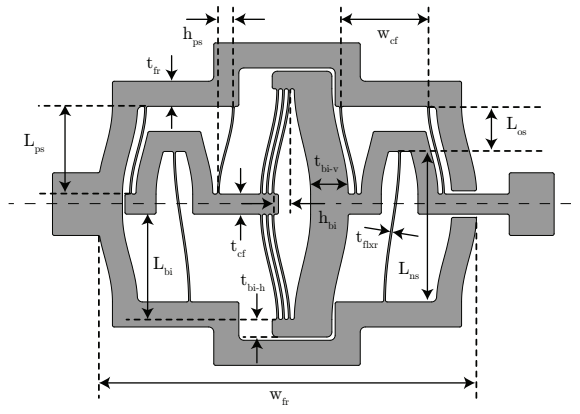
Figure 3.4: Finite element models. (a) Undeformed element plot of ocf mechanism. (b) Displacement solution of OCF mechanism. (c) Undeformed element plot of OCT mechanism. (d) Displacement solution of oct mechanism.

3.2.4. FINITE ELEMENT MODELS

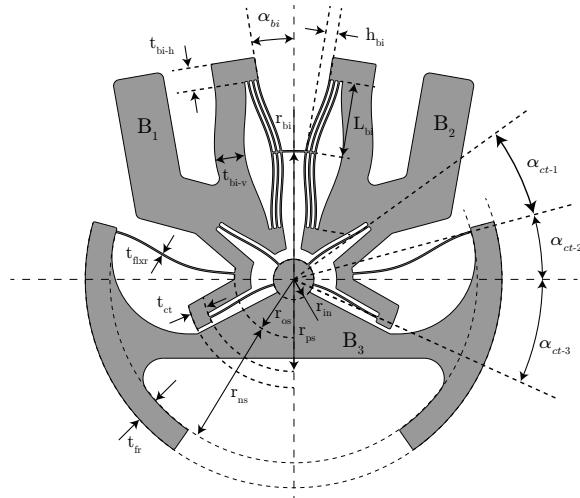
Both the individual CFM and CTM and fully compliant OCF and OCT mechanisms are modeled in ANSYS APDL. A parametric model is built with beam188 elements and all simulations are displacement controlled. A Young's modulus of 3.12 GPa is used with a poisson's ratio of 0.3 [34].

To determine the shape of the CFM and CTM all elements are given an arbitrary coefficient of thermal expansion of $5 \times 10^{-6} \text{ } ^\circ\text{C}^{-1}$. A linear buckling analysis is then performed under a uniform temperature of $1 \text{ } ^\circ\text{C}$ to get the first buckling mode shape. The resulting normalized mode shapes are then scaled and used as undeformed geometry. The CFM are scaled to an amplitude of 6 mm and the CFM to 9.5° . Next bistable mechanisms are constructed, resulting in the geometry given by Fig. 3.4a and Fig. 3.4c.

To simulate post buckling behavior imperfections are required. In each case the first 4 normalized buckling mode shapes are computed and added to the nodal coordinates with a scaling of 0.01. To compute this point C of the OCF mechanism (see Fig. 3.4a) is constrained in all directions, point D is constrained in the y-direction. A unit force is



(a) OCF mechanism



(b) OCT mechanism

Figure 3.5: Annotated CAD drawings with dimensions of (a) the OCF mechanism and (b) the OCT mechanism

applied at points A and B pointing towards each other. For the OCT mechanism A and C are fully constrained while a unit torque is applied at B.

Figures 3.4b and 3.4d show a displacement solution after the bistable switches have been activated and the mechanism is moved to the middle of the motion domain. In both cases this is done by first fully constraining points A and then moving B towards A. Once through the bistability, A is released and B is moved back to its starting position.

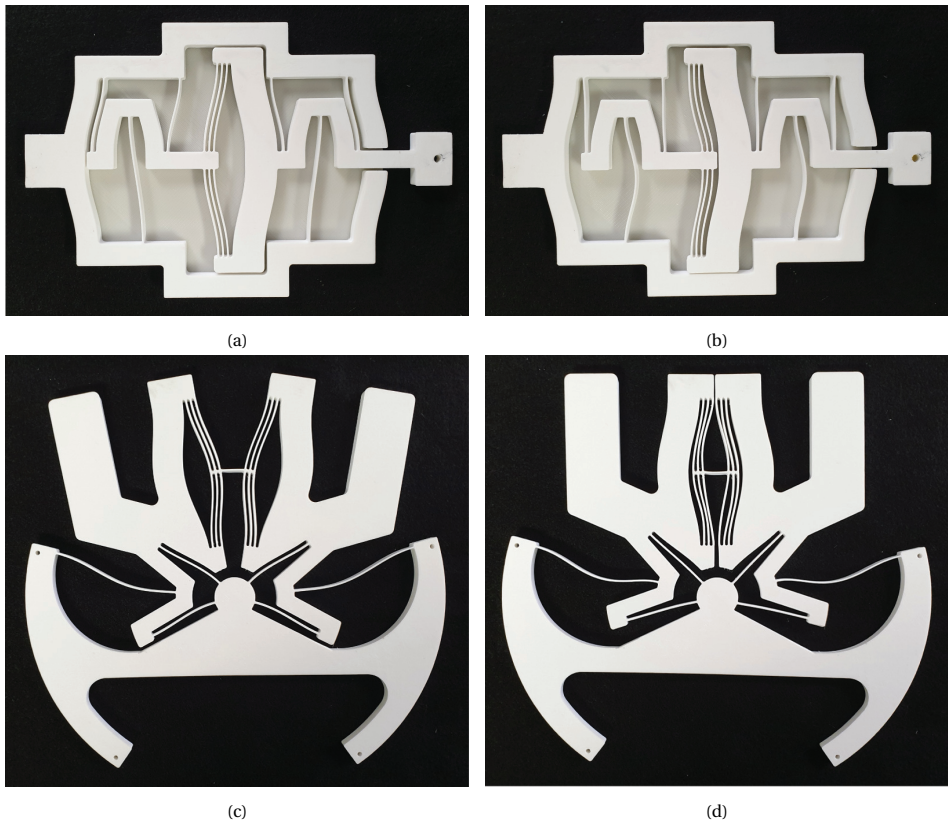


Figure 3.6: Photos of the 3d printed OCF and OCT mechanisms. the OCF mechanism is shown in a (a) stiff and (b) compliant configuration. The OCT mechanism is shown in a (c) stiff and (d) compliant configuration.

3.2.5. FINAL MECHANISM DESIGN AND MANUFACTURING

Dimensions from the parametric model are transferred to a 3D CAD drawing. All mechanisms have a thickness of 7 mm and all plate springs a thickness T_{flxr} of 0.7 mm providing a sufficient aspect ratio for out of plane stiffness. A fillet is added to each corner with radius 0.7 mm to reduce stress concentrations. Big fillets are used for aesthetic purposes.

In each case the length (L_{ps} and $r_{ps} - r_{in}$) of the plate springs of the stage, responsible for the kinematics, are 35 mm long before buckling mode shapes are computed. Since the analysis is linear, the scaled mode shapes will have plate springs that are slightly longer. Annotated CAD drawings of the OCF and OCT mechanisms are shown in Fig. 3.5. The dimensions are given in Tab. 3.1.

The mechanisms are 3D printed by fused deposition modeling (FDM) on a Original Prusa i3 MK3S out of polylactic acid (PLA) with default printer and slicing settings. Isotropic material properties are assumed based on FDM printed PLA with a layer raster angle of 0° [34]. A Young's modulus of 3.12 GPa and an ultimate tensile stress of 50.23 MPa are used with a Poisson's ratio of 0.3.

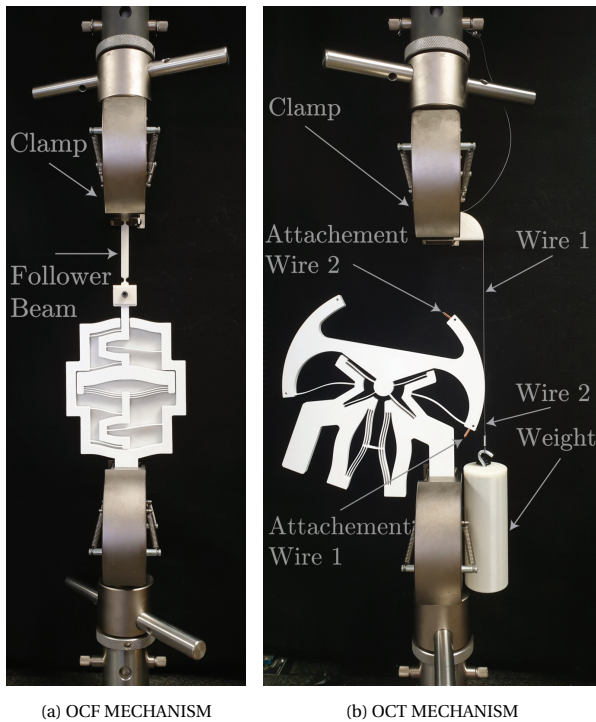


Figure 3.7: An (a) OCF and (b) OCT mechanism clamped in the tensile test bench

3.2.6. MEASUREMENTS

Force deflection measurements are done with an Instron 5966 tensile test bench. All mechanisms are cyclically measured in the motion direction for 5 cycles. Strain rate is 15 mm min^{-1} and force is bounded. An additional follower beam is added between the Instron and the translational device to account for parasitic motion, see Fig. 3.7a. Torque and angular displacement are measured in the same tensile test bench.

A circular arm is attached to the rotational stage centered around the initial center of rotation. Two steel wires run through grooves at the outside of the arm. The wire that runs up is attached to the Instron. The wire that runs down is attached to a 10.2 N weight for preloading, because wires can only pull. Since the radius is known (assumed to be constant), the measured displacement and force can be converted into angular displacement and torque. Both measurements are shown in Fig. 3.8.

Each measurement starts with the mechanism in the stiff configuration. The Instron is used to simultaneously actuate and measure the devices. We first measure the stiff configuration and transition to the compliant state by pushing or pulling through the bistable switches.

Table 3.1: Parameter values as shown in Fig. 3.5

CFM		CTM	
Parameter	Value	Parameter	Value
L_{ps}	35 mm	r_{ps}	45 mm
L_{ns}	60 mm	r_{ns}	62 mm
L_{bi}	42 mm	r_{bi}	63.3 mm
L_{os}	10 mm	r_{in}	10 mm
h_{ps}	6 mm	r_{os}	29.3 mm
h_{bi}	6.5 mm	L_{bi}	37 mm
t_{cf}	8 mm	h_{bi}	5.7 mm
t_{bi-v}	15 mm	t_{ct}	8 mm
t_{bi-h}	7 mm	t_{bi-v}	15 mm
t_{fr}	10 mm	t_{bi-h}	11 mm
t_{flxr}	0.7 mm	t_{fr}	12 mm
w_{cf}	35 mm	t_{flxr}	0.7 mm
w_{fr}	151.2 mm	α_{bi}	9.5°
		α_{ct-1}	20.5°
		α_{ct-2}	15°
		α_{ct-3}	24.5°

3.3. RESULTS

Figure 3.8g shows the force displacement measurement (EXP) and simulation (FEA) of the OCF mechanism transitioning from high to low stiffness. High and low stiffness are indicated with dotted lines, which are obtained by locally fitting the data with least squares. The actuation stiffness is reduced by 98.75 percent from 14.47 N mm^{-1} to -0.18 N mm^{-1} with an absolute range of motion of approximately 10 mm and a relative range of motion of 6.6% with respect to the frame width $w_{fr} = 151.2 \text{ mm}$. Transition by toggling the bistable switch requires 17.71 N as shown by the peak at 2.5 mm.

Figure 3.8h shows the angle moment measurement (EXP) and the simulation (FEA) of the OCT mechanism transitioning from stiff to compliant. The angular actuation stiffness is reduced by 90.5% from $3.99 \text{ N m rad}^{-1}$ to $0.38 \text{ N m rad}^{-1}$ with a range of motion of approximately 0.35 rad. Transition requires two bistable switches to toggle, shown as the two peaks with values of 1.15 N m and 1.26 N m at respectively 0.1 rad and 0.27 rad.

Both simulations are in good agreement with measurements. However, in the rotary mechanism a clear shift and some discontinuities can be observed in the two peaks. Both discrepancies can be explained by repeated contact and release between bodies B_2 and B_3 (see Fig. 3.5b) that is not simulated. In simulation, body B_2 is rotated towards body B_1 while B_1 and B_3 are fully constrained. In measurement however, B_3 is rotated towards B_1 while B_2 is free floating. Because of this, B_2 will have repeated contact and release with body B_3 . The events of contact and release are illustrated in Fig. 3.8a to 3.8f and annotated in Fig. 3.8h.

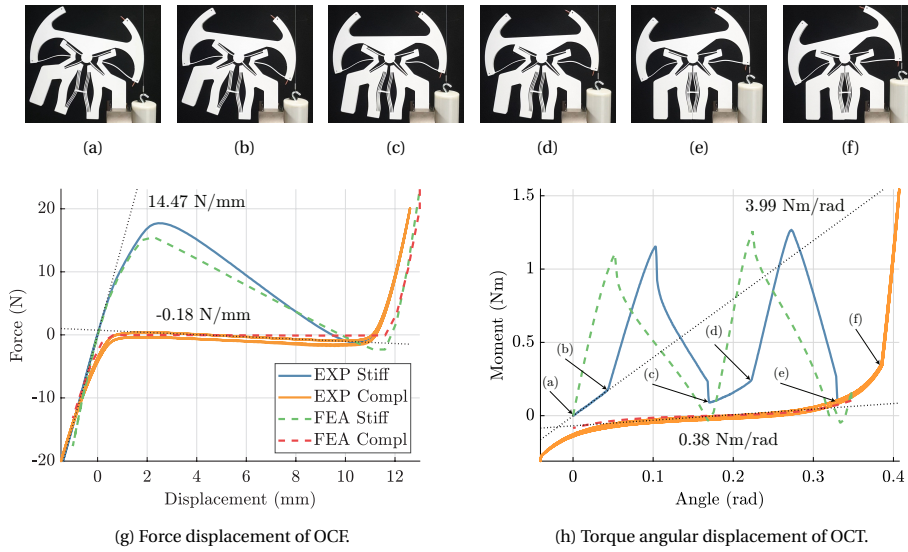


Figure 3.8: Measurement (EXP) and simulation (FEA) results of (g) CFM and (h) CTM mechanisms. In both cases the transition from stiff to compliant is shown. Figures (a) to (f) indicate specific moment of contact and release and correspond to the labels shown in (h). High and low stiffness is indicated with the dotted lines, they are locally fitted to the data with least squares.

3.4. DISCUSSION

We have demonstrated two fully compliant monolithic architectures that have dramatically different states of stiffness. Reversible static balancing is achieved by opposing two constant force and torque mechanisms with bistable mechanisms. We used constant force mechanisms based on [15], but instead of inducing buckling in combination with annealing we directly manufactured the buckling mode shape stress free. The same was done to create a novel constant torque mechanism.

A negative low stiffness for the device with rectilinear motion is reported in Fig. 3.8g and Section. 3.3. The stiffness is negative, because the individual constant force mechanisms display slight negative stiffness themselves in Fig. 3.3a. This is not observed in simulation and is likely caused by manufacturing errors increasing the negative stiffness generated by the long plate spring. By tuning the length of the long plate spring the slope can be increased or decreased even further [15].

For the CM with linear motion we have significantly reduced device complexity and doubled relative range of motion compared to the state of the art [17, 18] while maintaining a stiffness reduction between 98% and 99.5%. The total number of individual plate springs is reduced from 38 to 12 and relative range of motion doubled from 3.3% to 6.6%. Although no device dimensions are mentioned in [17, 18] they are estimated from the reported range of motion and visible clearance. The rotary mechanism is the first of his kind, so no comparison with literature is made.

One can reversibly change between both states of stiffness by switching the multistable mechanisms. However, after the compliant configuration has been entered, it

cannot return to the stiff configuration by manipulating the main stage in a quasi static fashion. Transitioning back requires the constant force and torque mechanisms to be pulled apart by an amount that exceeds the threshold force of the bistable elements. However, this threshold can never be exceeded, because the range of motion of the main stage is limited by the frame. Increased clearance may overcome this.

A relatively large difference in stiffness reduction between the linear and rotary mechanisms is observed, i.e. 98.75 % versus 90.5 %. This is easily understood from Fig. 3.3a and Fig. 3.3c. The more sudden and severe increase in stiffness at the tails of the graph in Fig. 3.3a, make the unpreloaded configuration in the linear case stiffer and hence a more dramatic decrease possible. In addition, the constant force behavior seems more linear compared to the constant torque behavior, making it less likely that two CTM exactly counteract each other when preloaded against each other. Shape optimization may improve our proposed CTM.

In general, the proposed devices may enhance the efficiency of compliant mechanisms, by reducing inherent stiffness in a permanent fashion. More specifically, they may revolutionize low-frequency sensor technology such as accelerometers and gravimeters [4], but also mechanical energy harvesters [21]. In addition they may be fundamentally required to make devices such as compliant transmission mechanisms practically usable [7, 22]. Although the proposed devices are on centimeter scale, their monolithic nature allows micro-manufacturing such as photo-lithography and two-photon stereo lithography [35]. In such micro devices, a low stiffness configuration could be permanently activated by switching the multistable mechanisms with, for example, a probe station or embedded actuators.

3.5. CONCLUSION

In this paper we have demonstrated fully compliant statically balanced mechanisms with rectilinear and rotational kinematics that do not require preloading assembly. They are capable of reversibly reducing linear and angular stiffness by 98.5 % and 90.5 % over 10 mm and 0.35 rad respectively. The mechanism with linear motion significantly reduces device complexity by using 12 plate springs instead of 38 while doubling the relative range of motion compared to the state of the art.

These dramatically different states of stiffness are obtained by preloading two constant force and torque mechanisms against each other with a monolithically integrated bistable switch. Toggling the bistable switch engages and disengages static balance, effectively turning off and on stiffness. A constant force mechanism based on existing literature is used while a new constant torque mechanism is created based on the same principle.

The prototyped devices are on centimeter scale and 3D printed out of polylactic acid (PLA) by fused deposition modeling (FDM). However their monolithic nature, enables miniaturization and micro-manufacturing by photo-lithography and two-photon stereo lithography. In such micro systems the low stiffness configuration can be activated by actuating the main stage once with high force. They may find applications in low-frequency sensor technology, energy harvesting, micro-compliant transmissions or provide robustness of sensitive sensors during launches to space.

REFERENCES

- [1] S. Kota, J. Joo, Z. Li, S. M. Rodgers, and J. Sniegowski, *Design of compliant mechanisms: applications to mems*, Analog integrated circuits and signal processing **29**, 7 (2001).
- [2] H.-W. Huang and Y.-J. Yang, *A mems bistable device with push-on–push-off capability*, Journal of Microelectromechanical Systems **22**, 7 (2012).
- [3] J. Qiu, J. H. Lang, and A. H. Slocum, *A centrally-clamped parallel-beam bistable mems mechanism*, in *Technical Digest. MEMS 2001. 14th IEEE International Conference on Micro Electro Mechanical Systems (Cat. No. 01CH37090)* (IEEE, 2001) pp. 353–356.
- [4] R. Middlemiss, A. Samarelli, D. Paul, J. Hough, S. Rowan, and G. Hammond, *Measurement of the earth tides with a mems gravimeter*, Nature **531**, 614 (2016).
- [5] R. Luharuka and P. J. Hesketh, *Design of fully compliant, in-plane rotary, bistable micromechanisms for mems applications*, Sensors and Actuators A: Physical **134**, 231 (2007).
- [6] M. Mayyas and H. Stephanou, *Electrothermoelastic modeling of mems gripper*, Microsystem Technologies **15**, 637 (2009).
- [7] D. Farhadi Machekposhti, J. L. Herder, and N. Tolou, *Frequency doubling in elastic mechanisms using buckling of microflexures*, Applied Physics Letters **115**, 143503 (2019).
- [8] A. Stapel and J. L. Herder, *Feasibility study of a fully compliant statically balanced laparoscopic grasper*, in *ASME 2004 International Design Engineering Technical Conferences and Computers and Information in Engineering Conference* (American Society of Mechanical Engineers, 2004) pp. 635–643.
- [9] N. Tolou and J. L. Herder, *Concept and modeling of a statically balanced compliant laparoscopic grasper*, in *ASME 2009 International Design Engineering Technical Conferences and Computers and Information in Engineering Conference* (American Society of Mechanical Engineers, 2009) pp. 163–170.
- [10] D. J. de Lange, M. Langelaar, and J. L. Herder, *Towards the design of a statically balanced compliant laparoscopic grasper using topology optimization*, in *ASME 2008 International Design Engineering Technical Conferences and Computers and Information in Engineering Conference* (American Society of Mechanical Engineers, 2008) pp. 293–305.
- [11] J. Lassooij, N. Tolou, G. Tortora, S. Caccavaro, A. Menciassi, and J. Herder, *A statically balanced and bi-stable compliant end effector combined with a laparoscopic 2dof robotic arm*, Mechanical Sciences, 3 (2), 2012 (2012).
- [12] N. Tolou, J. Gallego, and J. Herder, *Statically balanced compliant micro mechanisms (sb-mems): A breakthrough in precision engineering*, Mikroniek **50**, 20 (2010).

- [13] F. L. te Riele and J. L. Herder, *Perfect static balance with normal springs*, in *Proceedings of the 2001 ASME Design Engineering Technical Conferences*, Pittsburg, PA, Sept (2001) pp. 9–12.
- [14] F. M. Morsch and J. L. Herder, *Design of a generic zero stiffness compliant joint*, in *ASME 2010 International Design Engineering Technical Conferences and Computers and Information in Engineering Conference* (American Society of Mechanical Engineers, 2010) pp. 427–435.
- [15] P. R. Kuppens, J. L. Herder, and N. Tolou, *Permanent stiffness reduction by thermal oxidation of silicon*, *Journal of Microelectromechanical Systems* **28**, 900 (2019).
- [16] P. J. Pluimers, N. Tolou, B. D. Jensen, L. L. Howell, and J. L. Herder, *A compliant on/off connection mechanism for preloading statically balanced compliant mechanisms*, in *ASME 2012 International Design Engineering Technical Conferences and Computers and Information in Engineering Conference* (American Society of Mechanical Engineers, 2012) pp. 373–377.
- [17] P. Pluimers, *Design for specified stiffness in precision engineering*, Ph.D. thesis, TU Delft, Delft University of Technology (2012).
- [18] N. Tolou, *Statically balanced compliant mechanisms for mems and precision engineering*, Ph.D. thesis, PhD Thesis, Delft University of Technology, Delft, the Netherlands (2012).
- [19] G. Chen and S. Zhang, *Fully-compliant statically-balanced mechanisms without prestressing assembly: concepts and case studies*, *Mech. Sci* **2**, 169 (2011).
- [20] M. Barel, D. F. Machekposhti, J. Herder, N. Tolou, and M. Sitti, *Permanent preloading by acceleration for statically balancing mems devices*, in *2018 International Conference on Reconfigurable Mechanisms and Robots (ReMAR)* (IEEE, 2018) pp. 1–11.
- [21] M. Han, Q. Yuan, X. Sun, and H. Zhang, *Design and fabrication of integrated magnetic mems energy harvester for low frequency applications*, *Journal of Microelectromechanical Systems* **23**, 204 (2014).
- [22] D. F. Machekposhti, J. L. Herder, G. Sémon, and N. Tolou, *A compliant micro frequency quadrupler transmission utilizing singularity*, *Journal of Microelectromechanical Systems* **27**, 506 (2018).
- [23] K. Hoetmer, J. L. Herder, and C. J. Kim, *A building block approach for the design of statically balanced compliant mechanisms*, in *ASME 2009 International Design Engineering Technical Conferences and Computers and Information in Engineering Conference* (American Society of Mechanical Engineers, 2009) pp. 313–323.
- [24] Q. Xu, *Design of a large-stroke bistable mechanism for the application in constant-force micropositioning stage*, *Journal of Mechanisms and Robotics* **9**, 011006 (2017).

- [25] N. Tolou, P. Pluimers, B. D. Jensen, S. Magleby, L. Howell, and J. L. Herder, *Constant force micro mechanism out of carbon nanotube forest*, in *Proceedings of the 12th euspen International Conference Stockholm–Jun* (2011).
- [26] C.-W. Hou and C.-C. Lan, *Functional joint mechanisms with constant-torque outputs*, *Mechanism and Machine Theory* **62**, 166 (2013).
- [27] H. Nair Prakashah and H. Zhou, *Synthesis of constant torque compliant mechanisms*, *Journal of Mechanisms and Robotics* **8** (2016).
- [28] J. B. Hopkins and M. L. Culpepper, *Synthesis of multi-degree of freedom, parallel flexure system concepts via freedom and constraint topology (fact)–part i: Principles*, *Precision Engineering* **34**, 259 (2010).
- [29] J. B. Hopkins and M. L. Culpepper, *Synthesis of multi-degree of freedom, parallel flexure system concepts via freedom and constraint topology (fact). part ii: Practice*, *Precision Engineering* **34**, 271 (2010).
- [30] S. A. Zirbel, K. A. Tolman, B. P. Trease, and L. L. Howell, *Bistable mechanisms for space applications*, *PloS one* **11**, e0168218 (2016).
- [31] J. Qiu, J. H. Lang, and A. H. Slocum, *A curved-beam bistable mechanism*, *Journal of microelectromechanical systems* **13**, 137 (2004).
- [32] L. Berntsen, D. H. Gosenshuis, and J. L. Herder, *Design of a compliant monolithic internally statically balanced four-bar mechanism*, in *ASME 2014 International Design Engineering Technical Conferences and Computers and Information in Engineering Conference* (American Society of Mechanical Engineers, 2014) pp. V05AT08A040–V05AT08A040.
- [33] R. Luharuka and P. J. Hesketh, *A bistable electromagnetically actuated rotary gate microvalve*, *Journal of Micromechanics and Microengineering* **18**, 035015 (2008).
- [34] C. Casavola, A. Cazzato, V. Moramarco, and C. Pappalettere, *Orthotropic mechanical properties of fused deposition modelling parts described by classical laminate theory*, *Materials & design* **90**, 453 (2016).
- [35] S. Chizari, L. A. Shaw, and J. B. Hopkins, *Simultaneous printing and deformation of microsystems via two-photon lithography and holographic optical tweezers*, *Materials Horizons* **6**, 350 (2019).

4

BINARY STIFFNESS MECHANISMS FOR MECHANICAL DIGITAL MACHINES

We introduce two essential building blocks with binary stiffness for mechanical digital machines. The large scale fully compliant mechanisms have rectilinear and rotational kinematics and use a new V-shaped negative stiffness structure to create two extreme states of stiffness by static balancing. The use of a mechanical bistable switch allows us to toggle between near-zero-stiffness and high-stiffness states, effectively turning off and on stiffness. A stiffness reduction of 98.8% and 99.9% is achieved for linear and rotary motion over a range of 13.3% (20 mm) and 0.4 rad (23°) respectively. Stiffness states can be reversibly changed by toggling the mechanical switch, or irreversibly by actuating the stage.

These binary stiffness mechanisms could set the stage for a new type of mechanical logic, adaptive and programmable metamaterials and other types of digital mechanical devices. Practical mechanical digital machines and materials require miniaturized and easily micro-manufactured components. We have therefore carefully considered scalability by integrating all required structures into a planar and monolithic architecture. This allows miniaturization and fabrication with conventional surface-micro-machining and additive manufacturing such as photolithography, two-photon lithography and fused deposition modeling.

This chapter has been published as a scientific article: P. R. Kuppens, M. A. Bessa, J. L. Herder, and J. B. Hopkins. *Monolithic binary stiffness building blocks for mechanical digital machines*. Extreme Mechanics Letters, 42:101120, 2021. doi:10.1016/j.eml.2020.101120

4.1. INTRODUCTION

Mechanisms with variable stiffness have the ability to change their stiffness over a range of values. This can be done actively and passively in a multitude of different ways. For example, electrostatically, piezoelectrically, thermally and mechanically [1]. They are commonly used in microelectromechanical system (MEMS) [1], vibration isolation [2] and variable impedance actuators [3] for example for human friendly robots [4] and robot fingers [5].

More recently variable stiffness is used to create metamaterials where controlled changes in local stiffness enable adaptive bulk properties. Examples are architected materials with multiple Poisson's ratios [6], variable stiffness [7, 8] as well as robotic materials with programmable properties [9–11]. These materials exploit variable stiffness created by geometry [6], phase change [7], fluid channels [8] or by active feedback control of thermal actuators [9–11].

Instead of continuously variable stiffness mechanisms, binary stiffness mechanisms may be used. A binary stiffness mechanism can only change its stiffness between two different values that ideally have an infinite ratio. Two extremely different states of stiffness can be created by static balancing [12, 13]. It uses negative stiffness caused by preloading to counteract a positive stiffness elsewhere in the mechanism. Even though the upper limit of the stiffness is limited by bulk properties, the ratio between the upper and lower limit can be infinite if the lower limit is reduced to zero stiffness [14]. Zero stiffness can be achieved if negative stiffness is designed to be equal but opposite to the positive stiffness. Different techniques may be used such as preloading in postbuckling [15] or up to the critical buckling load [16], zero-free-length springs [17, 18] and curved surfaces [19, 20], see [21, 22] for an extensive overview. Binary states of stiffness can thus be achieved by enabling and disabling static balancing by engaging and disengaging preloading, effectively turning the stiffness off and on.

Programmable zero stiffness based on multistable mechanisms [23–25] has been previously reported in [26]. However, the reported device is not of a digital nature, since the flexible programming inputs are analog and require a sustained holding force to create both low or high stiffness. In addition, the zero stiffness (and zero force) monostable behavior is obtained in prebuckling which limits the low stiffness to small deflections, i.e. the zero-stiffness is instantaneous.

If binary stiffness mechanisms are used in large numbers, they may approach continuous properties and enable new types of digital mechanical machines and metamaterials [27]. Examples could include novel computing systems based on mechanical logic that could potentially be build on the molecular level [28, 29] and provide more robustness in extremely harsh environments such as high radiation, because they lack a significant electromagnetic signature [28, 30, 31].

In most existing mechanical logic systems each Boolean state is associated with a predefined displacement of the mechanism, such as the location of a dial. Examples are rigid body logic [32], multi-stable micro-flexural additively manufactured logic gates [31] and micro-flexural NOT and AND gates [33, 34]. All are examples of static logic, however in most modern computing systems dynamic logic is used because of its superior performance [35]. In dynamic logic a clocked signal is used to evaluate the state after input signals are applied, as opposed to static logic where the output is immediately available.

An example of mechanical dynamic logic is rod logic [36]. It uses sliding rods that block or unblock each other to create logic states in terms of potential sliding motion evaluated by an oscillating mechanical signal [28]. We can regard the blocked and unblocked configurations as states of high and low stiffness such that one rod logical element is essentially a binary stiffness mechanism. A more recent example modulates the linear resonance frequency of an arch beam resonator electrothermally to perform various 2-bit and 3-bit logic operations [37].

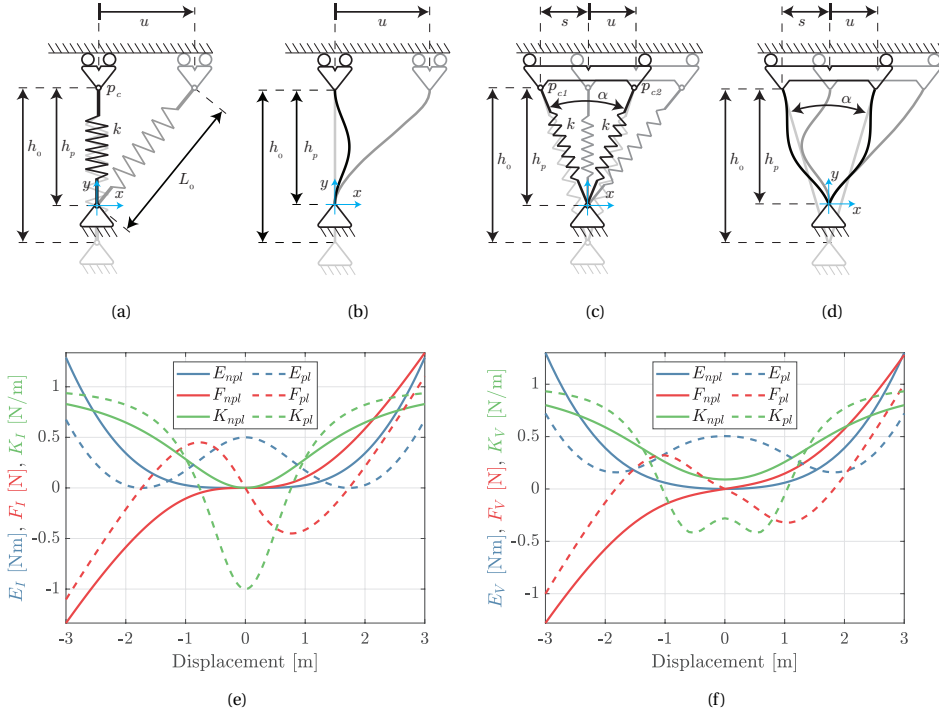


Figure 4.1: (a) Shows a canonical example of a negative stiffness mechanisms and (b) its compliant equivalent. In (c) the single spring has been decomposed into two springs in a V-shaped orientation and (d) shows its compliant equivalent. (e) Shows the potential energy E_I , force F_I and stiffness K_I with and without preloading. (f) Shows the potential energy E_V , force F_V and stiffness K_V with and without preloading. Solid lines refer to cases without preloading while dashed lines with preloading.

Practical mechanical digital machines and materials require binary stiffness elements to be easily miniaturized and micro-manufactured, since large numbers are needed in a small volume. It is therefore essential to avoid any form of assembly and account for micro-manufacturing techniques like photolithography and upcoming 3D printing technologies such as two-photon lithography [38]. Necessary properties are therefore a fully monolithic and planar architecture which can be created by exploiting the flexibility of materials in what is known as a compliant mechanism.

In this paper we present two fully compliant binary stiffness mechanisms with large deflection linear and rotary motion based on static balancing. A new V-shaped negative

stiffness structure is introduced that maximizes the ratio between high and low stiffness. The preloading required for negative stiffness is controlled by a reversible bistable switch independent of primary mobility. Kinematics are dictated by two parallel or angled plate springs.

The method for obtaining binary stiffness is first explained with compression springs and extended to a fully compliant mechanism by replacing them with buckled beams. Final mechanism dimensions are iteratively tuned by hand. This semi-autonomous process still relies on domain knowledge from the designer, but a fully automated process relying on machine learning and optimization could be used, as demonstrated in a different context [39]. Examples of design optimizations with this method include a super-compressible micro-structure [40] and an ultra-thin shell structure [41].

We have validated the designs by prototyping decimeter scale prototypes and performing mechanical tests. It is plausible that the presented designs can be scaled down to micro or nanoscale, because all required structures are planar and fully compliant and are integrated in a monolithic and planar device that avoids assembly. A scaled down version would rely on identical principles and only requires redesign for different material properties. The mechanisms are stress free and in their high stiffness configuration when manufactured. Low stiffness is enabled when the bistable switch is engaged. This can be done irreversibly by actuating the main stage, or reversibly by toggling the bistable switch itself.

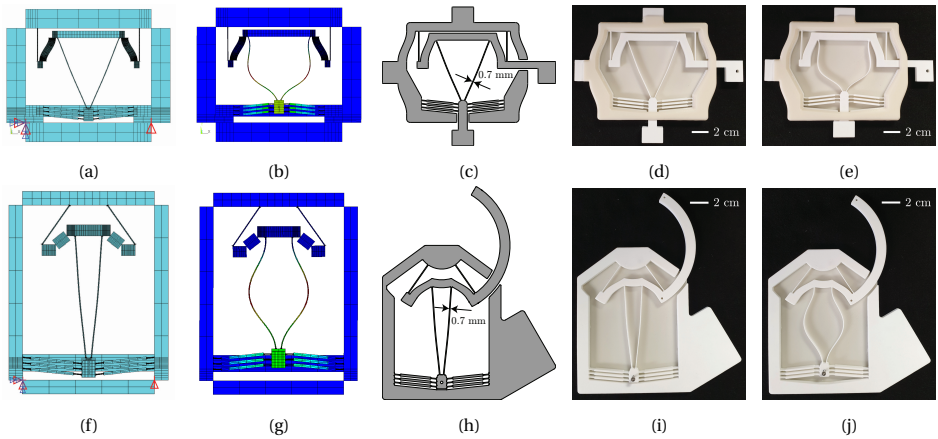


Figure 4.2: (a, f) Finite element plots of the linear and rotary devices, (b, g) displacement solutions, (c, h) CAD drawings, (d, i) photos of the prototypes in the stiff state and (e, j) the prototype in the compliant state.

4.2. METHOD FOR BINARY STIFFNESS

Binary variable stiffness is achieved by enabling and disabling static balancing. Static balancing is an approach to keep the potential energy in a system constant and consequently all net conservative forces and stiffness are zero [42]. It is achieved by adding an elastic structure with negative stiffness in parallel to the functional part with positive stiffness. If negative and positive stiffness exactly oppose, a net zero stiffness results. The

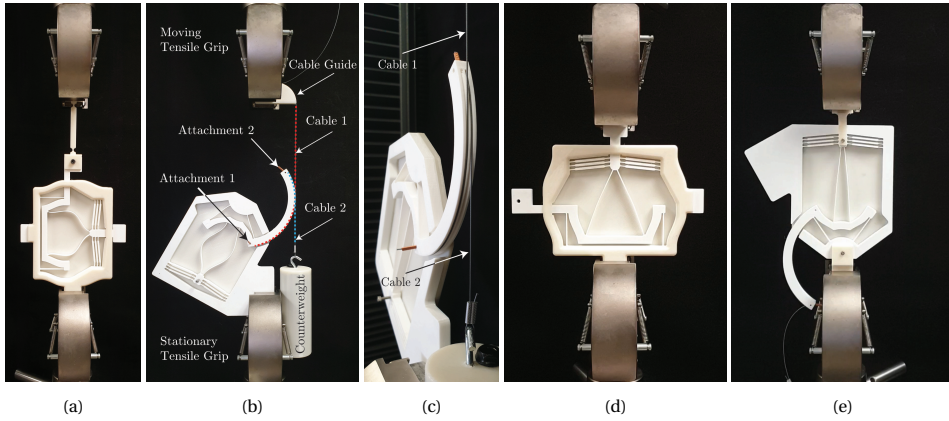


Figure 4.3: (a) Shows the measurement setup of the linear device. (b) Shows the measurement setup for the rotary device with cable system and preloading weight. (c) Shows how the cables run along grooves in the circular arm of the rotary device. Bistability is measured for the linear device as shown in (d) and for the rotary device as shown in (e).

required negative stiffness is a consequence of releasing elastic potential energy previously inserted by preloading. Therefore, we can toggle between balanced zero stiffness and unbalanced positive stiffness by engaging and disengaging preloading.

In its simplest form, negative stiffness is created by axially preloading an ordinary compression spring from its initial length L_0 to L_p as shown in figure 4.1a, note that $L_0 = h_0$ and $L_p = h_p$. This works for both linear [13, 20] and rotational motion [43] of the cart. The potential energy of the spring as function of cart displacement u is given by:

$$E_I(u) = \frac{1}{2}k \left(\sqrt{(\mathbf{p}_c^T \cdot \mathbf{p}_c)} - L_0 \right)^2 \quad (4.1)$$

where k is the spring stiffness, $\mathbf{p}_c = [u, h_p]^T$ the cart location, h_p the spring length at $u = 0$ and L_0 the initial length of the spring. Force and stiffness at the cart are given by:

$$F_I(u) = \frac{dE_I(u)}{du}, \quad K_I(u) = \frac{d^2E_I(u)}{du^2} \quad (4.2)$$

E_I , F_I and K_I are shown in figure 4.1e with $k = 1$, without preloading ($h_0 = h_p = 2$) and with preloading ($h_0 = 2, h_p = 1$). It shows that for large values of u the stiffness K_I converges to k independent of preloading, i.e. $\lim_{u \rightarrow \infty} K_I(u, h_p) = k$. Also if the spring is stretched by large amounts ($h_p \gg L_0$) K_I converges to k independent of u , i.e. $\lim_{h_p \rightarrow \infty} K_I(u, h_p) = k$. However, since compliant mechanisms have limited stroke, we are interested in behaviour around $u = 0$. And since negative stiffness is only created by compressing the spring, we are only interested in values of $0 \leq h_p \leq L_0$.

The stiffness K_I at $u = 0$ is given by:

$$K_I(u = 0) = -\frac{k(L_0 - h_p)}{h_p}, \quad h_p \geq 0 \quad (4.3)$$

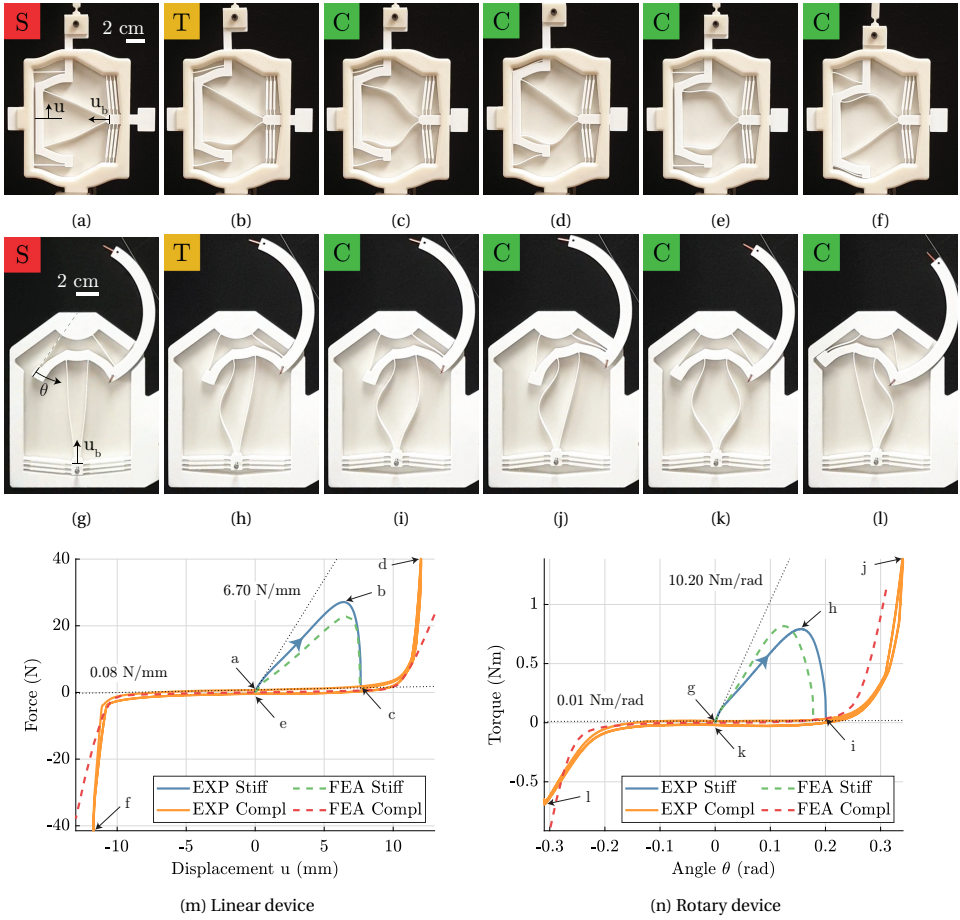


Figure 4.4: A chronological photo sequence of the linear device (a-f) and the rotary device (g-l) taken during measurement. Three different states can be identified, a stable stiff configuration in red (S), an unstable transition state in which the bistable switch is toggling in yellow (T) and a stable compliant configuration in green (C). The different mechanism configurations are correspondingly indicated in the force deflection diagrams from (m) and (n) with both measurements (EXP) and finite element simulations (FEA). The stiffness in both stiff and compliant states around the equilibrium position are shown as dotted lines.

which shows the stiffness $K_I(u=0) = 0$ when $h_p = L_0$ and becomes more negative as h_p decreases, i.e.

$$\lim_{h_p \rightarrow 0} K_I(u=0) = -\infty \quad (4.4)$$

This demonstrates the ability to turn negative stiffness on and off by controlling the preloading distance h_p . A compliant analogue is obtained by axially preloading a continuum plate in post buckling [13] see figure 4.1b, possibly with various boundary conditions such as pinned-pinned [20], clamped-pinned [15, 44] and clamped-clamped [44].

A preloaded continuum plate is in theory able to reduce the combined stiffness to zero, because the amount of negative stiffness can be tuned by changing its geometry

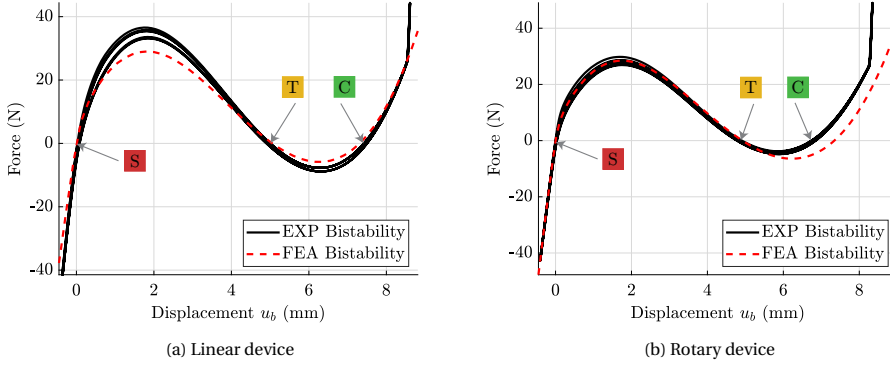


Figure 4.5: Measurement (EXP) and simulation (FEA) results of the bistable switch are in good agreement for both the linear (a) and rotary (b) device. All equilibrium points are associated with the different states, stiff (S), compliant (C) and toggle (T), as shown in figure 4.4.

[15]. In practice, perfectly matching positive and negative stiffness is hard and affected by modeling errors, manufacturing tolerances and nonlinear effects. It is therefore desirable to maximize the high stiffness state, because stiffness states become more distinguishable. This is done by increasing the stiffness without preloading around $u = 0$, while keeping the ability to generate negative stiffness when preloaded. Increasing the high stiffness state is done by decomposing the compression spring in a V-shaped configuration as shown in figure 4.1c.

The potential energy of the V-shaped springs on a cart is given by:

$$E_V = \frac{1}{2}k \left(\sqrt{\mathbf{p}_{c1}^T \mathbf{p}_{c1}} - L_0 \right)^2 + \frac{1}{2}k \left(\sqrt{\mathbf{p}_{c2}^T \mathbf{p}_{c2}} - L_0 \right)^2 \quad (4.5)$$

where k is spring stiffness, the initial length $L_0 = \sqrt{h_0^2 + s^2}$, $\mathbf{p}_{c1} = [u - s, h_p]^T$, $\mathbf{p}_{c2} = [u + s, h_p]^T$, with $s \geq 0$ half the distance between the springs on the cart. Force F_V and stiffness K_V are computed by differentiation of E_V as in equation (4.2). They are shown in figure 4.1f with $k = 0.5$, $\alpha = 35^\circ$, without preloading $h_p = h_0 = 2$ and with preloading $h_0 = 2$ and $h_p = s\sqrt{2}$.

The stiffness K_V at $u = 0$ is given by:

$$K_V(u = 0) = 2k \left(\frac{s^2}{L_p^2} \left(1 + \frac{L_0 - L_p}{L_p} \right) - \frac{L_0 - L_p}{L_p} \right) \quad (4.6)$$

where $L_p = \sqrt{h_p^2 + s^2}$. The minimum stiffness (i.e. max negative stiffness) achievable by preloading is determined by finding the roots of $\frac{dK_V(u=0)}{dh_p}$, which are given by $h_p = \pm s\sqrt{2}$. Substituting the positive value $h_p = s\sqrt{2}$ in equation (4.6) yields:

$$\min_{h_p} K_V(u = 0) = 2k - \frac{4kL_0}{3\sqrt{3}s}, \quad s \geq 0 \quad (4.7)$$

which shows that unbounded negative stiffness can be obtained for $\frac{2\sqrt{3}}{9}L_0 > s \geq 0$. On the other hand, the stiffness without preloading ($L_0 = L_p$) is given by

$$K_V(u=0) = 2k \frac{s^2}{L_p^2}, \quad s \geq 0 \quad (4.8)$$

which is positive for any nonzero s . Equations (4.7) and (4.8) show that two springs placed in a V-shaped configuration can generate negative stiffness when preloaded yet have positive stiffness without preloading.

A compliant analogue is shown in figure 4.1d which will be given exact dimension in an iterative design process. The advantage over a single or multiple vertical beams is the increased stiffness when not preloaded. Values for its negative and positive stiffness depend on geometry and preloading. Too much negative stiffness results in a combined system with negative stiffness. Too little negative stiffness and combined system stiffness is positive. Since we can continuously shift between these two behaviours, by changing for example V-shaped beam length or the geometry of the stage beams, an optimum can be found that results in zero combined stiffness.

4.2.1. CONTROLLING THE PRELOADING

Preloading is easily controlled by hand in many macro-scale statically balanced mechanisms, for example during assembly [45] or by using linear stages [13, 46]. On the micro-scale, preloading becomes a significant challenge because manual handling is difficult which makes assembly economically unjustifiable. Proposed monolithic solutions include shaking [47] and residual film stress [48], however these methods are irreversible. Reversible examples exist that make use of multistable compliant mechanisms (MSCMs) [12, 49–51]. However, their direction of preloading is aligned with the intended mechanical mobility and can therefore not be controlled independently.

We propose to attach a MSCM to the negative stiffness device from figure 4.1d. Since the direction of preloading and generated negative stiffness are perpendicular, preloading can be engaged and disengaged independently from the primary mobility. MSCMs are easily made fully compliant, because multistability is most often caused by snap-through of buckled beams [52]. This enables a monolithic system integration and hence miniaturization. Since only two stable states are required for binary stiffness, a bistable mechanism is used.

A myriad of bistable mechanisms are reported in literature both on large scale and small scale. Among them are chevron type bistable mechanisms [53, 54], a curved beam bistable mechanism [55], a tensural bistable micro-mechanism [56], two-link in-plane bistable micro-mechanisms [57, 58], bistable mechanisms based on slider mechanisms [59, 60] and a rotational bistable mechanism [61].

Although the above bistable mechanisms are passive devices, active implementations are equally common. These microrelays can switch between stable states by means of actuation, but do not require actuation to stay in either state. A wide variety of actuator-mechanism combinations is reported in literature, including rotary bistable mechanisms [62]. Most microrelays rely for their bistability on a set of at least two curved or chevron style beams centrally connected to prevent rotation. Actuation is most commonly done by chevron type thermal actuators [63–67], but also with bending beam

thermal actuators [68, 69], external electromagnetic actuation [62, 70, 71], a combination of thermal and electromagnetic [72] and electrostatic comb actuators [73–76].

In our large scale design a passive chevron type bistable mechanism is implemented. Maximizing the force required to switch equilibrium is important, because a higher threshold force means more negative stiffness can be created. To do this multiple chevron bistable beams are used in parallel. Also, lumped compliance is used instead of distributed compliance to further increase the severity of the bistability by thickening the beams in the middle [53]. The exact dimensions are determined by iterative design in combination with a parametric finite element model.

4.2.2. MODELING, DESIGN AND FABRICATION

Parametric finite element models of the proposed mechanisms are built in Ansys APDL out of two-node beam elements (beam188) based on Timoshenko beam theory, a linear shape function and a rectangular cross section. The models are iteratively to create devices that approximate zero stiffness over a maximized range of motion. In practice this entails a design cycle in which a grid search is performed to determine dimensions, simulations ran and prototypes manufactured to validate simulations and build intuition for manufacturing and materials.

The model carefully takes into account the geometry of the flexible elements and models elastic boundary conditions. Supporting back and front plates are added to reinforce the frame, which is needed due to the gate allowing the main stage to exit the frame. The devices are grounded by constraining the motion of the lower left corner in all directions and the motion of the lower right corner in the vertical direction as shown in figures 4.2a and 4.2f.

In order to compute post buckling behaviour, imperfections are added to the bistable mechanisms [77]. A linear buckling analysis is first performed by adding a unit force on the bistable element. Next the first five normalized buckling mode shapes are added to the undeformed geometry with an amplitude of 0.01. Only then the bistable element is connected to the negative stiffness structure. An element plot and a deformation plot in post buckling are shown in figures 4.2a, 4.2b, 4.2f and 4.2g.

All plate springs have a beam thickness of 0.7 mm and are 7 mm high. The plate springs of the stages have a length of 35 mm and are angled at 70° for the rotational stage. The angle α between the negative stiffness plate springs in the rectilinear case is 45° and they are 75 mm long. In case of rotation the plate springs are 89 mm long and the angle α between them is 10°. All negative stiffness plate springs have the shape of a cosine with an amplitude of 0.7 mm, making sure they will buckle outwards. Inwards buckling is prevented, because this may cause the V-shaped plate springs to touch each other and challenge performance by introducing for example friction and unwanted deformations. To save space, they are placed as far up as possible. The systems are designed for a range of motion of ± 10 mm and ± 0.2 rad ($\pm 11.5^\circ$) for translation and rotation. A fillet of at least 0.7 mm is added to each corner.

In both cases an identical bistable switch is used. Its parameters are chosen such that it can stay in either configuration without effort, while it maintains the load provided by the negative stiffness from the V-shaped plate spring. To create sufficient transition force within material limits, three parallel beams are used instead of two, similar to [53]. The

flexures have a total length of 43 mm where the thick part is 31 mm long and 2 mm wide. The offset between the outside of the flexures and the shuttle in the middle is 4.5 mm, such that elastic equilibrium is found when preloaded between 7 mm and 8 mm, see figure 4.5.

The mechanisms are 3D printed by fused deposition modeling (FDM) on a Original Prusa i3 MK3S out of polylactic acid (PLA) with default settings. Isotropic material properties are assumed based on FDM printed PLA with a layer raster angle of 0° [78]. A Young's modulus of 3.12 GPa and an ultimate tensile stress of 50.23 MPa are used with a Poisson's ratio of 0.3. A CAD drawing and photos of the fabricated linear and rotary devices are shown in figures 4.2c to 4.2e and 4.2h to 4.2j.

4.2.3. MEASUREMENTS

Force deflection measurements are done with an Instron 5966 tensile test bench. Transition from high to low stiffness is measured by actuating the linear stage bounded by a force of 40 N at a strain rate of 15 mm min^{-1} . Parasitic motion is accounted for by adding a follower beam between the clamp and the mechanism, see figure 4.3a. Gravity is not accounted for and bistability is measured the same way, see figures 4.3d and 4.3e.

By using a cable system, the rotational mechanism is measured on the same tensile test bench. Since cables cannot be loaded in compression, the combined system is preloaded in tension by a 10.2 N counterweight. Two cables run along grooves on an extended circular arm with a radius of 68.8 mm, see figures 4.3b and 4.3c. Cable one (in red in figure 4.3b) runs from attachment one to the moving tensile grip that is attached to the force sensor. Cable two (in blue) runs from attachment two to the counterweight that preloads the cablesystem. A constant arm radius is assumed to compute the moments and angles from the measured forces and displacements.

4.3. RESULTS

Measurement (EXP) and finite element simulation (FEA) results for the main stage, both linear and rotary, are shown in figure 4.4 and for the bistable switches in figure 4.5. All force displacement measurements are in good agreement with simulations.

The chronological photo sequences from figures 4.4a to 4.4f and figures 4.4g to 4.4l associate each mechanism state with a point on the force deflection graphs from figures 4.4m and 4.4n. Three different mechanism configurations can be identified. The first (red S) is a stable configuration with high stiffness in which the device is manufactured and thus stress free, see figures 4.4a and 4.4g. The second (yellow T) is unstable in which the bistable switch is toggling, see figures 4.4b and 4.4h. In this instantaneous state of transition the device is neither on nor off, but at the onset of snap through to either configurations. In the third configuration (green C) the bistable switch is toggled and the V-shaped plate spring buckled, it is highly compliant and also stable as shown in figures 4.4c to 4.4f and 4.4i to 4.4l. The configurations are also indicated in the force deflection characteristics of the bistable switch from figures 4.5a and 4.5b.

A dramatic reduction in stiffness can be readily observed. Around the equilibrium position at (0,0), translational stiffness is reduced by 98.8% from 6.70 Nmm^{-1} to 0.08 Nmm^{-1} and rotational stiffness is reduced by 99.9% from 10.20 Nmm^{-1} to 0.01 Nmm^{-1} .

$0.01 \text{ N m rad}^{-1}$. These states of stiffness differ by two and three orders of magnitude with a factor of 84 and 1020 respectively.

By pulling on the main stage a force and torque of 27.11 N and 0.79 N m are required to transition. However, if the bistable switch is directly actuated a force of 36.56 N and 29.81 N are required. By design the mechanisms cannot transition back from compliant to stiff by actuating the main stage, because the V-shaped plate spring cannot overcome the threshold force of the bistable switch. However, it is possible by directly actuating the bistable switch with -8.87 N and -4.82 N for the linear and rotary device, as can be seen in figures 4.5a and 4.5b

In each case the low stiffness domain is in accordance with the intended range of motion. In the linear case, low stiffness stretches 20 mm and by taking into account a 150 mm frame width (without the clamp brackets) this results in a relative range of motion of 13.3%. The range of motion in the stiff configuration is approximately 14 mm or 9.3%. In the rotary case, the low stiffness domain stretches 0.4 rad (23°) and high stiffness approximately 0.32 rad (18°). Beyond these ranges stiffness ramps up quickly and a slight discrepancy between measurement and simulation is observed. These differences may be attributed to issues such as parasitic motion and contact between frame and stage. Contact is also clearly observed at the right side of the curves in figure 4.5.

The discrepancy observed between the measurements and simulations of the stiff parts of figure 4.4, but also that of the bistability in figure 4.5, may be attributed to frame geometry. The stiffness of the boundary conditions of a bistable mechanisms are extremely important. If boundaries are too compliant, the bistable behavior may even disappear. Since we have only coarsely approximated the frame geometry, it would be possible to have a discrepancy between the modeled and actual frame stiffness, but the simulations show good agreement with the experiments.

4.4. CONCLUSION

In this paper we have introduced two mechanisms with binary stiffness that are essential building blocks for mechanical digital machines. Extreme states of linear and angular stiffness are achieved by enabling and disabling static balancing by engaging and disengaging preloading. A new V-shaped negative stiffness plate spring is used successfully to maximize the ratio between the two states of stiffness by controlling its preloading with a bistable switch.

Linear stiffness is reduced by 98.8% from 6.70 N mm^{-1} to 0.08 N mm^{-1} over an absolute range of motion of 20 mm and a relative range of motion of 13.3%. Angular stiffness is reduced by 99.9% from $10.20 \text{ N m rad}^{-1}$ to $0.01 \text{ N m rad}^{-1}$ over a range of 0.4 rad or 23° . This is a difference in stiffness by two and three orders of magnitude with a factor 84 and 1020 respectively. This is a significant improvement over previously reported statically balanced mechanisms with stiffness reduction factors of 46, -21.2 , -4.2 and 3.3 with corresponding reduction percentages 97.8%, -104.7% , -123% and 70% from [45, 47, 48, 79].

A force of 27.11 N and a torque of 0.79 N m on the main stage is required to transition irreversibly from high to low stiffness. Reversible transition is possible by actuating the bistable switch with 36.56 N and -8.87 N in the linear device, and 29.81 N and -4.82 N in the angular device. All measurements are in good agreement with simulations.

The presented mechanisms could set the stage for innovative mechanical logical systems, adaptive and programmable metamaterials and other types of mechanical digital machines. To enable miniaturization and micro-fabrication required for such machines we have carefully considered scalability. All required components are integrated in a single piece device that can be fabricated with conventional surface-micro-machining or upcoming micro 3D printing technologies. Although the introduced devices are passive, scaling down presents opportunities for actuator implementation by replacing the passive bistable switch with an active micro-relay commonly reported in scientific literature about MEMS.

REFERENCES

- [1] M. de Laat, H. P. Garza, J. Herder, and M. Ghatkesar, *A review on in situ stiffness adjustment methods in mems*, Journal of Micromechanics and Microengineering **26**, 063001 (2016).
- [2] C. B. Churchill, D. W. Shahan, S. P. Smith, A. C. Keefe, and G. P. McKnight, *Dynamically variable negative stiffness structures*, Science advances **2**, e1500778 (2016).
- [3] B. Vanderborght, A. Albu-Schäffer, A. Bicchi, E. Burdet, D. G. Caldwell, R. Carloni, M. Catalano, O. Eiberger, W. Friedl, G. Ganesh, *et al.*, *Variable impedance actuators: A review*, Robotics and autonomous systems **61**, 1601 (2013).
- [4] D. Hyun, H. S. Yang, J. Park, and Y. Shim, *Variable stiffness mechanism for human-friendly robots*, Mechanism and Machine Theory **45**, 880 (2010).
- [5] T. Morita and S. Sugano, *Design and development of a new robot joint using a mechanical impedance adjuster*, in *Proceedings of 1995 IEEE International Conference on Robotics and Automation*, Vol. 3 (IEEE, 1995) pp. 2469–2475.
- [6] K. Kim, H. Heo, and J. Ju, *A mechanism-based architected material: A hierarchical approach to design poisson's ratio and stiffness*, Mechanics of Materials **125**, 14 (2018).
- [7] R. Poon and J. B. Hopkins, *Phase-changing metamaterial capable of variable stiffness and shape morphing*, Advanced Engineering Materials , 1900802 (2019).
- [8] Y. Shan, M. Philen, A. Lotfi, S. Li, C. E. Bakis, C. D. Rahn, and K.-W. Wang, *Variable stiffness structures utilizing fluidic flexible matrix composites*, Journal of Intelligent Material Systems and Structures **20**, 443 (2009).
- [9] Y. Song, P. C. Dohm, B. Haghpanah, A. Vaziri, and J. B. Hopkins, *An active microarchitected material that utilizes piezo actuators to achieve programmable properties*, Advanced Engineering Materials **18**, 1113 (2016).
- [10] L. A. Shaw and J. B. Hopkins, *An actively controlled shape-morphing compliant microarchitected material*, Journal of Mechanisms and Robotics **8** (2016).

- [11] C. Luo, Y. Song, C. Zhao, S. Thirumalai, I. Ladner, M. A. Cullinan, and J. B. Hopkins, *Design and fabrication of a three-dimensional meso-sized robotic metamaterial with actively controlled properties*, *Materials Horizons* **7**, 229 (2020).
- [12] P. J. Pluimers, N. Tolou, B. D. Jensen, L. L. Howell, and J. L. Herder, *A compliant on/off connection mechanism for preloading statically balanced compliant mechanisms*, in *ASME 2012 International Design Engineering Technical Conferences and Computers and Information in Engineering Conference* (American Society of Mechanical Engineers, 2012) pp. 373–377.
- [13] K. Hoetmer, J. L. Herder, and C. J. Kim, *A building block approach for the design of statically balanced compliant mechanisms*, in *ASME 2009 International Design Engineering Technical Conferences and Computers and Information in Engineering Conference* (American Society of Mechanical Engineers, 2009) pp. 313–323.
- [14] S. Groothuis, R. Carloni, and S. Stramigioli, *A novel variable stiffness mechanism capable of an infinite stiffness range and unlimited decoupled output motion*, in *Actuators*, Vol. 3 (Multidisciplinary Digital Publishing Institute, 2014) pp. 107–123.
- [15] J. van Eijk and J. F. Dijkstra, *Plate spring mechanism with constant negative stiffness*, *Mechanism and Machine Theory* **14**, 1 (1979).
- [16] H. Zhao, D. Han, L. Zhang, and S. Bi, *Design of a stiffness-adjustable compliant linear-motion mechanism*, *Precision Engineering* **48**, 305 (2017).
- [17] R. Nathan, *A constant force generation mechanism*, *Journal of Mechanisms, Transmissions, and Automation in Design* **107**, 508 (1985).
- [18] J. L. Herder, *Energy-free Systems; Theory, conception and design of statically balanced spring mechanisms* (2001).
- [19] Y. Liu, D.-J. Li, D.-p. Yu, J.-g. Miao, and J. Yao, *Design of a curved surface constant force mechanism*, *Mechanics Based Design of Structures and Machines* **45**, 160 (2017).
- [20] S. Park and T. Luu, *Techniques for optimizing parameters of negative stiffness*, *Proceedings of the Institution of Mechanical Engineers, Part C: Journal of Mechanical Engineering Science* **221**, 505 (2007).
- [21] P. Wang and Q. Xu, *Design and modeling of constant-force mechanisms: A survey*, *Mechanism and Machine Theory* **119**, 1 (2018).
- [22] M. Schenk and S. D. Guest, *On zero stiffness*, *Proceedings of the Institution of Mechanical Engineers, Part C: Journal of Mechanical Engineering Science* , 0954406213511903 (2013).
- [23] G. Chen, Q. T. Aten, S. Zirbel, B. D. Jensen, and L. L. Howell, *A tristable mechanism configuration employing orthogonal compliant mechanisms*, *Journal of Mechanisms and Robotics* **2** (2010).

- [24] G. Chen, Y. Gou, and A. Zhang, *Synthesis of compliant multistable mechanisms through use of a single bistable mechanism*, *Journal of Mechanical Design* **133** (2011).
- [25] D. Younesian and M.-R. Alam, *Multi-stable mechanisms for high-efficiency and broadband ocean wave energy harvesting*, *Applied energy* **197**, 292 (2017).
- [26] M. Zanaty and S. Henein, *Programmable constant-force multistable mechanisms*, in *International Design Engineering Technical Conferences and Computers and Information in Engineering Conference*, Vol. 51807 (American Society of Mechanical Engineers, 2018) p. V05AT07A002.
- [27] A. Ion, L. Wall, R. Kovacs, and P. Baudisch, *Digital mechanical metamaterials*, in *Proceedings of the 2017 CHI Conference on Human Factors in Computing Systems* (ACM, 2017) pp. 977–988.
- [28] R. C. Merkle, *Two types of mechanical reversible logic*, *Nanotechnology* **4**, 114 (1993).
- [29] J. S. Hall, *Nanocomputers and reversible logic*, *Nanotechnology* **5**, 157 (1994).
- [30] P. Bergstrom, T. Tamagawa, and D. Polla, *Design and fabrication of micromechanical logic elements*, in *IEEE Proceedings on Micro Electro Mechanical Systems, An Investigation of Micro Structures, Sensors, Actuators, Machines and Robots*. (IEEE, 1990) pp. 15–20.
- [31] Y. Song, R. M. Panas, S. Chizari, L. A. Shaw, J. A. Jackson, J. B. Hopkins, and A. J. Pascall, *Additively manufacturable micro-mechanical logic gates*, *Nature communications* **10**, 882 (2019).
- [32] A. Sharma, W. S. Ram, and C. Amarnath, *Mechanical logic devices and circuits*, in *14th National Conference on Machines and Mechanisms (NaCoMM-09)*, Durgapur, India, Dec (2009) pp. 17–18.
- [33] A. Modi, P. S. Gandhi, H. Shah, and S. G. Singh, *Design, analysis and fabrication of microflexural not gate*, in *ASME 2007 International Mechanical Engineering Congress and Exposition* (American Society of Mechanical Engineers Digital Collection, 2007) pp. 501–508.
- [34] A. Modi, H. Shah, C. Amarnath, P. Gandhi, S. Singh, and R. Rashmi, *Design, analysis and fabrication of a microflexural and gate*, in *13th National Conference on Mechanisms and Machines (NaCoMM-07)*, Bangalore, India, Dec (2007) pp. 12–13.
- [35] T. J. Thorp, G. S. Yee, and C. M. Sechen, *Design and synthesis of dynamic circuits*, *IEEE Transactions on Very Large Scale Integration (VLSI) Systems* **11**, 141 (2003).
- [36] K. E. Drexler, *Rod logic and thermal noise in the mechanical nanocomputer*, in *Proc. Third Int. Symp. on Molecular Electronic Devices* (1988).
- [37] M. A. A. Hafiz, L. Kosuru, and M. I. Younis, *Microelectromechanical reprogrammable logic device*, *Nature communications* **7**, 1 (2016).

- [38] S. Chizari, L. A. Shaw, and J. B. Hopkins, *Simultaneous printing and deformation of microsystems via two-photon lithography and holographic optical tweezers*, *Materials Horizons* **6**, 350 (2019).
- [39] M. Bessa, R. Bostanabad, Z. Liu, A. Hu, D. W. Apley, C. Brinson, W. Chen, and W. K. Liu, *A framework for data-driven analysis of materials under uncertainty: Countering the curse of dimensionality*, *Computer Methods in Applied Mechanics and Engineering* **320**, 633 (2017).
- [40] M. A. Bessa, P. Glowacki, and M. Houlder, *Bayesian machine learning in metamaterial design: fragile becomes supercompressible*, *Advanced Materials* **31**, 1904845 (2019).
- [41] M. Bessa and S. Pellegrino, *Design of ultra-thin shell structures in the stochastic post-buckling range using bayesian machine learning and optimization*, *International Journal of Solids and Structures* **139**, 174 (2018).
- [42] J. A. Gallego and J. L. Herder, *Criteria for the static balancing of compliant mechanisms*, in *ASME 2010 International Design Engineering Technical Conferences and Computers and Information in Engineering Conference* (American Society of Mechanical Engineers, 2010) pp. 465–473.
- [43] J. Zhang, A. D. Shaw, M. Amoozgar, M. I. Friswell, and B. K. Woods, *Bidirectional torsional negative stiffness mechanism for energy balancing systems*, *Mechanism and Machine Theory* **131**, 261 (2019).
- [44] J. F. Dijkstra, *A study of some aspects of the mechanical behaviour of cross-spring pivots and plate spring mechanisms with negative stiffness*, (1979).
- [45] F. M. Morsch and J. L. Herder, *Design of a generic zero stiffness compliant joint*, in *ASME 2010 International Design Engineering Technical Conferences and Computers and Information in Engineering Conference* (American Society of Mechanical Engineers, 2010) pp. 427–435.
- [46] L. Berntsen, D. H. Gosenshuis, and J. L. Herder, *Design of a compliant monolithic internally statically balanced four-bar mechanism*, in *ASME 2014 International Design Engineering Technical Conferences and Computers and Information in Engineering Conference* (American Society of Mechanical Engineers, 2014) pp. V05AT08A040–V05AT08A040.
- [47] M. Barel, D. F. Machekposhti, J. Herder, N. Tolou, and M. Sitti, *Permanent preloading by acceleration for statically balancing mems devices*, in *2018 International Conference on Reconfigurable Mechanisms and Robots (ReMAR)* (IEEE, 2018) pp. 1–11.
- [48] P. R. Kuppens, J. L. Herder, and N. Tolou, *Permanent stiffness reduction by thermal oxidation of silicon*, *Journal of Microelectromechanical Systems* **28**, 900 (2019).
- [49] P. Pluimers, *Design for specified stiffness in precision engineering*, (2012).

- [50] G. Chen and S. Zhang, *Fully-compliant statically-balanced mechanisms without prestressing assembly: concepts and case studies*, *Mech. Sci* **2**, 169 (2011).
- [51] N. Tolou, P. Estevez, and J. L. Herder, *Collinear-type statically balanced compliant micro mechanism (sb-cmm): experimental comparison between pre-curved and straight beams*, in *ASME 2011 International Design Engineering Technical Conferences and Computers and Information in Engineering Conference* (American Society of Mechanical Engineers, 2011) pp. 113–117.
- [52] G. Chen, Y. Gou, and L. Yang, *Research on multistable compliant mechanisms: The state of the art*, in *Proceedings of the 9th International Conference on Frontiers of Design and Manufacturing* (2010) pp. 1–5.
- [53] S. A. Zirbel, K. A. Tolman, B. P. Trease, and L. L. Howell, *Bistable mechanisms for space applications*, *PloS one* **11**, e0168218 (2016).
- [54] B. D. Jensen, M. B. Parkinson, K. Kurabayashi, L. L. Howell, and M. S. Baker, *Design optimization of a fully-compliant bistable micro-mechanism*, in *Proceedings of ASME IMECE*, Vol. 2 (2001) pp. 2931–2937.
- [55] J. Qiu, J. Lang, and A. Slocum, *A curved-beam bistable mechanism*, *Microelectromechanical Systems*, *Journal of* **13**, 137 (2004).
- [56] D. L. Wilcox and L. L. Howell, *Fully compliant tensural bistable micromechanisms (ftbm)*, *Journal of Microelectromechanical Systems* **14**, 1223 (2005).
- [57] B. D. Jensen, L. L. Howell, and L. G. Salmon, *Introduction of two-link in-plane, bistable compliant mems*, in *Proceeding of the 1998 ASME Design Engineering Technical Conferences, DETC98/MECH-5837* (1998).
- [58] B. Jensen, L. Howell, and L. Salmon, *Design of two-link, in-plane, bistable compliant micro-mechanisms*, *Journal of Mechanical Design* **121**, 416 (1999).
- [59] B. D. Jensen, *Identification of macro-and micro-compliant mechanism configurations resulting in bistable behavior*, (2003).
- [60] B. D. Jensen and L. L. Howell, *Bistable configurations of compliant mechanisms modeled using four links and translational joints*, *Journal of Mechanical Design* **126**, 657 (2004).
- [61] R. Luharuka and P. J. Hesketh, *Design of fully compliant, in-plane rotary, bistable micromechanisms for mems applications*, *Sensors and Actuators A: Physical* **134**, 231 (2007).
- [62] R. Luharuka and P. J. Hesketh, *A bistable electromagnetically actuated rotary gate microvalve*, *Journal of Micromechanics and Microengineering* **18**, 035015 (2008).
- [63] H.-W. Huang and Y.-J. Yang, *A mems bistable device with push-on–push-off capability*, *Journal of Microelectromechanical Systems* **22**, 7 (2012).

- [64] B.-T. Liao, H.-H. Shen, H.-H. Liao, and Y.-J. Yang, *A bi-stable 2x2 optical switch monolithically integrated with variable optical attenuators*, Optics express **17**, 19919 (2009).
- [65] T. Gomm, L. Howell, and R. Selfridge, *In-plane linear displacement bistable microrelay*, Journal of Micromechanics and Microengineering **12**, 257 (2002).
- [66] C. Lee and C.-Y. Wu, *Study of electrothermal v-beam actuators and latched mechanism for optical switch*, Journal of Micromechanics and Microengineering **15**, 11 (2004).
- [67] M. S. Baker and L. L. Howell, *On-chip actuation of an in-plane compliant bistable micromechanism*, Journal of microelectromechanical systems **11**, 566 (2002).
- [68] J. Qiu, J. H. Lang, A. H. Slocum, and A. C. Weber, *A bulk-micromachined bistable relay with u-shaped thermal actuators*, Journal of Microelectromechanical Systems **14**, 1099 (2005).
- [69] J. Qui, J. H. Lang, A. H. Slocum, and R. Strumpler, *A high-current electrothermal bistable mems relay*, in *The Sixteenth Annual International Conference on Micro Electro Mechanical Systems, 2003. MEMS-03 Kyoto. IEEE* (IEEE, 2003) pp. 64–67.
- [70] J. S. Ko, M. G. Lee, J. S. Han, J. S. Go, B. Shin, and D.-S. Lee, *A laterally-driven bistable electromagnetic microrelay*, ETRI journal **28**, 389 (2006).
- [71] D.-A. Wang, H.-T. Pham, and Y.-H. Hsieh, *Dynamical switching of an electromagnetically driven compliant bistable mechanism*, Sensors and Actuators A: Physical **149**, 143 (2009).
- [72] A. Cao, J. Kim, and L. Lin, *Bi-directional electrothermal electromagnetic actuators*, Journal of Micromechanics and Microengineering **17**, 975 (2007).
- [73] R. A. Receveur, C. R. Marxer, R. Woering, V. C. Larik, and N.-F. de Rooij, *Laterally moving bistable mems dc switch for biomedical applications*, Microelectromechanical Systems, Journal of **14**, 1089 (2005).
- [74] M. Freudenreich, U. Mescheder, and G. Somogyi, *Simulation and realization of a novel micromechanical bi-stable switch*, Sensors and Actuators A: Physical **114**, 451 (2004).
- [75] J. Casals-Terre, A. Fargas-Marques, and A. M. Shkel, *Snap-action bistable micromechanisms actuated by nonlinear resonance*, Journal of microelectromechanical systems **17**, 1082 (2008).
- [76] H. N. Kwon, I.-H. Hwang, and J.-H. Lee, *A pulse-operating electrostatic microactuator for bi-stable latching*, Journal of Micromechanics and Microengineering **15**, 1511 (2005).
- [77] A. Dunning, N. Tolou, P. Pluimers, L. Kluit, and J. Herder, *Bistable compliant mechanisms: corrected finite element modeling for stiffness tuning and preloading incorporation*, Journal of Mechanical Design **134** (2012).

- [78] C. Casavola, A. Cazzato, V. Moramarco, and C. Pappalettere, *Orthotropic mechanical properties of fused deposition modelling parts described by classical laminate theory*, *Materials & design* **90**, 453 (2016).
- [79] A. Lamers, J. A. G. Sánchez, and J. L. Herder, *Design of a statically balanced fully compliant grasper*, *Mechanism and machine theory* **92**, 230 (2015).

5

PERMANENT STIFFNESS REDUCTION BY THERMAL OXIDATION OF SILICON

Stiffness in compliant micro mechanisms can negatively affect performance. Current methods for stiffness reduction in micro electro mechanical systems (MEMS) consume power, have a large footprint or are relatively complex to manufacture. In this paper stiffness is reduced by static balancing. A building block commonly used for stiffness reduction in large scale compliant mechanisms is made compatible with MEMS. Preloading required to create negative stiffness is obtained from residual film stress by thermal oxidation of silicon. Instead of buckling a plate spring by moving its end points, a SiO₂ film 1900 nm to 2500 nm thick will stretch micro-beams 24 μm wide, while the end points are fixed.

To show efficacy of our method, the building block is coupled with a simple linear stage. However, the building block can readily be combined with other compliant micro mechanisms to reduce their stiffness. Statically balanced MEMS will enable novel designs in low-frequency sensor technology, low-frequency energy harvesting and pave the way to autonomous micro-robotics. We show a stiffness reduction of a factor 9 to 46. The balancing effect remained after SiO₂ removal, due to plastic deformation of the beams.

This chapter has been published as a scientific article: P. R. Kuppens, J. L. Herder, and N. Tolou. *Permanent stiffness reduction by thermal oxidation of silicon*. Journal of Microelectromechanical Systems, 28(5):900–909, 2019. doi: 10.1109/JMEMS.2019.2935379

5.1. INTRODUCTION

Compliant mechanisms (CM) move due to deformation of slender segments. They are a necessity rather than a design choice for micro electro mechanical systems (MEMS), because CMs can be monolithic [1] and assembly is economically unjustifiable [2]. Even though CMs have many advantages over conventional mechanisms (e.g. increased precision, increased reliability, reduced wear and simplified manufacturing [3]) a disadvantage is that they store a significant part of the input energy as strain energy due to stiffness [4]. This may affect the input-output relation with an insufficient travel range, a low energy efficiency and a high natural frequency [5, 6].

Stiffness in MEMS can be reduced by active methods such as electrostatic actuation, piezo electric actuation and joule heating [7]. However, these methods consume power, have a large footprint and manufacturing complexity is relatively high. A passive alternative is static balancing (SB) [6].

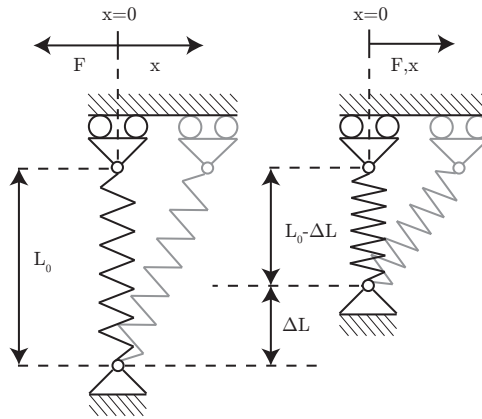


Figure 5.1: Balancer with negative stiffness used for static balancing, comprised of a compression spring with free length L_0 on a cart. In the unloaded configuration (left), displacement of the cart results in a returning force to the stable equilibrium at $x = 0$. If preloaded a distance ΔL , displacement of the cart results in a force away from the unstable equilibrium at $x = 0$, i.e. negative stiffness.

In a statically balanced system the potential energy is kept constant over the entire range of motion, instead of in just one or multiple positions [8]. A balancer (e.g. the mechanism in Fig. 5.1) is responsible for counteracting all elastic forces generated by the functional mechanism, ensuring a sustained static equilibrium. It is essentially a mechanisms with opposing (negative) stiffness in parallel to a functional mechanism.

Negative stiffness (NS) mechanisms may have different forms [9–12], but they all require some kind of embedded potential energy. An inverted pendulum for example, requires to be put upright. Compliant mechanisms with negative stiffness, require flexible elements to be preloaded in postbuckling [13].

Preloading in large scale CMs is relatively straightforward by displacing the end points of plate springs. Literature shows plenty of examples [14–18]. However, preloading on micro-scale becomes a significant challenge since physical handling of micro structures with high precision and without causing damage is difficult [19]. Even though

several concepts have been developed to circumvent preloading assembly, no methods are available for introducing the required potential energy to move the device into the statically balanced domain [19–21].

Statically balanced compliant micro mechanisms may find applications in low-frequency sensor technology [22, 23], low-frequency energy harvesting devices [24, 25] or compliant micro transmission mechanisms [26]. In addition they may revolutionize micro-robotics, because actuators do not have to overcome self-stiffness or the stiffness of the underlying kinematic structure. This would relax the energy requirements and pave the way to their autonomy. Applications of these robots in minimally invasive medicine are widespread [27].

In this paper a commonly used balancing building block [15] is made compatible with MEMS and their manufacturing techniques. We do so by stretching a silicon plate spring while keeping the endpoints fixed, instead of displacing the endpoints. The stretching is achieved by thermally growing a thin film of silicon dioxide on the silicon micro mechanism.

Thin films usually contain residual stresses. The film tends to expand if this stress is compressive and tends to shrink for a tensile stress [28]. Any film containing compressive residual stress will induce a tensile stress in the silicon substrate and stretch it. Surface stress has been suggested for removing inter component clearance and preloading [29] and is known to change the natural frequency of cantilever and doubly clamped microbeams [30–32]. However, it has never been used to create a building block for statically balancing compliant micro mechanisms.

The MEMS balancing building block could be used to balance any sort of MEMS structure, such as a gripper [15, 16] or a rotational mechanism [14]. In this paper we introduce our method by balancing a simple linear stage. A balanced and unbalanced stage are compared to show efficacy.

The method is compatible with semi-conductor batch manufacturing techniques, enabling mass fabrication. It consumes no power after manufacturing, has a low manufacturing complexity and has a high resolution by controlling the film thickness. The equations of motion of a beam show that our method is theoretically possible to reduce stiffness to zero [33]. And it has the potential to be 100% space efficient if positive and negative stiffness mechanisms are united in a single structure.

In Section 5.2 the stiffness reduction method is explained followed by an implementation in Section 5.4. Manufacturing is explained in Section 5.5 and simulations are discussed in Section 5.6. How measurements are done is given in Section 5.7 followed by the measurement results in Section 5.8. The implications of the results are discussed in Section 5.9 followed by a conclusion in Section 5.10.

5.2. STIFFNESS REDUCTION METHOD

The positive stiffness K_p of a CM can be reduced by coupling it with a mechanism with opposing negative stiffness K_n in parallel. The resulting equivalent stiffness is given by $K_{eq} = K_p + K_n$ and is zero if K_p and K_n are equal but opposite. These zero-stiffness compliant mechanisms are referred to as statically balanced [13].

Various negative stiffness mechanisms exist [9, 10, 15] that can be used as building blocks to balance an existing design [15]. One of the simplest is schematically shown in

Fig. 5.1. In this mechanism a compression spring with a free length L_0 is preloaded a distance ΔL , causing instability around $x = 0$.

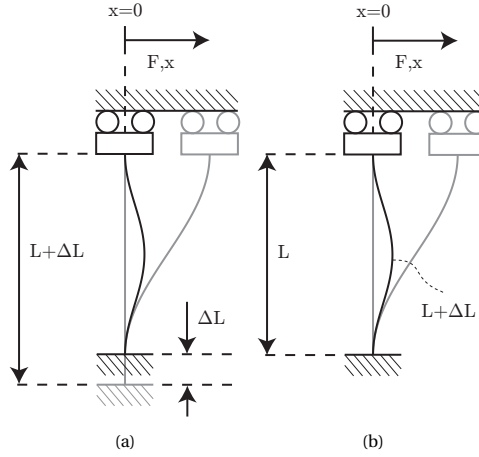


Figure 5.2: Commonly used compliant equivalent of the balancer from Fig. 5.1. (a) Shows preloading by moving the end point of the plate spring a distance ΔL . (b) Shows preloading by stretching the plate spring a distance ΔL . Both systems are equivalent.

A commonly used compliant equivalent is shown in Fig. 5.2a. It is obtained by axially preloading a plate spring into its post-buckled state. Normally, the plate spring is preloaded by moving its endpoint an amount ΔL as shown in Fig. 5.2a [10, 12, 14–16]. An alternative, yet equivalent approach, is to elongate the plate spring an amount ΔL , as shown in Fig 5.2b. We elongate the plate springs by uniformly depositing a thin film all around the silicon micro CM. Thin films virtually always contain residual stress, typically in the order of GPa [34]. They tend to expand if stress is compressive and tend to shrink for tensile stress [28].

In a freestanding substrate with a homogeneous thin film, the stress distribution follows from equilibrium of the normal forces and bending moments over the entire cross-section. Consequently, stress at the interface between film and substrate reverses sign and is small if the film thickness is small compared to substrate thickness [35].

If the film is in compression it will induce tension in the substrate. Hence, if the film is substantially thick, it will stretch the substrate. To prevent bending, the film should be applied uniformly around the substrate. This way all induced moments cancel each other. Generally speaking, large stresses should be avoided in thin films, because they can lead to cracking or buckling of the film itself. One typically aims to get a compressive stress in the order of a few hundred MPa [28].

5.3. MINIMUM REQUIRED FILM STRESS

The total residual film stress σ_f is a combination of intrinsic σ_I and thermal σ_T stress:

$$\sigma_f = \sigma_I + \sigma_T \quad (5.1)$$

Intrinsic stress σ_I is generally hard to predict due to dependency on processing parameters [36]. For example, the stress in sputtered thin films is dependent on gas pressure, substrate bias, gas atomic mass, target atomic mass, angle of deposition, angle of emission, target shape and cathode power [37].

Thermal stresses σ_T are caused by a mismatch in the coefficient of thermal expansion (CTE) between the bulk and film materials. It is well understood and easily calculated with the following equation:

$$\sigma_f(T) = (\alpha_b - \alpha_f) \Delta T \frac{E_f}{1 - \nu_f} \quad (5.2)$$

where α_s and α_f are the CTE of the bulk and film material respectively, ΔT is the temperature difference and E_f and ν_f are the Young's modulus and Poisson's ratio of the film.

In doubly-clamped beams film stress induces a net axial force [32]. It is given by the integral of the resulting axial stress over the beam cross-section. If the axial stress is due to a thin film only, this amounts to the integral of the stress in the thin film only [38]:

$$F_{axial} = \int_{A_f} \sigma_f dA \quad (5.3)$$

where F_{axial} is the net axial force, σ_f is a uniform strain-independent film stress and A_f is the cross sectional area of the thin film.

At sufficiently large axial loading the natural frequency of a beam becomes zero. This load can be derived from its dynamic equations and is called the Euler buckling load F_{cr} [33, 39–41]. For loads greater than F_{cr} the natural frequency becomes complex and the mode shape unstable [39], i.e. the beam buckles. For uniform beams under constant axial loading the Euler buckling load is given by:

$$F_{cr} = \frac{\pi^2 EI}{(KL)^2} \quad (5.4)$$

where E is the Young's modulus, I is the surface moment of inertia, L is the length of the beam (see Fig. 5.2) and K is the effective length factor that depends on the boundary conditions. For a doubly-clamped beam $K = 0.5$ [39].

By equating Eq. 5.3 and Eq. 5.4 we can get the surface stress σ_{cr} that would cause the critical load:

$$\int_A \sigma_{cr} dA_f = \frac{\pi^2 EI}{(KL)^2} \quad (5.5)$$

Assuming a uniform thin film of thickness t that is negligible compared to the bulk of a beam of width b and height h (as defined in Fig. 5.4c) and a constant film stress σ_{cr} we get:

$$\sigma_{cr} (2bt + 2ht + 4t^2) = \frac{\pi^2 EI}{(KL)^2} \quad (5.6)$$

such that the critical film stress σ_{cr} becomes:

$$\sigma_{cr} = \frac{\pi^2 EI}{(2bt + 2ht + 4t^2)(KL)^2} \quad (5.7)$$

Material properties of silicon according to [42] are substituted in Eq. 5.7 along with a beam height $h = 525\mu\text{m}$ and a film thickness $t = 1.9\mu\text{m}$. This yields a function for the critical stress σ_{cr} required for buckling a beam of width b and length L . It is plotted for various beam lengths in Fig. 5.3. It shows that thermally grown oxide can easily buckle silicon beams with lengths in the order of millimeters and a thickness in the order of tens of micrometers.

5.4. MECHANISM DESIGN

To demonstrate our stiffness reduction method the negative stiffness building block from Fig. 5.2b is placed in parallel with a linear stage, see Fig. 5.4. Although it could be combined with other mechanisms, see [14–16], this linear stage is arguably the simplest. The goal is to reduce the stiffness of the stage from Fig. 5.4a as much as possible.

Minimal stiffness is achieved by choosing the length L of the negative stiffness plate spring such that the critical loads (similar to F_{cr}) of the first two buckling modes (see Fig. 5.5) are the same. The critical load, induced by the film stress, is the load at which the system loses stability and its state bifurcates, i.e. the system can buckle left or right. The buckling modes give the shape in which the system will buckle. The modes and critical load can be computed with a linear buckling analysis (i.e. a linearized eigenvalue analysis) in any commercially available finite element program.

The residual stress in the SiO_2 will cause deformation in the shape of mode 1 or mode 2 (see Fig. 5.5) for large and small values of L respectively. However, for a particular value of L mode 1 and 2 can theoretically coexist, because they have the same critical load. Essentially, post buckling happens in the shape of mode 1 and 2 simultaneously, i.e. some linear combination of the eigenvectors associated with modeshape 1 and 2. This means that we can move the system from mode shape 1 to mode shape 2 without changing the potential energy in the system, which means the system is zero stiffness.

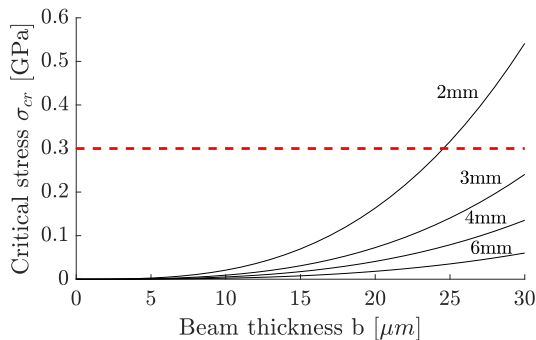


Figure 5.3: Required critical stress according to Eq. 5.7 versus beam widths b for various beam lengths L . The dashed line indicates the maximum reported residual film stress in thermal oxide.

In practice, the buckling modes will always be slightly separated, i.e. their critical loads are slightly different. This is affected by modeling errors and by manufacturing tolerances caused by for example overetching or underetching of silicon. Consequently the structure will always buckle in either mode 1 or mode 2. A system buckled in mode 1 will have a reduced stiffness. However if the system is buckled in mode 2 it should be bistable [12, 43].

The length of the negative stiffness plate spring is $L = 8.673$ mm and the plate springs of the stage are chosen to have a length of $L_S = 5$ mm. Please note that although the two plate springs of the stage are also stretched, they do not create any negative stiffness, because that would require them to buckle as shown in Fig. 5.2.

All plate springs have the same cross section A-A as shown in Fig. 5.4b and Fig. 5.4c. The width and height before oxidation are respectively $B = 24$ μm and $H = 525$ μm (wafer thickness). In practice B and H are slightly different from b and h , because some silicon is consumed during oxidation.

The shuttle is $S_w = 8$ mm wide and $S_h = 2.67$ mm high. It has a protrusion $P_w = 2$ mm wide with markers at height $P_h = 2.5$ mm. It enables us to measure force and displacement close to the center of compliance (CC). At our CC all orthogonal compliance components are fully decoupled, which ensures no parasitic motions (e.g. r and y directions in Fig. 5.4) are induced during loading in the desired motion direction (x -direction) [44]. The markers are added to optically align the sensor probe with the mechanism, see Fig. 5.4b.

5.5. MANUFACTURING

All mechanisms are produced with DRIE and wet oxidation at 1100 °C from (100) oriented 525 μm thick silicon wafers. Five different oxide thicknesses are grown, 1.9 μm , 2.05 μm , 2.2 μm , 2.35 μm and 2.5 μm on five different wafers. Oxidation times are determined with the Deal-grove model [45] and thickness is verified in five places across the front side of the wafer with spectral reflectance using a Leitz MPV SP. Wafers are oriented vertically in the oven to ensure uniform film growth on the front and back side. Before oxidation, one unbalanced stage is removed from each wafer.

Unbalanced linear stages with and without SiO_2 are manufactured and measured to determine the positive stiffness K_p to compensate. The balanced mechanisms with SiO_2 film are measured and compared with the unbalanced stiffness. In addition we remove the SiO_2 from the balanced mechanisms to investigate plastic effects of thermal oxidation on the Si beams. The SiO_2 is removed with a HF vapor etch using a SPTS Primaxx uEtch.

5.6. SIMULATIONS

Numerical modeling is done with ANSYS. Beam elements (beam188) with a custom trapezoidal cross sectional area are used. In case thin film is modeled a multi material (Si and SiO_2) cross section is defined as shown in Fig. 5.4. In case no thin film is modeled, a single material (Si) is defined. For the frame the effect of film stress is neglected, so a single material (Si) cross section is used. The frame is constrained in all directions to the ground at one corner.

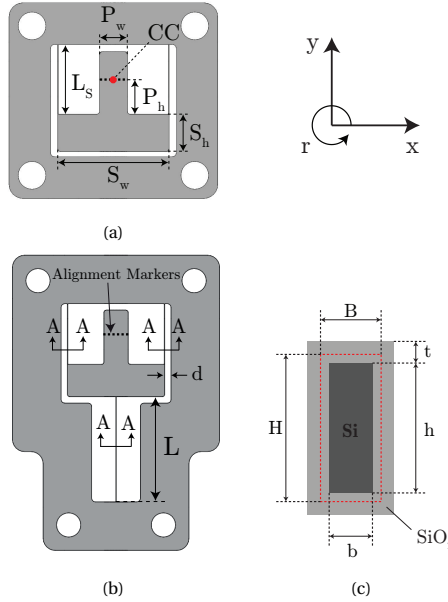


Figure 5.4: Stage designs. (a) Shows the unbalanced stage and (b) the balanced stage. (c) Shows the cross section A-A of the plate springs, which is the same everywhere. The dashed rectangle indicates the silicon beam before some of its material is consumed by oxidation.

The mono-crystalline silicon is assumed to be perfectly elastic. A constant orthotropic stiffness is used according to [42]. Which is equivalent to aligning all beams with the [010] crystal direction on the wafer, i.e. a 45 degree rotation with respect to the flat end. A temperature dependent CTE is used according to [46].

The reported material properties of thermally grown SiO_2 vary greatly [47]. Reported values for the CTE of silicon dioxide typically range from $0.5 \times 10^{-6} \text{ }^\circ\text{C}^{-1}$ to values as high as $4.1 \times 10^{-6} \text{ }^\circ\text{C}^{-1}$ [48]. And even negative values are reported. Young's moduli range from 50 to 100 GPa and Poisson's ratios between 0.15 and 0.20 [47]. We have adopted elastic properties ($E = 72 \text{ GPa}$, $\nu = 0.2$) from [49], where conditions are relatively comparable and are similar to data from [50]. A constant CTE of $0.5 \times 10^{-6} \text{ }^\circ\text{C}^{-1}$ is used as reported by [50]. Volume expansion during growth is accounted for by regarding the ratio of the atomic volume between Si and SiO_2 , i.e. 20 \AA to 40 \AA [51].

A linear buckling analysis to compute the buckling shape modes and critical loads is performed by cooling down the material $1 \text{ }^\circ\text{C}$. All elements are given an initial reference temperature of $970 \text{ }^\circ\text{C}$ (the viscous flow point of SiO_2) and a final uniform temperature of $969 \text{ }^\circ\text{C}$ to all nodes.

Modeling of the force deflection behaviour is done by a nonlinear static structural analysis. Again all elements are given an initial temperature of $970 \text{ }^\circ\text{C}$, but are now given a final uniform temperature of $20 \text{ }^\circ\text{C}$ to model the cooling down to room temperature. Although plasticity of Si is observed in the measurements of the balanced stages, we do not predict and model plastic behaviour. Instead, we determine how much the neutral

position has moved in the x-direction by measuring the distance d (see Fig. 5.4b) after oxide has been removed with a scanning electron microscope (SEM). It equals 55.10 μm , 98.59 μm , 101.80 μm , 90.86 μm and 110.14 μm for a film thickness of 1.9 μm to 2.5 μm respectively.

It is assumed the new equilibrium is stress free (without SiO_2) and that it has the shape of mode 2. Therefore we add buckling shape mode 2 with appropriate amplitude (distance d) to the original and undeformed neutral position. A uniform temperature of 20 $^\circ\text{C}$ is set to all nodes to model the cooling down of the sample. Force deflection behaviour is determined by computing reaction forces at regular intervals in the x-direction at the center of compliance.

Simulations are done for the balanced and unbalanced stages, both with and without oxide. The unbalanced stages with and without SiO_2 do not require any buckling modes to be added and are shown in Fig. 5.10b and Fig. 5.10a respectively. The balanced stages with and without oxide are shown in Fig. 5.6a and Fig. 5.6b respectively. Stiffness data is summarized in Tab. 5.3.

Since the beams are not perfectly straight in practice, we model the influence of such defects by introducing geometric imperfections. Imperfections are simulated by adding the first three buckling modes with increasing amplitude to the undeformed nodal coordinates. That is, the sum of the first three buckling modes (at the new equilibrium) is scaled such that the maximum sideways deviation of the beams is 0 μm , 4 μm , 8 μm , 12 μm , 16 μm and 20 μm . We do this only for the simulations of the balanced stage with film thickness 2.35 μm . Results are shown in Fig. 5.6c.

5.7. MEASUREMENTS

Stiffness is analyzed in the x-direction of each stage by measuring the force deflection behavior. For this a microforce sensing probe (FT-S10000) with a resolution of 0.5 μN is mounted on a precision linear stage (Physik Instrumente M-060.2DG) with a resolution of 8.5 nm. The sensor is mounted under an angle of 30 degrees with an aluminum sensor head and vertically aligned using a manual linear precision stage (Thorlabs PT1). Samples are placed on a 3D printed L-shaped base plate and positioned using two manual linear precision stages. A picture of the measurement setup is shown in Fig. 5.7.

The sensing probe is visually aligned with the alignment markers at the CC and vertically halfway the thickness by using a Dino-Lite digital microscope and the manual precision stages. All measurements are averaged over 10 repetitions to reduce constant measurement noise, see Fig. 5.10.

Beam thickness is measured by using a low vacuum SEM. In one device all beams are measured in three locations on the front and back to get an idea of the distribution. In all other devices the average is taken of two beams, measured in one location on front and back. For beam measurements of the unbalanced stages, devices that were never oxidized are used. For the balanced stages, oxide is first removed.

5.8. MEASUREMENT RESULTS

Pictures of the unbalanced and the balanced stages are shown in Fig. 5.8a and Fig. 5.8b respectively. Measurements of the SiO_2 thickness are given in Tab. 5.1. Film thickness on

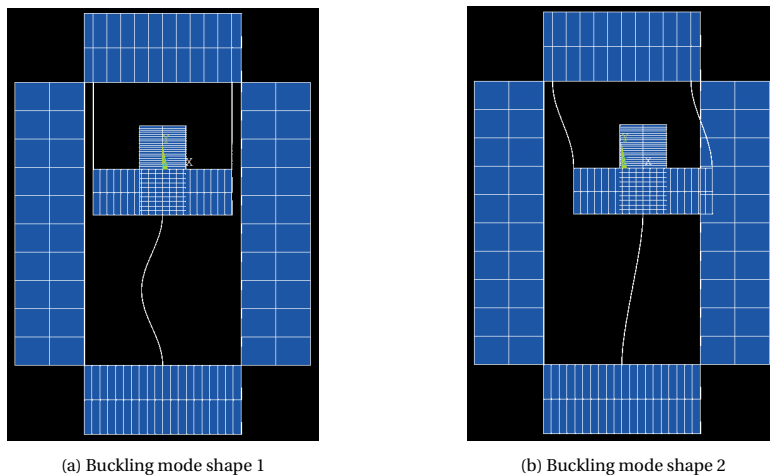


Figure 5.5: The first two buckling modes resulting from uniformly cooling down the sample. Modeling is done as described in Section 5.6.

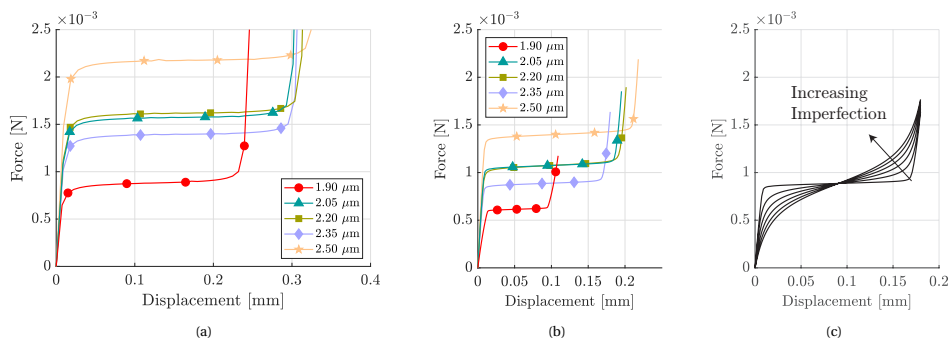


Figure 5.6: Simulation results for statically balanced stages (a) with (b) and without oxide for multiple oxide thicknesses. (c) Shows the influence of beam imperfections on the force deflection response for the stage where $2.35 \mu\text{m}$ of SiO_2 has been removed.

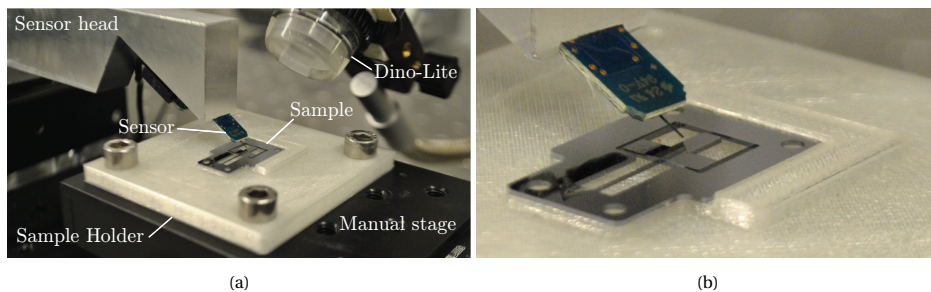


Figure 5.7: Picture of the force deflection measurement setup. (a) Shows a closeup of the stage, sensor holder and digital microscope. (b) Shows a closeup of the microforce sensing probe and a sample.

Table 5.1: SiO₂ Thickness per wafer in nm.

Target	Bottom	Right	Top	Left	Center
1900 nm	1892	1891	1890	1889	1886
2050 nm	2050	2050	2052	2050	2048
2200 nm	2189	2187	2191	2192	2185
2350 nm	2352	2351	2349	2350	2349
2500 nm	2506	2506	2511	2511	2503

Table 5.2: Measured average front and back beam width in μm for the unbalanced stage (SU) and balanced stage (SB) without SiO₂. Note that SU is never oxidized.

Thickness	Back		Front	
	SU	SB - SiO ₂	SU	SB - SiO ₂
1900 nm	20.60	19.01	24.94	22.29
2050 nm	20.30	19.30	25.31	22.42
2200 nm	20.82	19.44	25.44	22.65
2350 nm	21.60	19.04	23.15	21.28
2500 nm	23.94	21.47	25.87	22.40

Table 5.3: Simulated stiffness in N m^{-1} for the unbalanced stage (SU) and balanced stage (SB) with and without oxide.

Thickness	SU	SU + SiO ₂	SB + SiO ₂	SB
1900 nm	13.02	13.65	0.29	0.27
2050 nm	13.13	13.77	0.18	0.32
2200 nm	13.67	14.45	0.17	0.42
2350 nm	12.27	13.40	0.16	0.30
2500 nm	16.92	18.35	0.17	0.37

Table 5.4: Measured stiffness in Nm^{-1} of the unbalanced stage (SU) and the balanced stage (SB) with and without oxide.

Thickness	SU	SU + SiO ₂	SB + SiO ₂	SB
1900 nm	13.42	13.73	0.66	0.51
2050 nm	12.83	13.72	0.60	0.41
2200 nm	13.21	13.81	0.70	0.49
2350 nm	13.23	14.63	1.53	1.07
2500 nm	14.92	15.19	0.60	0.32

average varies -0.28 ± 4.13 nm from target thickness and are in agreement with expected values.

Measurements of beam width on the front and back side are reported in Tab. 5.2. A typical SEM measurement is shown in Fig. 5.9c. Measurements on the front and back side had a variation of $0.11 \mu\text{m}$ and $0.32 \mu\text{m}$ respectively. Fig. 5.9a shows that the balanced device is buckled in mode shape 2 from Fig. 5.5b. Fig. 5.9b shows a SEM image of the alignment markers at the CC.

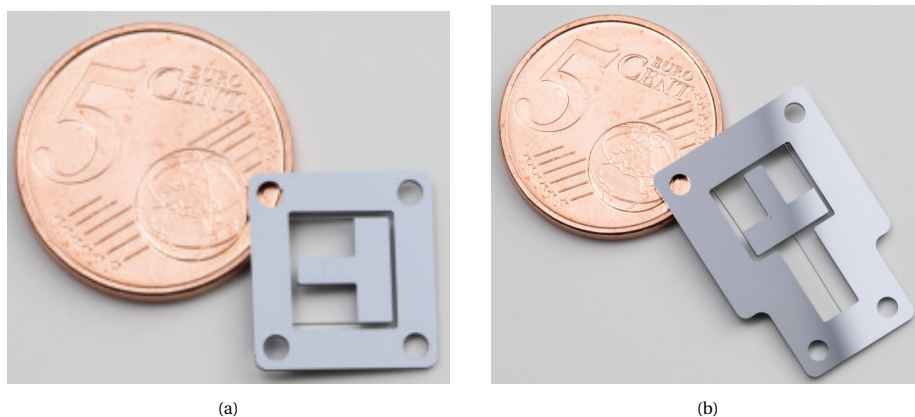


Figure 5.8: Manufactured stages. (a) Shows the unbalanced stage and (b) shows the balanced stage.

Force deflection measurements are shown in Fig. 5.10 and stiffness is summarized for all measurements in Tab. 5.4. Fig. 5.10a shows measurement data for one stage with SiO_2 , including the linear fit and simulation results. Fig. 5.10b shows the same for one stage without $1.9 \mu\text{m}$ SiO_2 . Measurements are in good agreement with simulations and stiffness increases $0.694 \pm 0.47 \text{ N m}^{-1}$ on average when oxidized. Measurement results of the balanced stages with oxide present and after it has been removed are given in Sections 5.8.1 and 5.8.2 respectively.

5.8.1. BALANCE WITH OXIDE

Fig. 5.10c shows all force deflection measurements for the balanced stages for all SiO_2 thicknesses. Fig. 5.10c also includes a linear fit to the low stiffness plateau. A clear reduction in stiffness can be observed compared to the non-balanced stages over a range of approximately $300 \mu\text{m}$ to $380 \mu\text{m}$. The linear fit reveals a stiffness reduction of approximately a factor 9 to 25 compared to the unbalanced non-oxidized stage.

The low stiffness range increases for thicker films, but it also increases a constant force offset from approximately $0.2 \times 10^{-3} \text{ N}$ to $0.9 \times 10^{-3} \text{ N}$, which can be explained by an increased change in neutral position, see Sec. 5.8.2. In addition it is remarkable that the curve of the balance stage with $2.35 \mu\text{m}$ SiO_2 is more rounded. It is likely that the beams in this mechanisms are less straight than in the other mechanisms, because Fig. 5.6c shows that with increasing beam imperfections the force deflection behaviour becomes more curvy.

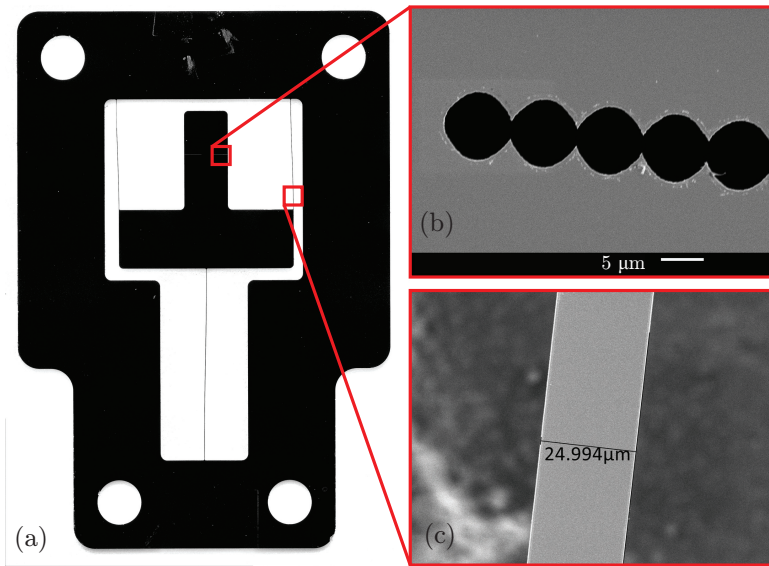


Figure 5.9: Micrographs of a balanced stage. (a) A picture of a balanced stage. It can be observed it is buckled in the mode from Fig. 5.5b. (b) A SEM image of the markers used to align the microforce sensing probe with the center of compliance, see Fig. 5.4b. In figure (c) a typical SEM image used for measuring the beam width is shown.

5.8.2. BALANCE WITHOUT OXIDE

Surprisingly, the balancing effect remained after oxide removal. Force deflection data, along with a linear curve fit, is shown in Fig. 5.10d. The linear fit reveals a stiffness reduction of approximately a factor 12 to 46 compared to the unbalanced non-oxidized stage. Almost half the stiffness of the balanced stages with SiO_2 .

After oxide removal the balancing effect should completely disappear under purely elastic deformations. The remaining effect and the asymmetrical stiffness profiles (they are not centered around displacement 0 mm) in Fig. 5.10c and in Fig. 5.10d suggest irreversible plastic deformations in the silicon beams. That is, the oxidation process has permanently stretched the silicon beams, causing the post-buckling state to become the new equilibrium. However, stresses were not fully relaxed by plastic yielding, since the balancing domain and the force offset decreased upon oxide removal.

This shift in neutral position also explains the constant force offset, because it adds positive stiffness to the originally bistable mechanism. If bistability is combined with positive stiffness, a constant force mechanism results [52]. The constant force offset increases for thicker films, because the severity of the bistability is increased for larger rotations of the plate springs. A parameter study of such a constant force mechanism can be found in [52].

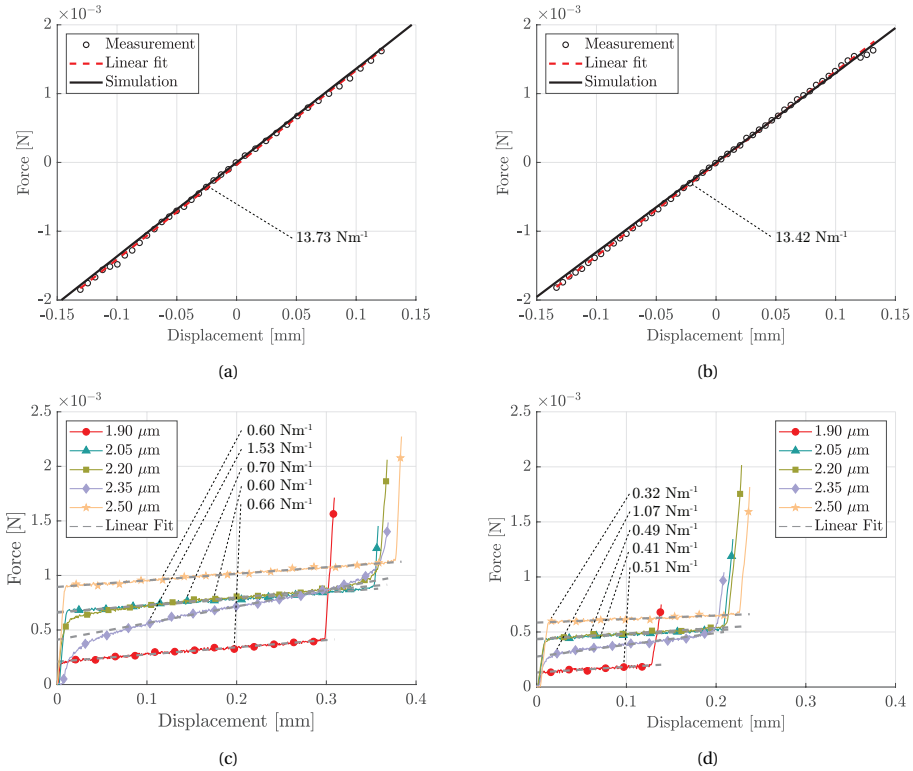


Figure 5.10: Force deflection measurements averaged over 10 repetitions to reduce constant measurement noise. (a) A typical measurement with linear fit along with a simulation of an unbalanced oxidized stage. (b) A typical measurement with linear fit along with a simulation of a non-oxidized unbalanced stage. (c) Measurements of the balanced devices with SiO_2 with a linear fit to the low stiffness domain. (d) Measurements of the balanced devices with SiO_2 removed with a linear fit to the low stiffness domain.

5.9. DISCUSSION

In this paper we have demonstrated, for the first time, one-time preloading for permanent stiffness reduction of flexible mechanisms at micro scale. A static balancing building block is made compatible with MEMS by exploiting residual stress from thermal oxidation of silicon. Efficacy is shown by coupling the building block to a simple linear stage, however it can be combined with other mechanisms as well [14–16].

The mechanism is unintentionally buckled in shape mode 2 instead of shape mode 1. Tolerances in manufacturing, caused by for example overetching or underetching of silicon, most likely changed the length and width of the beams causing a separation of the buckling modes with preference for mode shape 2. Sideways buckling may be prevented by properly separating the buckling modes, accounting for manufacturing tolerances. Ensuring the buckling shape mode 1 assures negative stiffness to be lower than the positive stiffness (stage flexures). As such, the negative stiffness acts around a stable equilibrium position and bistability or a constant force offset is avoided. This can be

easily achieved by making the negative stiffness flexure longer.

However, in some cases a force offset may be desirable. For example when the motion direction is aligned with gravity. By using an appropriately sized proof mass, a constant force offset is able to counteract the gravitational pull, allowing for low frequency oscillations in this direction. A similar approach was taken in [23].

If the induced deformation were purely elastic, each device should have been bistable, as shown in [12, 43]. However, plastic deformation in the silicon beams has caused buckling shape mode 2 to become the new neutral position. Although monocrystalline silicon is often considered brittle, plastic deformation is known to occur [53]. Plastic deformation of the silicon most likely happens during cool down between approximately 630 °C and 970 °C. This region is above the brittle-to-ductile transition temperature of silicon [54] and below the viscous flow point of silicon dioxide [55, 56]. However, we have no data to confirm this.

Simulations of the unbalanced stages are in good agreement with measurements. Simulations of the balanced stages model the general behaviour, however there is discrepancy in the force offset. The discrepancy may be explained by violation of the assumption that the permanently deformed shape is stress free. Indeed stress is relieved due to plastic deformation, however only those that exceed the yield stress. Stress just below the yield stress will still be present. Properly modeling this phenomenon requires implementation of constitutive models for the elasto-viscoplastic behaviour of monocrystalline silicon, such as [54, 57, 58].

Alternatively one may work with thin films below the brittle-to-ductile transition temperature of silicon to prevent plastic deformation. Here we are not limited to thermally grown SiO₂, because Si₃Ni₄ (plasma 50 kHz at 350 °C and poly Si (LPCVD between 560 °C and 670 °C are reported to contain residual compressive stress between -0.1 GPa and -2.1 GPa [59]). It can even be argued that static balance can be achieved with residual tensile film stress, because a mechanisms that buckles under tensile dead load is reported in [60].

We have improved upon the state of the art [19–21], by investigating a versatile permanent preloading method for micro compliant mechanisms. Our method enables static balancing of mechanisms by stretching micro beams. By using the balancing structure as an isolated building block, it should be able to permanently reduce stiffness in existing mechanisms such as shown in [26].

The method is suited for massive parallelized fabrication, since thermal oxidation of silicon is a common method in semi-conductor manufacturing. It consumes no power after manufacturing and has a low manufacturing complexity. It is able to theoretically reduce stiffness to 0 N m⁻¹ [33] and has the potential to be 100 % space efficient if positive and negative stiffness are united in a single structure. Our method is well suited for further miniaturization, since surface effects become predominant at smaller scales.

5.10. CONCLUSION

In this paper we have demonstrated, for the first time, permanent stiffness reduction on micro scale suited for mass production by exploiting stress induced by thin films. A building block commonly used for stiffness reduction in large scale compliant mechanisms is made compatible with MEMS. Stiffness of a simple linear stage is reduced by a

factor 9 to 46 over a range of maximally 380 μm by coupling with the balancing building block. The negative stiffness is created by stretching all beams by preloading the monocrystalline silicon with thermally grown oxide at 1100 °C.

It can be concluded that film stress is a feasible, simple and promising permanent preloading method for permanent stiffness reduction of compliant micro mechanisms. It is completely passive, allows parallelized and low complexity manufacturing, can potentially eliminate stiffness completely, has the potential to be extremely space efficient and is scalable.

REFERENCES

- [1] S. Kota, J. Joo, Z. Li, S. M. Rodgers, and J. Sniegowski, *Design of compliant mechanisms: applications to mems*, Analog Integr. Circuits Signal Process. **29**, 7 (2001).
- [2] G. Ananthasuresh and L. L. Howell, *Mechanical design of compliant microsystems—a perspective and prospects*, Journal of Mechanical Design **127**, 736 (2005).
- [3] L. L. Howell, *Compliant mechanisms* (John Wiley & Sons, 2001).
- [4] J. A. Gallego and J. L. Herder, *Criteria for the static balancing of compliant mechanisms*, in *ASME 2010 IDETC and CIE* (2010) pp. 465–473.
- [5] N. Tolou, V. A. Henneken, and J. L. Herder, *Statically balanced compliant micro mechanisms (sb-mems): Concepts and simulation*, in *ASME 2010 IDETC and CIE* (American Society of Mechanical Engineers, 2010) pp. 447–454.
- [6] N. Tolou, J. Gallego, and J. Herder, *Statically balanced compliant micro mechanisms (sb-mems): A breakthrough in precision engineering*, Mikroniek **50**, 20 (2010).
- [7] M. de Laat, H. P. Garza, J. Herder, and M. Ghatkesar, *A review on in situ stiffness adjustment methods in mems*, J. Micromechanics Microengineering **26**, 063001 (2016).
- [8] J. L. Herder, *Design of spring force compensation systems*, Mechanism and machine theory **33**, 151 (1998).
- [9] S. Park and T. Luu, *Techniques for optimizing parameters of negative stiffness*, Proceedings of the Institution of Mechanical Engineers, Part C: Journal of Mechanical Engineering Science **221**, 505 (2007).
- [10] J. van Eijk and J. F. Dijkman, *Plate spring mechanism with constant negative stiffness*, Mechanism and Machine Theory **14**, 1 (1979).
- [11] D. L. Platus, *Negative-stiffness-mechanism vibration isolation systems*, in *San Jose-DL tentative* (International Society for Optics and Photonics, 1992) pp. 44–54.
- [12] J. F. Dijkman, *A study of some aspects of the mechanical behaviour of cross-spring pivots and plate spring mechanisms with negative stiffness*, (1979).
- [13] M. Schenk and S. D. Guest, *On zero stiffness*, Proceedings of the Institution of Mechanical Engineers, Part C: Journal of Mechanical Engineering Science , 0954406213511903 (2013).

- [14] L. Berntsen, D. H. Gosenshuis, and J. L. Herder, *Design of a compliant monolithic internally statically balanced four-bar mechanism*, in *ASME 2014 International Design Engineering Technical Conferences and Computers and Information in Engineering Conference* (American Society of Mechanical Engineers, 2014) pp. V05AT08A040–V05AT08A040.
- [15] K. Hoetmer, J. L. Herder, and C. J. Kim, *A building block approach for the design of statically balanced compliant mechanisms*, in *ASME 2009 IDETC and CIE* (American Society of Mechanical Engineers, 2009) pp. 313–323.
- [16] J. Lassooij, N. Tolou, G. Tortora, S. Caccavaro, A. Menciassi, and J. Herder, *A statically balanced and bi-stable compliant end effector combined with a laparoscopic 2dof robotic arm*, *Mechanical Sciences*, 3 (2), 2012 (2012).
- [17] F. M. Morsch and J. L. Herder, *Design of a generic zero stiffness compliant joint*, in *ASME 2010 IDETC and CIE* (American Society of Mechanical Engineers, 2010) pp. 427–435.
- [18] L. C. Leishman, D. J. Ricks, and M. B. Colton, *Design and evaluation of statically balanced compliant mechanisms for haptic interfaces*, in *ASME 2010 DSCC* (American Society of Mechanical Engineers, 2010) pp. 859–866.
- [19] P. J. Pluimers, N. Tolou, B. D. Jensen, L. L. Howell, and J. L. Herder, *A compliant on/off connection mechanism for preloading statically balanced compliant mechanisms*, in *ASME 2012 IDETC and CIE* (American Society of Mechanical Engineers, 2012) pp. 373–377.
- [20] N. Tolou, P. Estevez, and J. L. Herder, *Collinear-type statically balanced compliant micro mechanism (sb-cmm): experimental comparison between pre-curved and straight beams*, in *ASME 2011 IDETC and CIE* (American Society of Mechanical Engineers, 2011) pp. 113–117.
- [21] G. Chen and S. Zhang, *Fully-compliant statically-balanced mechanisms without prestressing assembly: concepts and case studies*, *Mech. Sci* **2**, 169 (2011).
- [22] F. Acernese, R. De Rosa, G. Giordano, R. Romano, and F. Barone, *Tunable mechanical monolithic sensor with interferometric readout for low frequency seismic noise measurement*, in *SPIE Remote Sensing* (International Society for Optics and Photonics, 2008) pp. 711011–711011.
- [23] R. Middlemiss, A. Samarelli, D. Paul, J. Hough, S. Rowan, and G. Hammond, *Measurement of the earth tides with a mems gravimeter*, *Nature* **531**, 614 (2016).
- [24] M. Han, Q. Yuan, X. Sun, and H. Zhang, *Design and fabrication of integrated magnetic mems energy harvester for low frequency applications*, *J. Microelectromech S.* **23**, 204 (2014).
- [25] Y. Naruse, N. Matsubara, K. Mabuchi, M. Izumi, and S. Suzuki, *Electrostatic micro power generation from low-frequency vibration such as human motion*, *J. Micromechanics Microengineering* **19**, 094002 (2009).

- [26] D. F. Machekposhti, J. L. Herder, G. Sémon, and N. Tolou, *A compliant micro frequency quadrupler transmission utilizing singularity*, Journal of Microelectromechanical Systems **27**, 506 (2018).
- [27] B. J. Nelson, I. K. Kaliakatsos, and J. J. Abbott, *Microrobots for minimally invasive medicine*, Annual review of biomedical engineering **12**, 55 (2010).
- [28] G. Janssen, *Stress and strain in polycrystalline thin films*, Thin Solid Films **515**, 6654 (2007).
- [29] M. W. Judy, Y.-H. Cho, R. T. Howe, and A. P. Pisano, *Self-adjusting microstructures (sams)*, in *Micro Electro Mechanical Systems, 1991, MEMS'91, Proceedings. An Investigation of Micro Structures, Sensors, Actuators, Machines and Robots. IEEE* (IEEE, 1991) pp. 51–56.
- [30] M. J. Lachut and J. E. Sader, *Effect of surface stress on the stiffness of cantilever plates*, Physical review letters **99**, 206102 (2007).
- [31] M. J. Lachut and J. E. Sader, *Effect of surface stress on the stiffness of thin elastic plates and beams*, Physical Review B **85**, 085440 (2012).
- [32] R. B. Karabalin, L. Villanueva, M. Matheny, J. E. Sader, and M. L. Roukes, *Stress-induced variations in the stiffness of micro-and nanocantilever beams*, Physical review letters **108**, 236101 (2012).
- [33] M. I. Younis, *MEMS linear and nonlinear statics and dynamics*, Vol. 20 (Springer Science & Business Media, 2011).
- [34] M. Ohring, *Materials science of thin films* (Academic press, 2001).
- [35] J. A. Thornton and D. Hoffman, *Stress-related effects in thin films*, Thin solid films **171**, 5 (1989).
- [36] M. F. Doerner and W. D. Nix, *Stresses and deformation processes in thin films on substrates*, Critical Reviews in Solid State and Material Sciences **14**, 225 (1988).
- [37] D. Hoffman and J. A. Thornton, *Internal stresses in cr, mo, ta, and pt films deposited by sputtering from a planar magnetron source*, Journal of Vacuum Science and Technology **20**, 355 (1982).
- [38] R. B. Karabalin, L. Villanueva, M. Matheny, J. E. Sader, and M. L. Roukes, *Stress-induced variations in the stiffness of micro-and nanocantilever beams*, Physical review letters **108**, 236101 (2012).
- [39] F. J. Shaker, *Effect of axial load on mode shapes and frequencies of beams*, (1975).
- [40] A. Bokaian, *Natural frequencies of beams under compressive axial loads*, Journal of sound and vibration **126**, 49 (1988).

- [41] H. Guckel, T. Randazzo, and D. Burns, *A simple technique for the determination of mechanical strain in thin films with applications to polysilicon*, Journal of Applied Physics **57**, 1671 (1985).
- [42] M. A. Hopcroft, W. D. Nix, and T. W. Kenny, *What is the young's modulus of silicon?* J. Microelectromech S. **19**, 229 (2010).
- [43] J. Qiu, J. Lang, and A. Slocum, *A curved-beam bistable mechanism*, J. Microelectromech S. **13**, 137 (2004).
- [44] D. M. Brouwer, J. P. Meijaard, and J. B. Jonker, *Large deflection stiffness analysis of parallel prismatic leaf-spring flexures*, Precision engineering **37**, 505 (2013).
- [45] B. E. Deal and A. Grove, *General relationship for the thermal oxidation of silicon*, Journal of Applied Physics **36**, 3770 (1965).
- [46] Y. Okada and Y. Tokumaru, *Precise determination of lattice parameter and thermal expansion coefficient of silicon between 300 and 1500 K*, Journal of Applied Physics **56**, 314 (1984).
- [47] F. Maseeh, M. Arnone, and S. D. Senturia, *Mechanical Properties of Microelectronics Thin Films: Silicon Dioxide (SiO₂)*, Tech. Rep. (MIT, 1989).
- [48] H. Tada, A. E. Kumpel, R. E. Lathrop, J. B. Slanina, P. Nieva, P. Zavracky, I. N. Miaoulis, and P. Y. Wong, *Thermal expansion coefficient of polycrystalline silicon and silicon dioxide thin films at high temperatures*, Journal of Applied Physics **87**, 4189 (2000).
- [49] G. Carlotti, L. Doucet, and M. Dupeux, *Comparative study of the elastic properties of silicate glass films grown by plasma enhanced chemical vapor deposition*, Journal of Vacuum Science & Technology B: Microelectronics and Nanometer Structures Processing, Measurement, and Phenomena **14**, 3460 (1996).
- [50] J.-H. Zhao, T. Ryan, P. S. Ho, A. J. McKerrow, and W.-Y. Shih, *Measurement of elastic modulus, poisson ratio, and coefficient of thermal expansion of on-wafer submicron films*, Journal of applied physics **85**, 6421 (1999).
- [51] D.-B. Kao, J. P. McVittie, W. D. Nix, and K. C. Saraswat, *Two-dimensional thermal oxidation of silicon—i. experiments*, IEEE Transactions on Electron Devices **34**, 1008 (1987).
- [52] Q. Xu, *Design of a large-stroke bistable mechanism for the application in constant-force micropositioning stage*, Journal of Mechanisms and Robotics **9**, 011006 (2017).
- [53] J. Kim, H. Choo, L. Lin, and R. S. Muller, *Microfabricated torsional actuators using self-aligned plastic deformation of silicon*, J. Microelectromech S. **15**, 553 (2006).
- [54] H.-S. Moon, L. Anand, and S. Spearing, *A constitutive model for the mechanical behavior of single crystal silicon at elevated temperature*, MRS Online Proceedings Library Archive **687** (2001).

- [55] E. EerNisse, *Viscous flow of thermal sio₂*, Applied Physics Letters **30**, 290 (1977).
- [56] E. EerNisse, *Stress in thermal sio₂ during growth*, Applied Physics Letters **35**, 8 (1979).
- [57] J. Cochard, I. Yonenaga, S. Gouttebroze, M. M'Hamdi, and Z. Zhang, *Constitutive modelling of silicon: Parameters identification of classical models using crystal plasticity*, (2009).
- [58] J. Cochard, I. Yonenaga, S. Gouttebroze, M. M'Hamdi, and Z. Zhang, *Constitutive modeling of intrinsic silicon monocrystals in easy glide*, Journal of Applied Physics **107**, 033512 (2010).
- [59] S. Hu, *Stress-related problems in silicon technology*, Journal of Applied Physics **70**, R53 (1991).
- [60] D. Zaccaria, D. Bigoni, G. Noselli, and D. Misseroni, *Structures buckling under tensile dead load*, in *Proceedings of the Royal Society of London A: Mathematical, Physical and Engineering Sciences* (The Royal Society, 2011) p. rspa20100505.

6

DISCUSSION AND CONCLUSION

In this chapter we consider the impact of the presented work and compare it to the state of the art followed by a conclusion. In particular we discuss scalability of the presented devices and discuss the balancing quality.

6.1. SCALABILITY

In this thesis we have demonstrated meter, decimeter and centimeter scale devices that use zero-free-length and plate springs, yet have zero or near-zero stiffness. They can be directly applied in for example robotics [1], rehabilitation [2, 3] and medical devices [4, 5], mechanical oscillators for applications in horology [6, 7] and sensors [8–11] to make them more energy efficient, improve haptic feedback and decrease natural frequencies of oscillation. The same design paradigm can be used to create smaller devices on the microscale for mechanical meta materials with variable Poisson's ratios [12], variable stiffness [13, 14] and even adaptivity in robotic materials with programmable properties [15–17], mechanical logic [18, 19], mechanical nanocomputers robust against radiant environment [20, 21] and other mechanical digital machines [22].

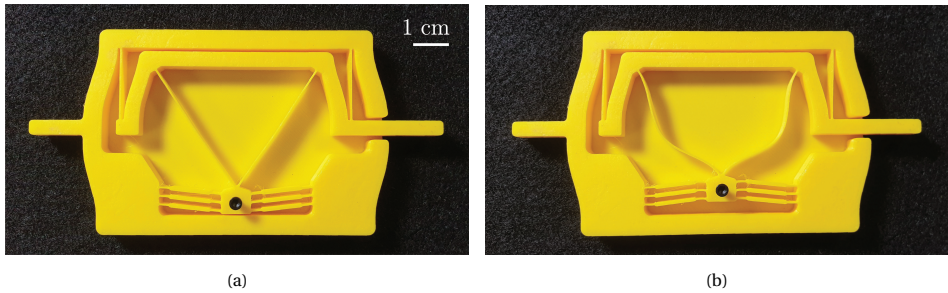


Figure 6.1: The linear statically balanced mechanism from chapter 4 scaled down by a factor of two. The mechanism is manufactured on a Prusa MK3 by fused deposition modeling with a nozzle size of 0.25 mm. (a) shows the high stiffness configuration and (b) shows the low stiffness configuration.

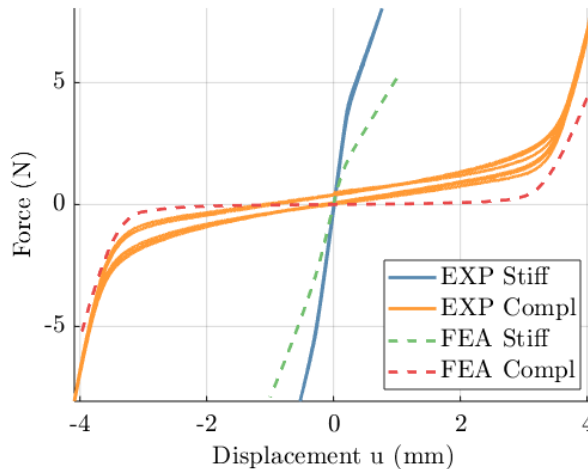


Figure 6.2: Experimental (EXP) and simulation (FEA) results of the mechanism from figure 6.1. Measurements and finite element simulations are done the same way as described in chapter 4.

The monolithic nature and the planar architecture of the devices from chapters 3 to 5 are primarily responsible for enabling scalability. Monolithicity eliminates assembly which means the devices can be scaled down to manufacturing limits. Planarity enables the use of well established surface-micro-machining techniques and additive manufacturing to be used, such as photolithography and two-photon lithography [23, 24], which are capable of producing micrometer sized features. Two demonstrations of scalability are given below.

The first demonstration of scalability is given in figure 6.1, where the characteristic length of the linear device from chapter 4 is reduced by a factor of two. This device is also 3D printed by using FDM, albeit with a smaller nozzle size of 0.25 mm, enabling smaller features compared to a 0.4 mm nozzle size. Measurements and simulations show its behavior in figure 6.2, which are done the same way as was done in chapter 4. Although no transition measurement is shown, high and low stiffness modes are clearly visible.

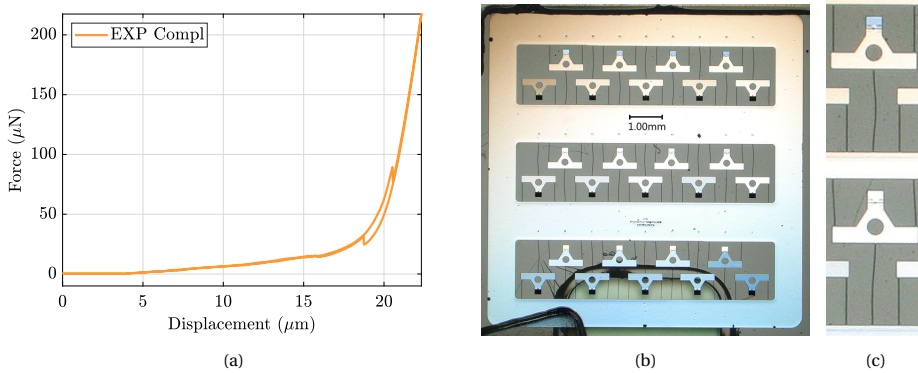


Figure 6.3: Permanent stiffness reduction by thermal oxidation of silicon is demonstrated on scale reduced by a factor 9 compared to the devices from chapter 5. (a) Shows preliminary experimental force displacement results on a Femtotools FT-NMT03, which are typical for a statically balanced compliant mechanism. (b) Shows an array of 27 devices in which the length L (see chapter 5) of the negative stiffness flexure is increased with each successive device, with top left the largest L . (c) Shows two buckling modes. The variation of length L is chosen such that the first two buckling modes will switch order at some unknown L , at which point the lowest stiffness should occur.

A second demonstration of scalability is given in figure 6.3 in which the characteristic length of the devices from chapter 5 is scaled down by a factor of 9 approximately. The devices are simultaneously manufactured with the devices from [25]. A silicon on insulator (SOI) wafer is used with a 300 μm handling layer, 2 μm silicon dioxide and a 50 μm thick device layer out of epitaxial silicon. A front and back are etched by DRIE and vapor hydrofluoric acid (VHF) is used to release the devices. Subsequently, a silicon dioxide thin film of approximately 1 μm is uniformly grown on the 5 μm wide beams by using wet thermal oxidation around 1100 °C.

Although many devices were broken for unknown reasons and unsuitable for executing the intended experiment, the two buckling modes from chapter 5 can be clearly observed. In addition one random but intact device in buckling mode 1 was measured to one side with a Femtotools FT-NMT03. Highly non-linear stiffness is observed in accor-

dance with results from both chapters 4 and 5. A low stiffness domain can be observed which indicates the generation of negative stiffness followed by a high stiffness as the stage reaches its motion limit indicating all beams are strained axially.

Apart from the design paradigm presented in this thesis, literature shows microscale statically balanced compliant mechanisms are possible today. Extensive numbers of micro-scale compliant mechanisms have been reported, such as passive bistable mechanisms [26–34] and active microrelays [35, 35–49]. These studies demonstrate good manufacturability of micro compliant mechanisms that store strain energy. Since storing strain energy has been the primary obstacle in statically balanced micro compliant mechanisms, they imply good manufacturability of the proposed systems from chapters 3 to 5 as well and suggest they can be made active with current technology. Actively controlled binary stiffness in micro compliant mechanisms will for example enable adaptive robotic metamaterials [15–17] that can change their bulk stiffness with local changes.

In addition, research into MEMS and semiconductor manufacturing has extensively focused on controlling stresses in thin film deposition to prevent damage [50]. However, instead of prevention, the same knowledge can form a basis for maximizing and exploiting those stresses for the preloading in the devices from chapters 3 to 5.

6.2. BALANCING QUALITY

It is observed that with reducing the length scale through the chapters, balancing quality deteriorates. In chapter 2 perfect balance is achieved, in chapters 3 and 4 a maximum factor of 1020 and in chapter 5 the best reduction factor is 46. Perfect balance from chapter 2 can only be achieved mathematically. Any embedding, be it in silico or in reality, will have approximate balance, due to the finite precision of computers and manufacturing.

In engineering the variation of any part dimensions is accounted for by specifying a tolerance. It is essential in ensuring all the parts of an assembly go together and to meet mechanical performance specifications. By analyzing the tolerance stack-up, i.e. the cumulative effect of all individual component tolerances, an engineer is able to analyze lower and upper bounds of mechanical performance, in this case balancing quality. Of course, by maintaining stricter engineering tolerances the cumulative effect is reduced, but producing high precision components is generally more difficult and thus more expensive.

Since the compliant mechanisms presented in chapters 3 to 5 do not require assembly, the cumulative effect of tolerances is smaller compared to rigid body mechanisms. However, the relative impact of manufacturing imperfections increases as length scales are reduced. One way to increase balancing quality at small scales is to account for uncertainty in the design process. A design that is insensitive to certain geometric variations can be obtained with the modular Bayesian machine learning framework from [51]. Here a (digital) experiment is set up to sample the effects of certain geometric variations, followed by a predictive analysis to generate a full solution space. Next machine learning establishes a mapping from the obtained solution space to actual device responses which is then used for computationally efficient design optimization. Even though modeling errors will always be present, this data-driven design approach is advantageous compared to experimentally guided design and is applicable to the design of stretch-

and bending-dominated structures under uncertainty [52].

Even when directly accounting for uncertainty, large-downward (top-down) fabrication, in which progressively smaller pieces of material are manipulated, is intrinsically limited. An alternative fabrication approach is small-upward (bottom-up) in which the smallest available building blocks, molecules, are assembled to form increasingly larger pieces of matter [53]. Various molecular mechanical devices have been fabricated such as gears, crank slider mechanisms, switches, rotors, tweezers and hinges by using self-assembly [54] but also active artificial molecular machines such as motors and an electrically driven car [55–57]. Active machines machine components have been realized by exploiting molecular bistability induced by input signals such as light and redox reactions, but are also possible by pH changes, metal ion binding, temperature and chemical stimuli [56].

Since stiffness is not an emergent property in bulk material it can be measured in individual molecules [58] and proteins [59]. As such, it should be theoretically possible to achieve artificial molecular machines that achieve their mobility from the deformation of individual molecules and proteins. Such molecular compliant mechanisms could be designed accounting for specific kinematic and dynamic properties and fabricated with a bottom-up approach by self assembly. Since the notion of storing and releasing strain energy is equally valid on the molecular scale, chemical bistability can be actively controlled and many mechanical molecular machines have been demonstrated, I look forward to the first nano-scale artificial molecular statically balanced compliant mechanism.

6.3. CONCLUSION

It can be concluded that statically balanced mechanisms with invariant potential energy are scalable to the micro scale. They have been investigated at various scales working towards smaller scales as we progressed.

At the large scale, the method from chapter 2 enables the analysis and synthesis of statically balanced rigid body mechanisms, which are often used as a precursor in the design process of compliant mechanisms. It is capable of balancing mechanisms with an infinite complexity by allowing symbolic derivation of balancing conditions for an arbitrary number of links and zero-free-length springs in 2D and 3D. To accommodate an easily solvable method, the principle of virtual transmissions has been introduced. It temporarily constrains the system to a single degree of freedom such that only one equation needs solving. The conditions generalize to the full unconstrained mobility.

We conclude that preloading difficulties has been primarily responsible for preventing the state of the art from miniaturization. This is solved by directly accounting for the manufacturability of micro compliant mechanisms. In various designs all required elastic structures are integrated into a monolithic and two-dimensional architecture. That is, components responsible for kinematics, negative stiffness and preloading are all integrated in a single-piece planar component. This makes them directly compatible with established micro fabrications techniques such as photo-lithography and two-photon lithography.

The principle of opposing constant force mechanisms has been extended to rotation with opposing constant torque. New constant force and constant torque mechanisms

have been introduced that significantly reduce device complexity. When preloaded against each other with bistable mechanisms, stiffness reduction of 98.5 % and 90.5 % is achieved for translation and rotation, respectively, with superior relative range of motion. Bistable mechanisms are responsible for preloading either by directly engaging them or by moving the central stage over a force threshold.

In addition, a novel elastic structure is introduced that is able to provide negative stiffness when preloaded, but also provides positive stiffness in the unpreloaded configuration. This allows maximization of the ratio between soft and hard modes resulting in an unprecedented stiffness reduction of 98.5 % (factor 84) and 99.9 % (factor 1020) for linear and rotational motion respectively, compared to the state of the art which reports reductions of -104.7 %, 91 %, -123 % and 70 % and (factors -21.2, 11.1, -4.2 and 3.3 respectively) [60–63]. A stiffness reduction by three orders of magnitude is sufficient for considering these mechanisms to be binary in stiffness, enabling binary digital machines that compute with stiffness.

We conclude that it is possible to preload microscale devices by exploiting residual stress in thin films. A stiffness reduction of a factor 9 to 46 is achieved by thermal oxidation of silicon, which could potentially be improved by using more severely stressed thin films such as Si_3Ni_4 and poly Si. The method is passive and nearly 100 % space efficient. It is a global method, enabling batch processing for massive parallelization at any level of complexity and since surface effects become more dominant at small scales by definition scalable.

Although scale and balancing quality are intrinsically limited by the current top-down approach of fabrication, extremely small artificial molecular machines have been fabricated in bottom-up fabrication approaches. Such nano-scale mechanical devices make it likely that mechanisms that exploit the flexibility of molecules and proteins can also be developed on those scales. Since the notion of negative stiffness is independent of the particular elastic element, it is likely to assume energy buffers and balancing modules can be developed by preloading molecules and proteins. These molecular negative stiffness building blocks could then be used to counteract the elastic properties of other molecules, achieving molecular sized statically balanced machines, moving closer actual nano-computers, robust in extreme environments.

REFERENCES

- [1] V. Arakelian, *Gravity compensation in robotics*, *Advanced Robotics* **30**, 79 (2016).
- [2] A. Alamdari, R. Haghghi, and V. Krovi, *Gravity-balancing of elastic articulated-cable leg-orthosis emulator*, *Mechanism and Machine Theory* **131**, 351 (2019).
- [3] P.-Y. Lin, W.-B. Shieh, and D.-Z. Chen, *A theoretical study of weight-balanced mechanisms for design of spring assistive mobile arm support (mas)*, *Mechanism and Machine Theory* **61**, 156 (2013).
- [4] A. Stapel and J. L. Herder, *Feasibility study of a fully compliant statically balanced laparoscopic grasper*, in *ASME 2004 IDETC and CIE* (2004) pp. 635–643.
- [5] J. Lassooui, N. Tolou, G. Tortora, S. Caccavaro, A. Menciassi, and J. Herder, *A stat-*

- ically balanced and bi-stable compliant end effector combined with a laparoscopic 2dof robotic arm*, *Mechanical Sciences* **3**, 85 (2012).
- [6] *Zenith watches*, <https://www.zenith-watches.com/int/collection/defy>, accessed: 2021-02-18.
- [7] S. L. Weeke, N. Tolou, G. Semon, and J. L. Herder, *A fully compliant force balanced oscillator*, in *ASME 2016 International Design Engineering Technical Conferences and Computers and Information in Engineering Conference* (American Society of Mechanical Engineers, 2016) pp. V05AT07A008–V05AT07A008.
- [8] R. P. Middlemiss, S. G. Bramsiepe, R. Douglas, S. Hild, J. Hough, D. J. Paul, A. Samarelli, S. Rowan, and G. D. Hammond, *Microelectromechanical system gravimeters as a new tool for gravity imaging*, *Philosophical Transactions of the Royal Society A: Mathematical, Physical and Engineering Sciences* **376**, 20170291 (2018).
- [9] R. Middlemiss, A. Samarelli, D. Paul, J. Hough, S. Rowan, and G. Hammond, *Measurement of the earth tides with a mems gravimeter*, *Nature* **531**, 614 (2016).
- [10] J. Laine and D. Mougnot, *A high-sensitivity mems-based accelerometer*, *The Leading Edge* **33**, 1234 (2014).
- [11] U. Krishnamoorthy, R. Olsson Iii, G. R. Bogart, M. Baker, D. Carr, T. Swiler, and P. Clews, *In-plane mems-based nano-g accelerometer with sub-wavelength optical resonant sensor*, *Sensors and Actuators A: Physical* **145**, 283 (2008).
- [12] K. Kim, H. Heo, and J. Ju, *A mechanism-based architected material: A hierarchical approach to design poisson's ratio and stiffness*, *Mechanics of Materials* **125**, 14 (2018).
- [13] R. Poon and J. B. Hopkins, *Phase-changing metamaterial capable of variable stiffness and shape morphing*, *Advanced Engineering Materials*, 1900802 (2019).
- [14] Y. Shan, M. Philen, A. Lotfi, S. Li, C. E. Bakis, C. D. Rahn, and K.-W. Wang, *Variable stiffness structures utilizing fluidic flexible matrix composites*, *Journal of Intelligent Material Systems and Structures* **20**, 443 (2009).
- [15] Y. Song, P. C. Dohm, B. Haghpanah, A. Vaziri, and J. B. Hopkins, *An active microarchitected material that utilizes piezo actuators to achieve programmable properties*, *Advanced Engineering Materials* **18**, 1113 (2016).
- [16] L. A. Shaw and J. B. Hopkins, *An actively controlled shape-morphing compliant microarchitected material*, *Journal of Mechanisms and Robotics* **8** (2016).
- [17] C. Luo, Y. Song, C. Zhao, S. Thirumalai, I. Ladner, M. A. Cullinan, and J. B. Hopkins, *Design and fabrication of a three-dimensional meso-sized robotic metamaterial with actively controlled properties*, *Materials Horizons* **7**, 229 (2020).
- [18] R. C. Merkle, *Two types of mechanical reversible logic*, *Nanotechnology* **4**, 114 (1993).

- [19] A. Sharma, W. S. Ram, and C. Amarnath, *Mechanical logic devices and circuits*, in *14th National Conference on Machines and Mechanisms (NaCoMM-09)*, Durgapur, India, Dec (2009) pp. 17–18.
- [20] J. S. Hall, *Nanocomputers and reversible logic*, *Nanotechnology* **5**, 157 (1994).
- [21] K. E. Drexler, *Rod logic and thermal noise in the mechanical nanocomputer*, in *Proc. Third Int. Symp. on Molecular Electronic Devices* (1988).
- [22] A. Ion, L. Wall, R. Kovacs, and P. Baudisch, *Digital mechanical metamaterials*, in *Proceedings of the 2017 CHI Conference on Human Factors in Computing Systems* (ACM, 2017) pp. 977–988.
- [23] S. Chizari, L. A. Shaw, and J. B. Hopkins, *Simultaneous printing and deformation of microsystems via two-photon lithography and holographic optical tweezers*, *Materials Horizons* **6**, 350 (2019).
- [24] Y. Song, R. M. Panas, S. Chizari, L. A. Shaw, J. A. Jackson, J. B. Hopkins, and A. J. Pascall, *Additively manufacturable micro-mechanical logic gates*, *Nature communications* **10**, 882 (2019).
- [25] K. V. Sweers, P. R. Kuppens, and N. Tolou, *Measuring plastic deformation in epitaxial silicon after thermal oxidation*, in *2019 International Conference on Manipulation, Automation and Robotics at Small Scales (MARSS)* (2019) pp. 1–8.
- [26] S. A. Zirbel, K. A. Tolman, B. P. Trease, and L. L. Howell, *Bistable mechanisms for space applications*, *PloS one* **11**, e0168218 (2016).
- [27] B. D. Jensen, M. B. Parkinson, K. Kurabayashi, L. L. Howell, and M. S. Baker, *Design optimization of a fully-compliant bistable micro-mechanism*, in *Proceedings of ASME IMECE*, Vol. 2 (2001) pp. 2931–2937.
- [28] J. Qiu, J. Lang, and A. Slocum, *A curved-beam bistable mechanism*, *Microelectromechanical Systems*, *Journal of* **13**, 137 (2004).
- [29] D. L. Wilcox and L. L. Howell, *Fully compliant tensural bistable micromechanisms (ftbm)*, *Journal of Microelectromechanical Systems* **14**, 1223 (2005).
- [30] B. D. Jensen, L. L. Howell, and L. G. Salmon, *Introduction of two-link in-plane, bistable compliant mems*, in *Proceeding of the 1998 ASME Design Engineering Technical Conferences, DETC98/MECH-5837* (1998).
- [31] B. Jensen, L. Howell, and L. Salmon, *Design of two-link, in-plane, bistable compliant micro-mechanisms*, *Journal of Mechanical Design* **121**, 416 (1999).
- [32] B. D. Jensen, *Identification of macro-and micro-compliant mechanism configurations resulting in bistable behavior*, (2003).
- [33] B. D. Jensen and L. L. Howell, *Bistable configurations of compliant mechanisms modeled using four links and translational joints*, *Journal of Mechanical Design* **126**, 657 (2004).

- [34] R. Luharuka and P. J. Hesketh, *Design of fully compliant, in-plane rotary, bistable micromechanisms for mems applications*, Sensors and Actuators A: Physical **134**, 231 (2007).
- [35] R. Luharuka and P. J. Hesketh, *A bistable electromagnetically actuated rotary gate microvalve*, Journal of Micromechanics and Microengineering **18**, 035015 (2008).
- [36] H.-W. Huang and Y.-J. Yang, *A mems bistable device with push-on–push-off capability*, Journal of Microelectromechanical Systems **22**, 7 (2012).
- [37] B.-T. Liao, H.-H. Shen, H.-H. Liao, and Y.-J. Yang, *A bi-stable 2x2 optical switch monolithically integrated with variable optical attenuators*. Optics express **17**, 19919 (2009).
- [38] T. Gomm, L. Howell, and R. Selfridge, *In-plane linear displacement bistable microrelay*, Journal of Micromechanics and Microengineering **12**, 257 (2002).
- [39] C. Lee and C.-Y. Wu, *Study of electrothermal v-beam actuators and latched mechanism for optical switch*, Journal of Micromechanics and Microengineering **15**, 11 (2004).
- [40] M. S. Baker and L. L. Howell, *On-chip actuation of an in-plane compliant bistable micromechanism*, Journal of microelectromechanical systems **11**, 566 (2002).
- [41] J. Qiu, J. H. Lang, A. H. Slocum, and A. C. Weber, *A bulk-micromachined bistable relay with u-shaped thermal actuators*, Journal of Microelectromechanical Systems **14**, 1099 (2005).
- [42] J. Qui, J. H. Lang, A. H. Slocum, and R. Strumpler, *A high-current electrothermal bistable mems relay*, in *The Sixteenth Annual International Conference on Micro Electro Mechanical Systems, 2003. MEMS-03 Kyoto. IEEE* (IEEE, 2003) pp. 64–67.
- [43] J. S. Ko, M. G. Lee, J. S. Han, J. S. Go, B. Shin, and D.-S. Lee, *A laterally-driven bistable electromagnetic microrelay*, ETRI journal **28**, 389 (2006).
- [44] D.-A. Wang, H.-T. Pham, and Y.-H. Hsieh, *Dynamical switching of an electromagnetically driven compliant bistable mechanism*, Sensors and Actuators A: Physical **149**, 143 (2009).
- [45] A. Cao, J. Kim, and L. Lin, *Bi-directional electrothermal electromagnetic actuators*, Journal of Micromechanics and Microengineering **17**, 975 (2007).
- [46] R. A. Receveur, C. R. Marxer, R. Woering, V. C. Larik, and N.-F. de Rooij, *Laterally moving bistable mems dc switch for biomedical applications*, Microelectromechanical Systems, Journal of **14**, 1089 (2005).
- [47] M. Freudenreich, U. Mescheder, and G. Somogyi, *Simulation and realization of a novel micromechanical bi-stable switch*, Sensors and Actuators A: Physical **114**, 451 (2004).

- [48] J. Casals-Terre, A. Fargas-Marques, and A. M. Shkel, *Snap-action bistable micromechanisms actuated by nonlinear resonance*, Journal of microelectromechanical systems **17**, 1082 (2008).
- [49] H. N. Kwon, I.-H. Hwang, and J.-H. Lee, *A pulse-operating electrostatic microactuator for bi-stable latching*, Journal of Micromechanics and Microengineering **15**, 1511 (2005).
- [50] S. Hu, *Stress-related problems in silicon technology*, Journal of Applied Physics **70**, R53 (1991).
- [51] M. Bessa and S. Pellegrino, *Design of ultra-thin shell structures in the stochastic post-buckling range using bayesian machine learning and optimization*, International Journal of Solids and Structures **139**, 174 (2018).
- [52] M. A. Bessa, P. Glowacki, and M. Houlder, *Bayesian machine learning in metamaterial design: fragile becomes supercompressible*, Advanced Materials **31**, 1904845 (2019).
- [53] V. Balzani, A. Credi, F. M. Raymo, and J. F. Stoddart, *Artificial molecular machines*, Angewandte Chemie International Edition **39**, 3348 (2000).
- [54] S. Erbas-Cakmak, D. A. Leigh, C. T. McTernan, and A. L. Nussbaumer, *Artificial molecular machines*, Chemical reviews **115**, 10081 (2015).
- [55] N. Koumura, R. W. Zijlstra, R. A. van Delden, N. Harada, and B. L. Feringa, *Light-driven monodirectional molecular rotor*, Nature **401**, 152 (1999).
- [56] B. L. Feringa, *The art of building small: from molecular switches to molecular motors*. The Journal of organic chemistry **72**, 6635 (2007).
- [57] T. Kudernac, N. Ruangsapichat, M. Parschau, B. Maciá, N. Katsonis, S. R. Harutyunyan, K.-H. Ernst, and B. L. Feringa, *Electrically driven directional motion of a four-wheeled molecule on a metal surface*. Nature **479**, 208 (2011).
- [58] A. Maitra and G. Arya, *Model accounting for the effects of pulling-device stiffness in the analyses of single-molecule force measurements*, Physical review letters **104**, 108301 (2010).
- [59] M. M. Claessens, M. Bathe, E. Frey, and A. R. Bausch, *Actin-binding proteins sensitively mediate f-actin bundle stiffness*, Nature materials **5**, 748 (2006).
- [60] A. Lamers, J. A. G. Sánchez, and J. L. Herder, *Design of a statically balanced fully compliant grasper*, Mechanism and machine theory **92**, 230 (2015).
- [61] P. J. Pluimers, N. Tolou, B. D. Jensen, L. L. Howell, and J. L. Herder, *A compliant on/off connection mechanism for preloading statically balanced compliant mechanisms*, in *ASME 2012 International Design Engineering Technical Conferences and Computers and Information in Engineering Conference* (American Society of Mechanical Engineers, 2012) pp. 373–377.

- [62] M. Barel, D. F. Machekposhti, J. Herder, N. Tolou, and M. Sitti, *Permanent preloading by acceleration for statically balancing mems devices*, in *2018 International Conference on Reconfigurable Mechanisms and Robots (ReMAR)* (IEEE, 2018) pp. 1–11.
- [63] F. M. Morsch and J. L. Herder, *Design of a generic zero stiffness compliant joint*, in *ASME 2010 International Design Engineering Technical Conferences and Computers and Information in Engineering Conference* (American Society of Mechanical Engineers, 2010) pp. 427–435.

A

APPENDIX

This appendix contains a table with all the references graphically summarized in figure 1.2 in chapter 1. The table lists the references in correspondence with the numbers on the x-axis along with the characteristic device length.

Nr.	Length (mm)	Reference
1	0.6	S. A. Zirbel, Q. T. Aten, M. Easter, B. D. Jensen, and L. L. Howell. Compliant constant-force micro-mechanism for enabling dual-stage motion. In <i>International Design Engineering Technical Conferences and Computers and Information in Engineering Conference</i> , volume 45035, pages 191–198. American Society of Mechanical Engineers, 2012
2	7.3	N. Tolou, P. Pluimers, B. D. Jensen, S. Magleby, L. Howell, and J. L. Herder. Constant force micro mechanism out of carbon nanotube forest. In <i>Proceedings of the 12th euspen International Conference Stockholm–Jun</i> , 2011
3	9.804	B. D. Jensen and C. H. Jenkins. Design of small-scale statically balanced compliant joints. In <i>ASME 2011 International Design Engineering Technical Conferences and Computers and Information in Engineering Conference</i> , pages 85–92. American Society of Mechanical Engineers, 2011

Nr.	Length (mm)	Reference
4	10	M. Tolou, P. Estevez, and J. L. Herder. Collinear-type statically balanced compliant micro mechanism (sb-cmm): experimental comparison between pre-curved and straight beams. In <i>Proceedings of the ASME Design Engineering Technical Conferences and Computers and Information in Engineering Conference, Aug</i> , pages 28–31, 2011
5	24.3	P. R. Kuppens, J. L. Herder, and N. Tolou. Permanent stiffness reduction by thermal oxidation of silicon. <i>Journal of Microelectromechanical Systems</i> , 28(5):900–909, 2019
6	60	M. Plooij, T. Van Der Hoeven, G. Dunning, and M. Wisse. Statically balanced brakes. <i>Precision Engineering</i> , 43:468–478, 2016
7	75	A. Bruyas, F. Geiskopf, and P. Renaud. Towards statically balanced compliant joints using multimaterial 3d printing. In <i>International Design Engineering Technical Conferences and Computers and Information in Engineering Conference</i> , volume 46360, page V05AT08A033. American Society of Mechanical Engineers, 2014
8	97.5	A. Dunning, N. Tolou, and J. Herder. A compact low-stiffness six degrees of freedom compliant precision stage. <i>Precision Engineering</i> , 37(2):380–388, 2013
9	99.8	Y.-H. Chen and C.-C. Lan. An adjustable constant-force mechanism for adaptive end-effector operations. <i>Journal of Mechanical Design</i> , 134(3):031005, 2012
10	104	Z.-W. Yang and C.-C. Lan. An adjustable gravity-balancing mechanism using planar extension and compression springs. <i>Mechanism and Machine Theory</i> , 92:314–329, 2015
11	105	H. Nair Prakashah and H. Zhou. Synthesis of constant torque compliant mechanisms. <i>Journal of Mechanisms and Robotics</i> , 8(6), 2016
12	110	Q. Xu. Design of a large-stroke bistable mechanism for the application in constant-force micropositioning stage. <i>Journal of Mechanisms and Robotics</i> , 9(1):011006, 2017

Nr.	Length (mm)	Reference
13	110	C.-W. Hou and C.-C. Lan. Functional joint mechanisms with constant-torque outputs. <i>Mechanism and Machine Theory</i> , 62: 166–181, 2013
14	116	P. Bilancia, S. P. Smith, G. Berselli, S. P. Magleby, and L. L. Howell. Zero torque compliant mechanisms employing pre-buckled beams. <i>Journal of Mechanical Design</i> , 142(11), 2020
15	117	A. Lamers, J. A. G. Sánchez, and J. L. Herder. Design of a statically balanced fully compliant grasper. <i>Mechanism and machine theory</i> , 92:230–239, 2015
16	125	D. Sarojini, T. Lassche, J. Herder, and G. Ananthasuresh. Statically balanced compliant two-port bistable mechanism. <i>Mechanism and Machine Theory</i> , 102:1–13, 2016
17	136.5	D. F. Machekposhti, N. Tolou, and J. Herder. A statically balanced fully compliant power transmission mechanism between parallel rotational axes. <i>Mechanism and Machine Theory</i> , 119:51–60, 2018
18	160	J. Zhang, A. D. Shaw, M. Amoozgar, M. I. Friswell, and B. K. Woods. Bidirectional torsional negative stiffness mechanism for energy balancing systems. <i>Mechanism and Machine Theory</i> , 131:261–277, 2019
19	170	J.-Y. Wang and C.-C. Lan. A constant-force compliant gripper for handling objects of various sizes. <i>Journal of Mechanical Design</i> , 136(7):071008, 2014
20	188	J. L. Herder. <i>Energy-free Systems. Theory, conception and design of statically</i> , volume 2. 2001
21	214	J. Lassoij, N. Tolou, G. Tortora, S. Caccavaro, A. Menciassi, and J. Herder. A statically balanced and bi-stable compliant end effector combined with a laparoscopic 2dof robotic arm. <i>Mechanical Sciences</i> , 3(2):85–93, 2012
22	250	G. Chen and S. Zhang. Fully-compliant statically-balanced mechanisms without prestressing assembly: concepts and case studies. <i>Mechanical Sciences</i> , 2(2):169–174, 2011

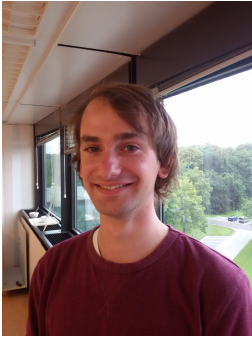
Nr.	Length (mm)	Reference
23	269.1	E. G. Merriam, M. Colton, S. Magleby, and L. L. Howell. The design of a fully compliant statically balanced mechanism. In <i>ASME 2013 International Design Engineering Technical Conferences and Computers and Information in Engineering Conference</i> . American Society of Mechanical Engineers Digital Collection, 2013
24	274.4	M. Barel, D. F. Macheuposhti, J. Herder, N. Tolou, and M. Sitti. Permanent preloading by acceleration for statically balancing mems devices. In <i>2018 International Conference on Reconfigurable Mechanisms and Robots (ReMAR)</i> , pages 1–11. IEEE, 2018
25	294	L. Berntsen, D. H. Gosenshuis, and J. L. Herder. Design of a compliant monolithic internally statically balanced four-bar mechanism. In <i>ASME 2014 International Design Engineering Technical Conferences and Computers and Information in Engineering Conference</i> , pages V05AT08A040–V05AT08A040. American Society of Mechanical Engineers, 2014
26	300	B. M. Wisse, W. D. Van Dorsser, R. Barents, and J. L. Herder. Energy-free adjustment of gravity equilibrators using the virtual spring concept. In <i>2007 IEEE 10th International Conference on Rehabilitation Robotics</i> , pages 742–750. IEEE, 2007
27	300	H. Pham and D. Wang. A constant-force bistable mechanism for force regulation and overload protection. <i>Mechanism and Machine Theory</i> , 2011
28	310	K. Hoetmer, J. L. Herder, and C. J. Kim. A building block approach for the design of statically balanced compliant mechanisms. In <i>ASME 2009 International Design Engineering Technical Conferences and Computers and Information in Engineering Conference</i> , pages 313–323. American Society of Mechanical Engineers, 2009
29	378	G. Radaelli, J. A. Gallego, and J. L. Herder. An energy approach to static balancing of systems with torsion stiffness. <i>Journal of Mechanical Design</i> , 133(9):091006, 2011

Nr.	Length (mm)	Reference
30	400	F. M. Morsch and J. L. Herder. Design of a generic zero stiffness compliant joint. In <i>ASME 2010 International Design Engineering Technical Conferences and Computers and Information in Engineering Conference</i> , pages 427–435. American Society of Mechanical Engineers, 2010
31	415	P. J. Pluimers, N. Tolou, B. D. Jensen, L. L. Howell, and J. L. Herder. A compliant on/off connection mechanism for preloading statically balanced compliant mechanisms. In <i>ASME 2012 International Design Engineering Technical Conferences and Computers and Information in Engineering Conference</i> , pages 373–377. American Society of Mechanical Engineers, 2012
32	420	C. Cho, W. Lee, and S. Kang. Static balancing of a manipulator with hemispherical work space. In <i>2010 IEEE/ASME International Conference on Advanced Intelligent Mechatronics</i> , pages 1269–1274. IEEE, 2010
33	450	M. Schenk, J. L. Herder, and S. D. Guest. Design of a statically balanced tensegrity mechanism. In <i>International Design Engineering Technical Conferences and Computers and Information in Engineering Conference</i> , volume 42568, pages 501–511, 2006
34	480	S. R. Deepak, A. N. Hansoge, and G. Ananthasuresh. Application of rigid-body-linkage static balancing techniques to reduce actuation effort in compliant mechanisms. <i>Journal of Mechanisms and Robotics</i> , 8(2):021005, 2016
35	489	P.-Y. Lin, W.-B. Shieh, and D.-Z. Chen. A theoretical study of weight-balanced mechanisms for design of spring assistive mobile arm support (mas). <i>Mechanism and Machine Theory</i> , 61:156–167, 2013
36	500	P. Pluimers. Design for specified stiffness in precision engineering. 2012
37	520	M. French and M. Widden. The spring-and-lever balancing mechanism, george carwardine and the anglepoise lamp. <i>Proceedings of the Institution of Mechanical Engineers, Part C: Journal of Mechanical Engineering Science</i> , 214(3):501–508, 2000

Nr.	Length (mm)	Reference
38	590	R. Rizk, S. Krut, and E. Dombre. Design of a 3d gravity balanced orthosis for upper limb. In <i>2008 IEEE International Conference on Robotics and Automation</i> , pages 2447–2452. IEEE, 2008
39	600	B. G. Bijlsma, G. Radaelli, and J. L. Herder. Design of a compact gravity equilibrator with an unlimited range of motion. <i>Journal of Mechanisms and Robotics</i> , 9(6):061003, 2017
40	600	J. L. Herder. Development of a statically balanced arm support: Armon. In <i>9th International Conference on Rehabilitation Robotics, 2005. ICORR 2005.</i> , pages 281–286. IEEE, 2005
41	700	J. L. Herder and G. J. Tuijthof. Two spatial gravity equilibrators. In <i>Proc. of ASME 2000 Design Engineering Technical Conferences and Computers and Information in Engineering Conference</i> , pages 1–9, 2000
42	900	S. K. Agrawal and A. Fattah. Gravity-balancing of spatial robotic manipulators. <i>Mechanism and machine theory</i> , 39(12):1331–1344, 2004
43	960	T. Laliberté, C. M. Gosselin, and M. Jean. Static balancing of 3-dof planar parallel mechanisms. <i>IEEE/ASME transactions on mechatronics</i> , 4(4):363–377, 1999
44	985	G. Endo, H. Yamada, A. Yajima, M. Ogata, and S. Hirose. A weight compensation mechanism with a non-circular pulley and a spring: Application to a parallel four-bar linkage arm. <i>SICE Journal of Control, Measurement, and System Integration</i> , 3(2):130–136, 2010
45	1000	S. K. Banala, S. K. Agrawal, A. Fattah, V. Krishnamoorthy, W.-L. Hsu, J. Scholz, and K. Rudolph. Gravity-balancing leg orthosis and its performance evaluation. <i>IEEE Transactions on robotics</i> , 22(6):1228–1239, 2006
46	1024	P.-Y. Lin, W.-B. Shieh, and D.-Z. Chen. Design of statically balanced planar articulated manipulators with spring suspension. <i>IEEE Transactions on Robotics</i> , 28(1):12–21, 2011

Nr.	Length (mm)	Reference
47	1270	P.-Y. Lin, W.-B. Shieh, and D.-Z. Chen. Design of a gravity-balanced general spatial serial-type manipulator. <i>Journal of Mechanisms and Robotics</i> , 2(3):031003, 2010
48	1750	A. Gopalswamy, P. Gupta, and M. Vidyasagar. A new parallelogram linkage configuration for gravity compensation using torsional springs. In <i>Proceedings 1992 IEEE International Conference on Robotics and Automation</i> , pages 664–669. IEEE, 1992
49	2000	C. M. Gosselin and J. Wang. Static balancing of spatial six-degree-of-freedom parallel mechanisms with revolute actuators. <i>Journal of Robotic Systems</i> , 17(3):159–170, 2000
50	2200	A. Alamdari and V. N. Krovi. Static balancing of highly reconfigurable articulated wheeled vehicles for power consumption reduction of actuators. <i>International Journal of Mechanisms and Robotic Systems</i> , 3(1):15–31, 2016
51	43000	G. Stepanov. Design of movable bridges. <i>Structural Engineering International</i> , 1(1):9–11, 1991
52	55000	G. Stepanov. Design of movable bridges. <i>Structural Engineering International</i> , 1(1):9–11, 1991
53	84000	G. Stepanov. Design of movable bridges. <i>Structural Engineering International</i> , 1(1):9–11, 1991
54	120450	G. Stepanov. Design of movable bridges. <i>Structural Engineering International</i> , 1(1):9–11, 1991
55	169000	J. Akkermann, T. Runte, and D. Krebs. Ship lift at three gorges dam, china—design of steel structures. <i>Steel Construction: Design and Research</i> , 2(2):61–71, 2009

ABOUT THE AUTHOR



June 7, 1990

Born in Gorinchem, The Netherlands.

2002-2007

Havo at Lyceum de Hoven in Gorinchem. Profile: Natuur en Techniek and Natuur en Gezondheid.

2007-2012

B.Eng. Human Kinetic Technology at The Hague University of Applied Sciences. Graduation project topic: *The design of a linkage based continuously variable transmission.*

2012-2013

Bridging program Mechanical Engineering at Delft University of Technology.

2013-2016

M.Sc. Mechanical Engineering focused on Biomechanical Design and Biorobotics. Graduation project topic: *Evolutionary design of dynamical mechanisms.*

2016-2020

Ph.D. Mechanical Engineering in the Mechatronic System Design group at the department of Precision and Microsystems Engineering at Delft University of Technology. Project topic is this thesis entitled: *Energy Invariant Mechanisms.*

2019-2020

Visiting Graduate Student at The Flexible Research Group at UCLA in Los Angeles as part of Ph.D program.

2020-present

Bright Member at Bright Society and Design Engineer at ASML.

LIST OF PUBLICATIONS

JOURNAL PAPERS

5. P. R. Kuppens, M. A. Bessa, and J. L. Herder. Static balancing of planar and spatial serial chains with virtual transmissions. *IN PREPARATION*, 2021
4. P. R. Kuppens, M. A. Bessa, J. L. Herder, and J. B. Hopkins. Monolithic binary stiffness building blocks for mechanical digital machines. *Extreme Mechanics Letters*, 42:101120, 2021. doi: 10.1016/j.eml.2020.101120
3. P. R. Kuppens, M. A. Bessa, J. L. Herder, and J. B. Hopkins. Compliant mechanisms that use static balancing to achieve dramatically different states of stiffness. *Journal of Mechanisms and Robotics*, 13(2), 2021. doi: 10.1115/1.4049438
2. P. R. Kuppens, J. L. Herder, and N. Tolou. Permanent stiffness reduction by thermal oxidation of silicon. *Journal of Microelectromechanical Systems*, 28(5):900–909, 2019. doi: 10.1109/JMEMS.2019.2935379
1. P. R. Kuppens and W. J. Wolfslag. A string-based representation and crossover operator for evolutionary design of dynamical mechanisms. *IEEE Robotics and Automation Letters*, 3(3):1600–1607, 2018. doi: 10.1109/LRA.2018.2800102

CONFERENCE PAPERS

2. K. V. Sweers, P. R. Kuppens, and N. Tolou. Measuring plastic deformation in epitaxial silicon after thermal oxidation. In *2019 International Conference on Manipulation, Automation and Robotics at Small Scales (MARSS)*, pages 1–8, 2019. doi: 10.1109/MARSS.2019.8860984
1. K. Vermeer, P. R. Kuppens, and J. L. Herder. Kinematic synthesis using reinforcement learning. In *International Design Engineering Technical Conferences and Computers and Information in Engineering Conference*, volume 51753, page V02AT03A009. American Society of Mechanical Engineers, 2018. doi: 10.1115/DETC2018-85529

OTHER

1. P. R. Kuppens. Finding the fittest spring mechanism. *Mikroniek*, 1(6), 2018

ACKNOWLEDGEMENTS

There are many people that I owe sincere gratitude. First I would like to thank Just and Nima for giving me the opportunity to do a PhD in their laboratory. In particular I would like to thank Just for his inexhaustible support, patience and enthusiasm. His technical insight, foresight and scientific vision have been truly inspiring. I would like to thank Nima for teaching me about the business side of research, for his strong personal involvement in the project and for pushing me further than I ever considered possible. I would also like to thank Miguel for his superb guidance, creative input and the many interesting discussions we had over the years. These are all qualities of great teachers, and I consider myself very lucky to have been given the opportunity to learn from you.

A special thanks goes out to all my colleagues from the department of Precision and Microsystems Engineering. I feel grateful that I have been part of a group of excellent scientists and support staff. In particular I would like to thank my direct colleagues from the Mechatronic System Design group, Davood, Freek, Jelle R., Werner, Niranjan, Stefan, Thijs, Joep, Jelle S., Ad, Ali A.D., Ali A.N., Nima, Andres, Wan, Giuseppe, Patrice, for all the support, the travels, the discussions, the laughs, and for the great company. It is hard to express how valuable you have been. I also owe a debt of gratitude to the engineers at Flexous Mechanisms B.V.: thank you Wout, Sybren, Maarten, Wouter and Sjoerd, it has been a pleasure to work with you. In addition I would like to express sincere gratitude to my colleagues Thomas, Vincent, Guy, Florian and Thuy-Anh that have been working at Tag Heuer Institute.

Jonathan has given me the opportunity to be a guest researcher in his Flexible Research Group at UCLA for which I am ever grateful. Thank you for providing me with an inspiring environment in which I had the freedom to do the research I love to do. This visit would not have been the same without Ryan, Miles, Rudy, Samira and Amin; thank you for making me feel welcome and for helping me every which way you could.

I have been lucky enough to interact with many brilliant students. Thank you Boran, Kaz, Lola, Korné and Abel, for the enthusiasm, creativity and the many inspiring discussions about your graduation project. I probably learned more from you than you ever did from me.

Last but not least, I would like to thank my friends and family. Thank you mom and dad, thank you Jilles, Casper, Pieter, Siska and Jocefe. This all would have been impossible if it wasn't for you. A final and most special word of thanks goes to Nina. Thank you Nina for the time we have spent, for being there whenever I needed it, for listening, for caring.

Reinier Kuppens
May 2021, Eindhoven

